3.0 Physical Environment

The physical environment including geology, climate, oceanography and ice influences the biological environment and also has the potential to affect the Project. A detailed description of the physical environment for the Laurentian Sub-basin is provided in the following sections.

3.1. Geological Overview

The evolution of Canada's southeastern continental margin can be traced to the closing of the ancient Iapetus Ocean during the Paleozoic. Colliding plates associated with a sequence of major tectonic events compressed the continental margin bordering this ocean to produce highly deformed rocks of the Appalachians (Humber Zone) and accreted onto it four terrains of exotic paleographic origin (Dunnage, Gander, Avalon, and Meguma Zones).

Following a long period of quiescence, a new "Wilson Cycle" of ocean opening and closing began in the Mesozoic (about 230 million years ago) to form the Atlantic Ocean and the passive continental margins that border it. This new cycle began in southeastern Atlantic Canada with rifting and breakup of the landmass that once joined Nova Scotia and southeastern Newfoundland to the Moroccan coast of Africa. Subsequent cooling and thermal contraction of the lithosphere accompanied by subsidence and rapid sedimentation along the margin has produced exceptionally thick Mesozoic-Cenozoic sedimentary basins that characterize much of the eastern seaboard of North America and which may hold vast petroleum resources.

Scotian Basin is one such basin, as shown on Figure 3.1. It occupies an area of about 300,000 km^2 and extends a distance of 1,200 km from Georges Bank (at the US/Canada boundary) to the southwestern Grand Banks of Newfoundland. Scotian Basin consists of a number of subbasins that are separated by areas of thinner sediment accumulation. From west to east these are the Shelburne, Sable, Abenaki, Laurentian and South Whale subbasins (Wade and MacLean 1990).

3.1.1. Physiography

The Project Area lies in the eastern portion of the Scotian Basin, spans across the relatively shallow and flat continental shelf, which generally has bathymetries of less than 200 m, and terminates partway down the continental slope. Maximum water depths of about 3,000 m are found in the southeastern part of the Project Area along the St Pierre Slope.

The bathymetry in the Project Area is relatively complex with depths ranging from about 100 m to depths over 3,500 m, including the shelves, slopes and abyssal plain (see Figure 1.1). The area contains the mouth of the Laurentian Channel and Halibut Channel and is bounded on the west by Banquereau

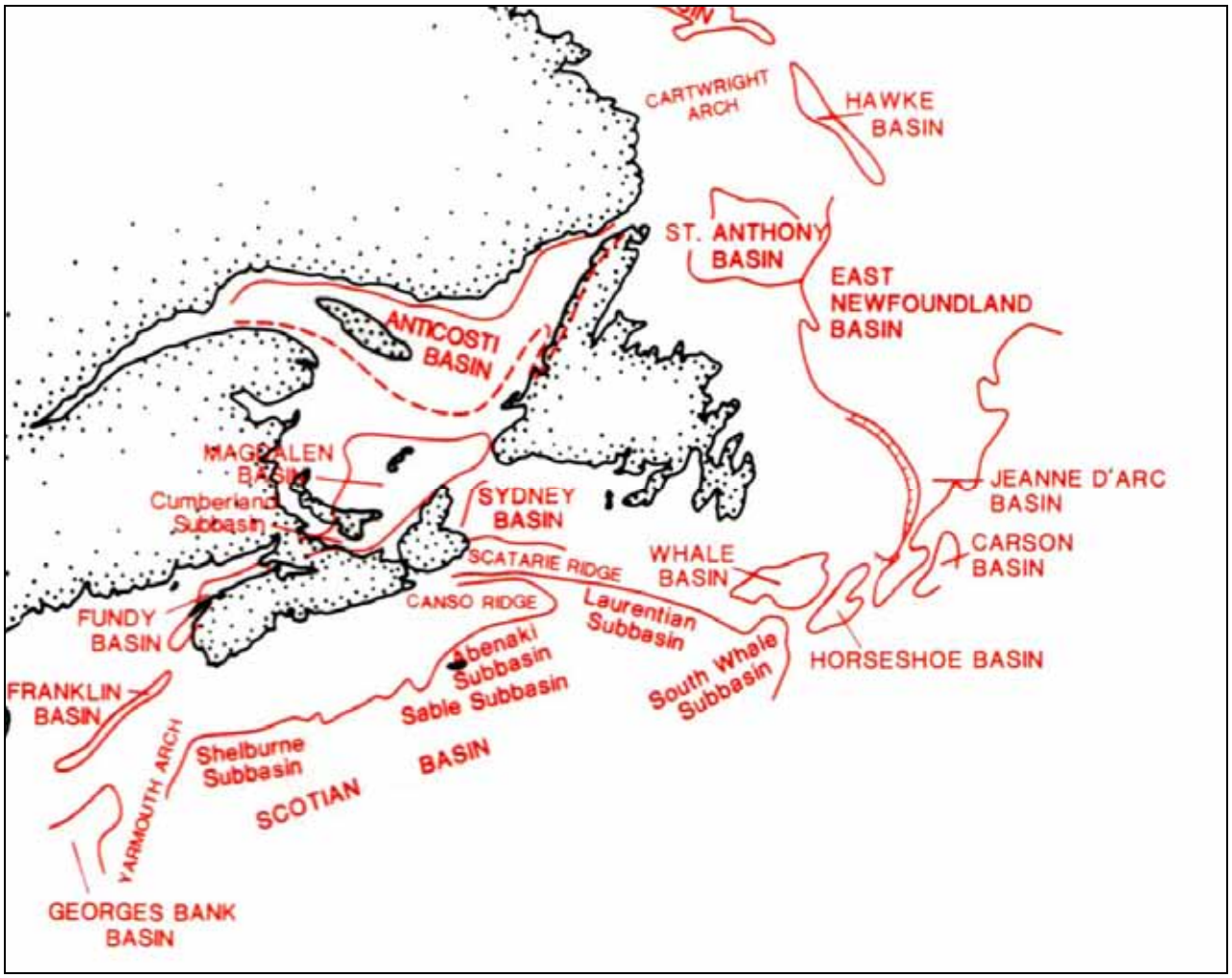

Figure 3.1. Sedimentary Basins of Offshore Eastern Canada (after Keen and Piper 1990).

Bank which forms the northeast corner of the Scotian Shelf, on the north by St. Pierre Bank and on the northeast by Green Bank both of which are part of the western Grand Banks. Whale Bank is immediately to the northeast of the Project Area.

3.1.1.1. Continental Shelf

The continental shelf to the south of Newfoundland is divided into two physiographic regions as shown on Figure 3.2: the Canadian Appalachian and Atlantic Coastal Plan. The Canadian Appalachians are further divided into the Atlantic Uplands and the Carboniferous-Triassic Lowlands (Fader et al. 1982). The geomorphology of these regions is primarily the result of Quaternary glaciations, including deposition of unconsolidated sediments that characterize the Project Area.

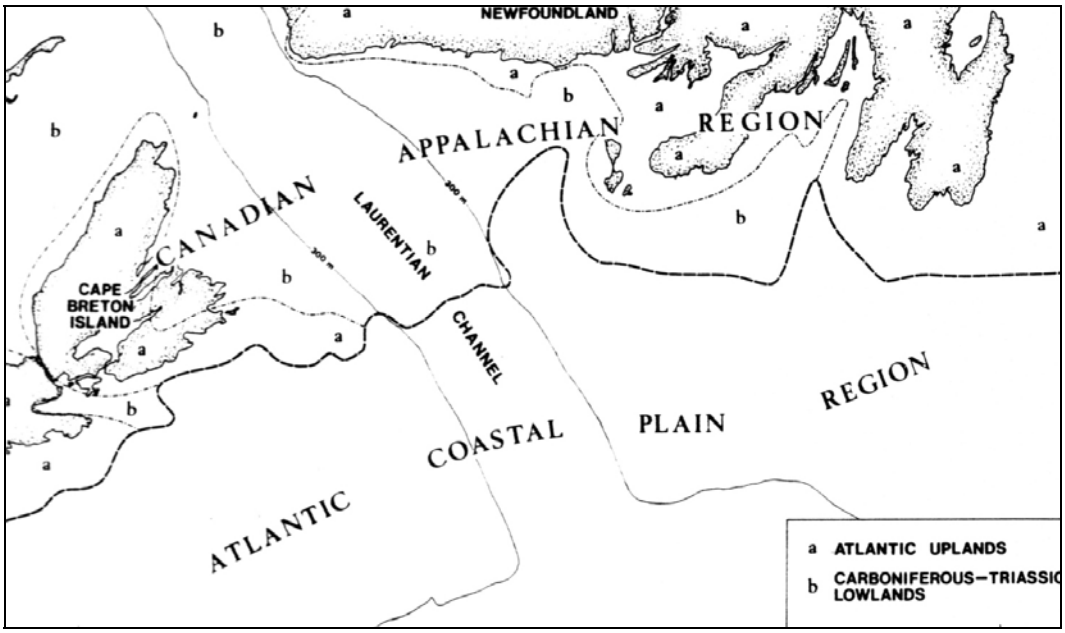

Figure 3.2. Physiographic Regions around the Project Area (after Fader et al. 1982).

Canadian Appalachian Region

The Atlantic Uplands is the largest geomorphic unit of the Appalachian Region, consisting of a southeasterly dipping peneplain of Precambrian and Paleozoic bedrock. This surface extends into offshore areas along the south coast of Newfoundland and generally coincides with areas of rough topography. In some places glacial erosion has resulted in overdeepened transverse troughs. Fortune Bay is an example of a submerged upland zone consisting of a linear isolated depression that is 30 km wide and 93 km long with water depths of over 512 m (Fader et al. 1982).

The Carboniferous – Triassic Lowlands is developed primarily in submerged rocks of that age. Several isolated banks occur within this area, including the Rose Blanche and Burgeo Banks (Figure 3.3). Glacial erosion has been extensive within the Lowlands Region as well, as evidenced by the Hermitage Channel which possesses the typical geomorphic character of a hanging valley where it intersects the deeper Laurentian Channel (Fader et al. 1982).

Atlantic Coastal Plain Region

The Atlantic Coastal Plain is underlain by Mesozoic and Cenozoic coastal plain sediments. The characteristic landforms that developed across this surface (mesas, cuestas, and deep incised valleys) formed during a period of subaerial erosion when sea levels were comparatively low. St Pierre Bank is a typical bank of the Atlantic Coastal Plain region (and the southwestern-most bank of the Grand Banks

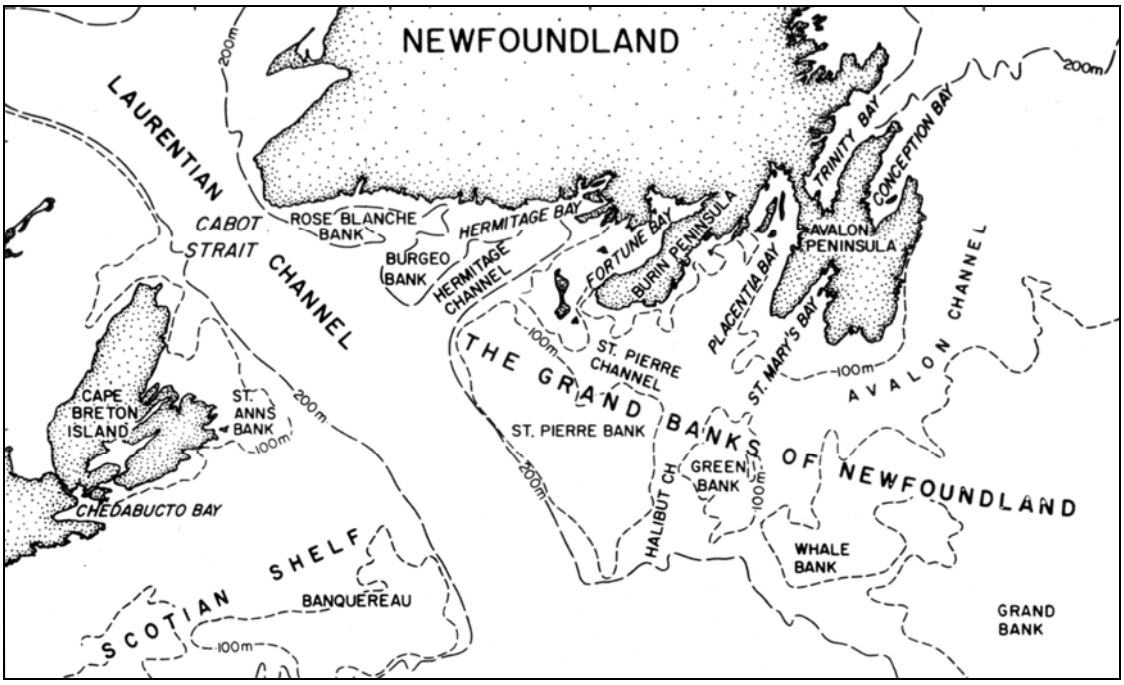

Figure 3.3. Index Map of the Grand Banks and the Eastern Scotian Shelf (after Fader et al. 1982).

of Newfoundland), with its shallowest point (31 m) occurring at its northwest corner, but in general being less than 115-120 m deep (corresponding to low sea levels 14,000 – 15,000 years before present). Halibut Channel is an extension of Placentia Bay, borders the eastern side of St Pierre Bank, and separates it from Green Bank further to the east (Wade and MacLean 1990; Fader et al. 1982).

The Laurentian Channel, which cuts across both physiographic regions, is a dominant morphological feature that extends from the St Lawrence River valley, through the Gulf of St Lawrence, across the continental shelf that separates Nova Scotia from Newfoundland, and terminates at the edge of the continental shelf. It began as a series of Late Cretaceous fluvial drainage systems that eroded subaerial Paleozoic and Mesozoic bedrock to form incised river valleys. Glaciers subsequently carved out and overdeepened these and sea levels rose to produce the broad, U-shaped submarine channel evident today. It has relatively straight sides, an average width of 93 km, and isolated depressions that reach depths below sea level of 538 m (north of Cabot Strait) and 485 m (south of the mouth of Hermitage Channel). At its mouth where it crosses the shelf break, the Laurentian Channel is floored by a sill having a minimum depth of 364 m and which extends three-quarters of the way across the channel starting from St Pierre Bank. Numerous slump features lie seaward of the sill along the continental slope (Josenhans and Lehman 1999; Fader et al. 1982).

3.1.1.2. Continental Slope

Along the continental margin of southeastern Canada a well defined transition exists, known as the shelf break, that separates the slightly southeast dipping shelf from the steep incline of the slope. At this

break, the slope profile is generally concave with the greatest gradient (up to 6°) on the upper slope. The large scale morphology of the slope reflects thick Mesozoic-Cenozoic sedimentary wedges that make up the sedimentary basins, as well as late Quaternary processes of slope progradation and erosion. The Paleozoic basement has minor influence on the geomorphology of the area because of the very thick sedimentary accumulations upon it.

The down-slope movement of sediment under gravity involves a continuum of processes from slow creep with bedding deformation to rotational slumping, translational sliding, debris flow, and turbidity currents. The upper and mid-slope areas are dominated by rotational slumps that appear to lead downslope into debris flows. The transition from debris flows to turbidity currents is presumed to occur at water depths of 700 to 1,500 m on the continental slope (Piper et al. 1999).

The Laurentian Fan, a major sedimentary depositional centre located seaward of the Laurentian Channel, provides evidence for the existence of a turbidity current precipitated by the 1929 Grand Banks earthquake. Seamarc side scan surveys of the Laurentian Fan reveal gravel-size sediment waves on its Eastern Valley floor, attesting to the high speed of the flow. This turbidity current traveled at a speed that peaked at more than 19 m/s and deposited more than 150 km^3 of sediment on the Sohm Abyssal Plain. Deep-towed sidescan imagery over the St Pierre Slope show "fresh" sediment failures interpreted as rotational slides and debris flow deposits associated with the 1929 event. These features show a prominent line of headscarps on the upper slope at depths between 500 and 700 m. At lesser depths the sediments appear to have been stable (Piper et al. 1999; 2005).

Such sediment transport processes have resulted in erosive features such as steep sided submarine valleys, particularly in areas seaward of major transverse troughs like the Laurentian and Halibut Channels. In contrast, the slope off St Pierre Bank shows progradational sedimentation broken only by minor erosional events throughout much of the Quaternary. Exceptions to this would be the St Pierre Valley and Grand Banks Valley, which are also prominent slope valleys that lead to the Eastern Valley of the Laurentian Fan (Piper et al. 2005).

3.1.2. Quaternary Sediments

Lying above Tertiary and older bedrock are unconsolidated Quaternary sediments deposited during and subsequent to the Wisconsinian glaciation. Five surficial sedimentary formations are recognized within the Project Area: Grand Banks Drift, Downing Silt, Adolphus Sand, Placentia Clay, and Grand Banks Sand and Gravel. These units are stratigraphic equivalents of Scotian Shelf sediments (i.e., Scotian Shelf Drift, Emerald Silt, Sambro Sand, LaHave Clay, and Sable Island Sand and Gravel) and consist of glacial tills, proglacial silts, sublittoral sands, recent mud, and basal transgressive sand and gravel. Figure 3.4 shows the distribution of these sediments where they are exposed along the shelf. Figure 3.5 is a schematic cross-section that illustrates the stratigraphic relationships between the formations. Fader et al. (1982), Piper et al. (1990), and Brown (1990) discuss each of these sedimentary units in detail. A summary of their descriptions is provided below.

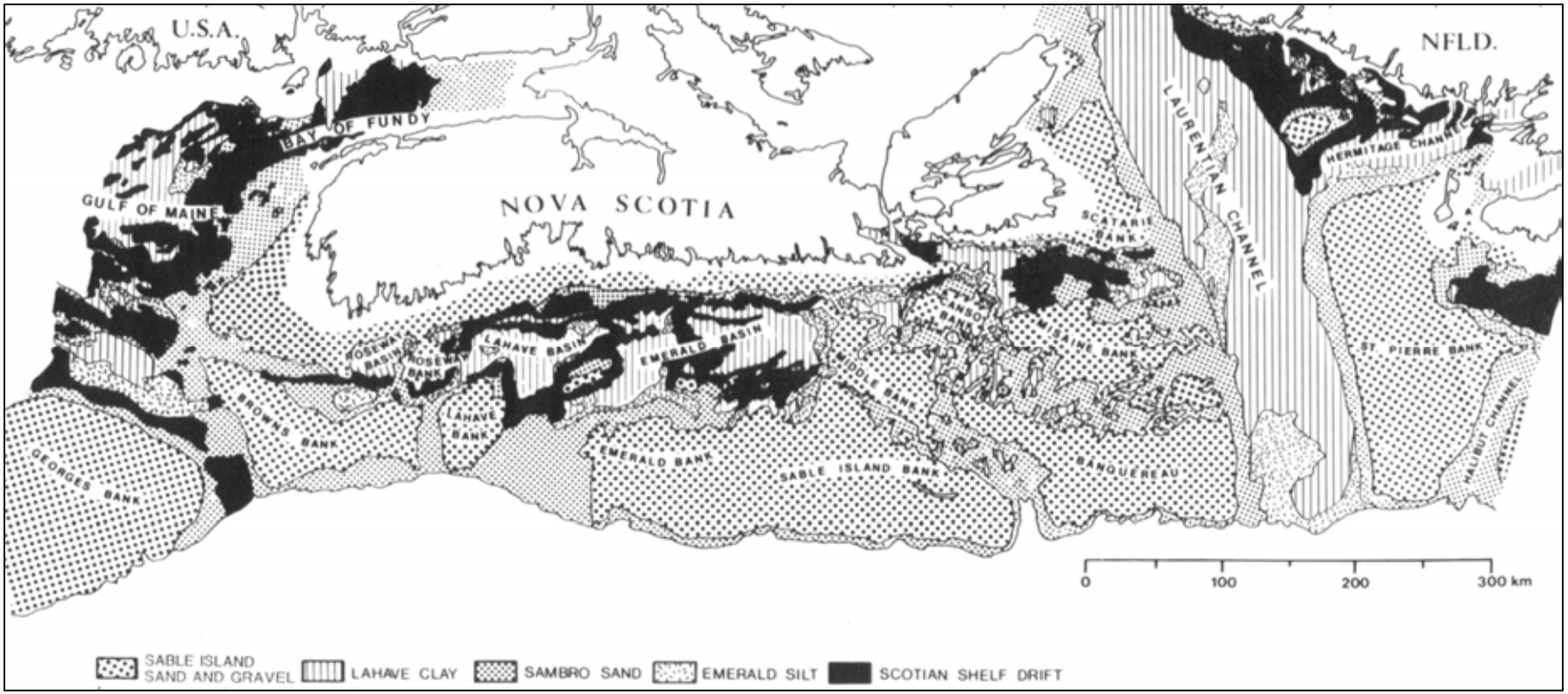

Figure 3.4. Surficial Geology of the Scotian Shelf and Southwestern Grand Banks (after Piper et al. 1990).

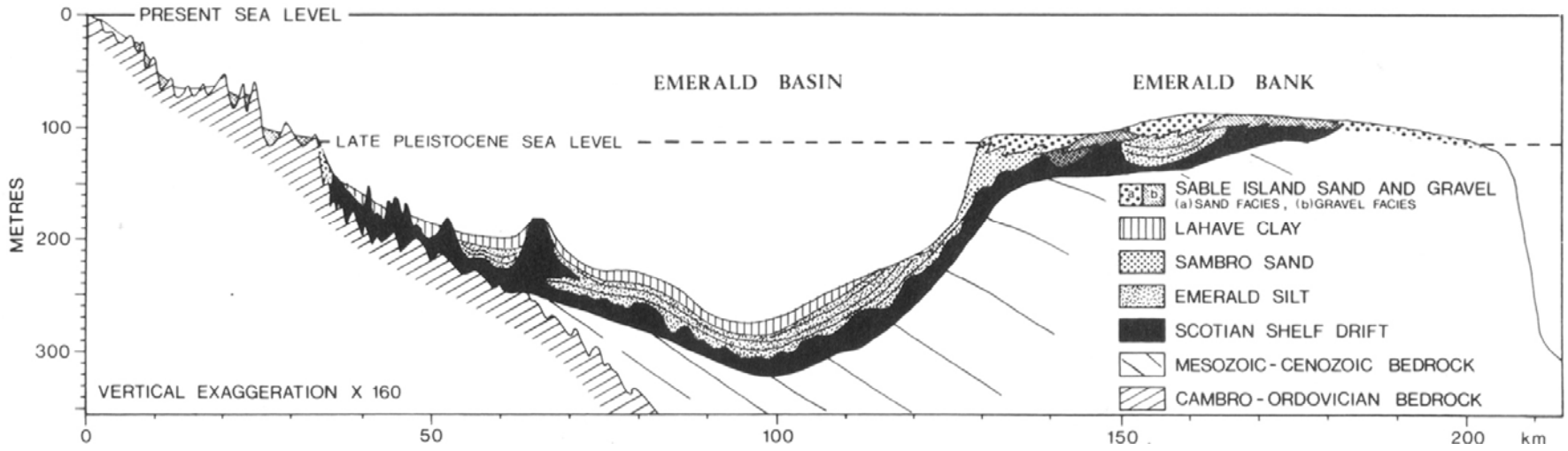

Figure 3.5. Schematic Northwest-Southeast Profile across the Emerald Basin and Emerald Bank of the Scotian Shelf showing the Stratigraphic Relationship of Quaternary Sediments (after Piper et al. 1990).

3.1.2.1. Grand Banks Drift

Grand Banks Drift (stratigraphic equivalent of Scotian Shelf Drift) consists of till deposited at the base of a grounded ice sheet, generally in contact with bedrock surfaces. This unit is less than 60 m thick and found at water depths of up to 500 m, as on the upper continental slope. It is an olive-grey to reddish-brown, poorly sorted till, composed of sand, silt, and clay with various amounts of pebbles, cobbles, and boulders. Where this unit is exposed at the seabed it appears as protruding cobbles and boulders within a matrix of sandy mud. It occurs as a thin veneer or ground moraine, as infillings in old subaerial erosional channels in underlying bedrock, or in thick morainal ridges. Although this unit is not exposed in the Project Area, it does occur as a thin, discontinuous sheet under later Quaternary sediments.

3.1.2.2. Downing Silt

Downing Silt (stratigraphic equivalent of Emerald Silt) is a unit that overlies and locally interfingers with Grand Banks Drift. It is typically less than 90 m thick and is interpreted to have been deposited at the front of a grounded ice sheet, beneath an ice shelf, or as a proglacial deposit. Downing Silt is a dark greyish-brown to greenish-brown, clayey and sandy silt that locally grades to a silty and clayey sand with minor angular gravel. In the Project Area Downing (Emerald) Silt is exposed primarily at the base of the Laurentian Channel and in isolated depressions of the Halibut Channel. Below the seabed, this unit occurs in the northeastern St Pierre Bank and over most of the Laurentian Channel. Where exposed, the surface of this unit is smooth with gentle undulations. In areas where this formation is thin and overlies rough glacial till, its surface mimics that of the underlying till.

This unit is extensively furrowed by icebergs. Furrows can be up to 10 m deep.

3.1.2.3. Adolphus Sand

Adolphus Sand (stratigraphic equivalent of Sambro Sand) is a formation found below the post-Wisconsinian low sea level at 115 – 120 m water depths. It is a dark, greyish-brown, fine to coarse-grained sand containing some silt and clay sized fractions and gravel that generally is found as a thin veneer less than 10 m thick. Foraminiferal tests, sponge spicules, radiolaria, and broken shell fragments occur in abundance within this formation. In the Project Area, this unit is found along the flanks of the Laurentian Channel and at the base of the Halibut Channel. Iceberg furrows occur across many areas of Adolphus Sand, particularly along the edges of the Laurentian Channel. In the Halibut Channel, the seabed is characterized by numerous sand waves with maximum heights of 8 m and wavelengths of 305 m.

3.1.2.4. Placentia Clay

Placentia Clay (stratigraphic equivalent of LaHave Clay) is a dark greyish brown to dark olive, homogeneous silty clay to clayey silt formation. It is less than 30 m thick and its generally flat surface comprises most of the seabed of the Laurentian Channel within the Project Area. This unit originates

primarily from reworking of Downing (Emerald) Silt and glacial tills during the marine transgression of the Holocene.

3.1.2.5. Grand Banks Sand and Gravel

Grand Banks Sand and Gravel (stratigraphic equivalent of Sable Island Sand and Gravel) is a basal marine transgressive sand and gravel deposit that occurs in water depths of less than 115 - 120 m and is generally less than 20 m thick. This unit consists of reddish to greyish-brown, fine to coarse grained, well sorted sand that grades locally to coarse, well rounded gravel with large boulders. The fine silt and clay sized fraction characteristic of the Adolphus Sand is absent in this unit. Grand Banks Sand and Gravel is exposed at the seabed over most of St Pierre Bank as sand waves and megaripples with wavelengths of between one and 200 m.

3.1.3. Seismicity

Eastern Canada is located in a stable continental region of the North American plate and as a consequence has a relatively low rate of seismic activity typical of "passive" continental margins (see Figure 3.6 to compare this region's seismic activity with that of the "active" margin off Canada's west coast). Nevertheless, numerous earthquakes have been recorded along the eastern continental margin (Figures 3.7 and 3.8), including the devastating Laurentian Slope, or "Grand Banks", earthquake of November 1929 (epicentre at 44.69° N latitude, 56.00° W, 20 km depth) which ripped apart numerous transatlantic cables and caused a tsunami that, coupled with a storm surge, resulted in a death toll of 27 people along the Burin Peninsula of Newfoundland. This magnitude 7.2 event could be felt as far away as New York, Ottawa, and Montreal, and also damaged structures in northeastern Nova Scotia (NRCan 2006).

Each year, about 300 earthquakes occur in eastern Canada[1]. Along Canada's eastern continental margin, instrument-recorded earthquake epicentres are concentrated in a few "source zones" of relatively intense seismic activity such as at Baffin Island, northern Baffin Bay, the northern Labrador Sea, and the Laurentian Slope in and around the Project Area.

Earthquake epicentres within the Labrador Sea show a strong seismotectonic association with the mid-ocean spreading axis of that area. Other earthquakes, such as those along the Laurentian Slope, do not show such clear associations and may indeed be related to postglacial unloading, ocean-continent boundary interactions, and sediment loading along the continental margin.

It has been suggested that stress relief along old zones of crustal weakness, such the Cobequid-Chedbucto Fault (which separates the Meguma and Avalon terrains) or the Glooscap Fault of the Newfoundland Fracture Zone may play some part in the earthquakes recorded within the Project Area

[1] A recent event recorded near the Project Area was on 3 February 2006 with a Magnitude of 2.8 and an epicentre located in the Laurentian Channel at latitude 45.96° N, longitude 57.76° W.

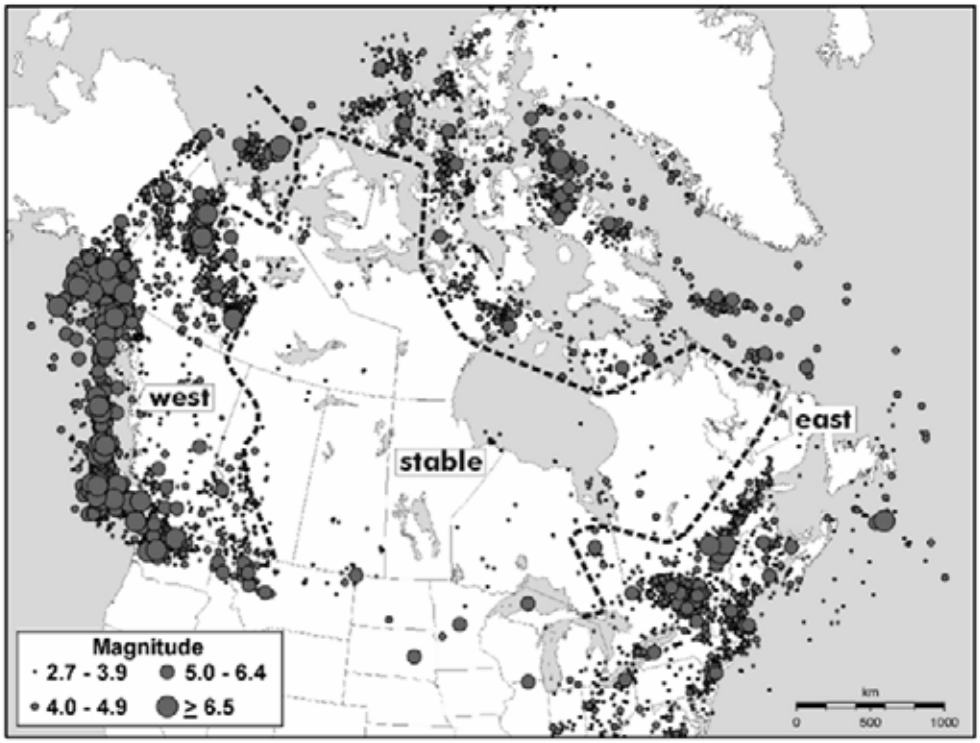

Figure 3.6. Earthquake Catalogue used to Generate Seismic Hazard Maps for Inclusion in the 2005 National Building Code of Canada.

Note: The dashed lines delimit the eastern and western seismic regions and the stable Canada central region (after Adams and Halchuk 2003).

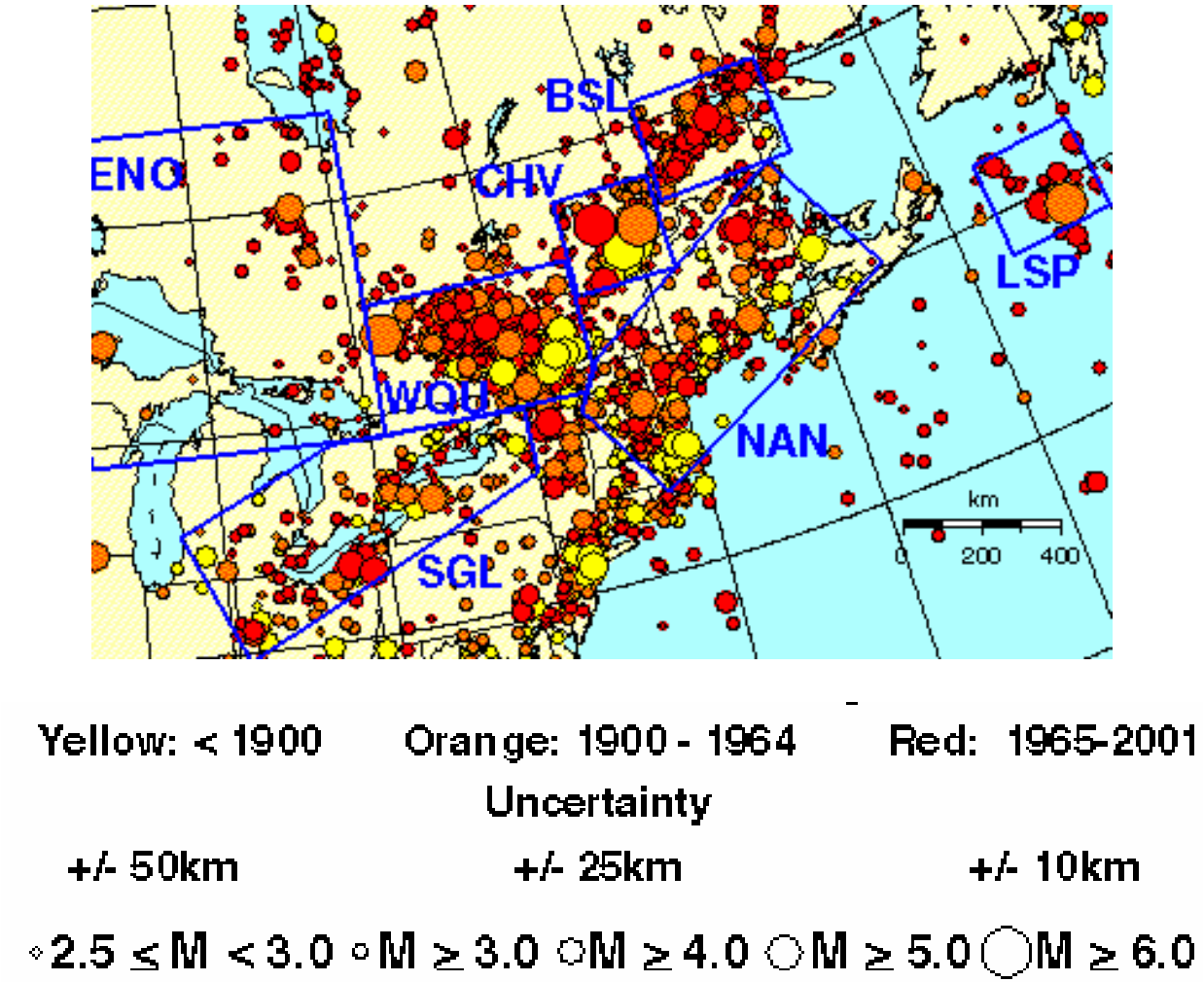

Figure 3.7. Historic Seismicity in Central, Eastern, and Offshore Eastern Canada.

Note: The blue box labeled LSP is the Laurentian Slope seismic zone (NRCan 2006).

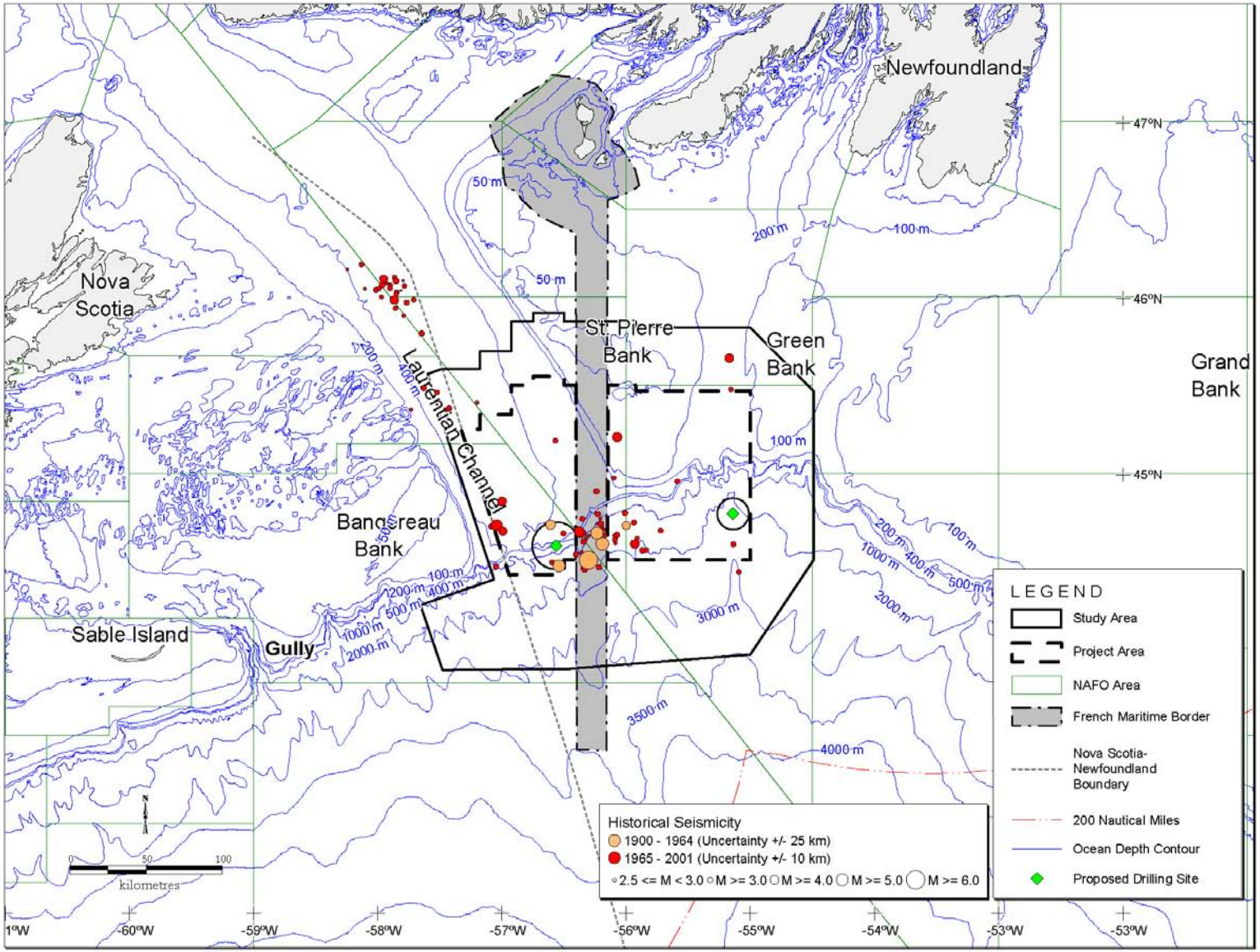

Figure 3.8. Historic Seismicity in the Laurentian Slope Region (NRCan 2006).

(JWEL 2003; Miller 1995). However, these structures are relatively far removed from the measured epicentres and the historical instrument-recorded earthquake database is too small to unequivocally support such an assertion (Keen et al. 1990; S. Dehler, personal communication).

3.1.3.1. Seismic Hazard[2]

Earthquakes can pose hazards to offshore structures and activities. These effects may include ground shaking; surface faulting; regional scale subsidence and uplift; seabed liquefaction and effects such as slides, slumps, and turbidity currents; tsunamis; and possible damage to floating structures due to acoustic shock waves (Keen et al. 1990).

The damage potential of an earthquake is determined by how the ground moves and how the buildings within the affected region are constructed. Expected ground motion can be calculated on the basis of probability, and the expected ground motions are referred to as seismic hazard.

In Canada, the evaluation of regional seismic hazard is the responsibility of the Geological Survey of Canada. The seismic hazard maps prepared by the Geological Survey are derived from statistical analysis of past earthquakes and from advancing knowledge of Canada's tectonic and geological structure. On the maps, seismic hazard is expressed as the most powerful ground motion that is expected to occur in an area for a given probability level. Contours delineate regions likely to experience similar ground motions. Figure 3.9 is a simplified seismic hazard map that indicates relative seismic hazard across Canada.

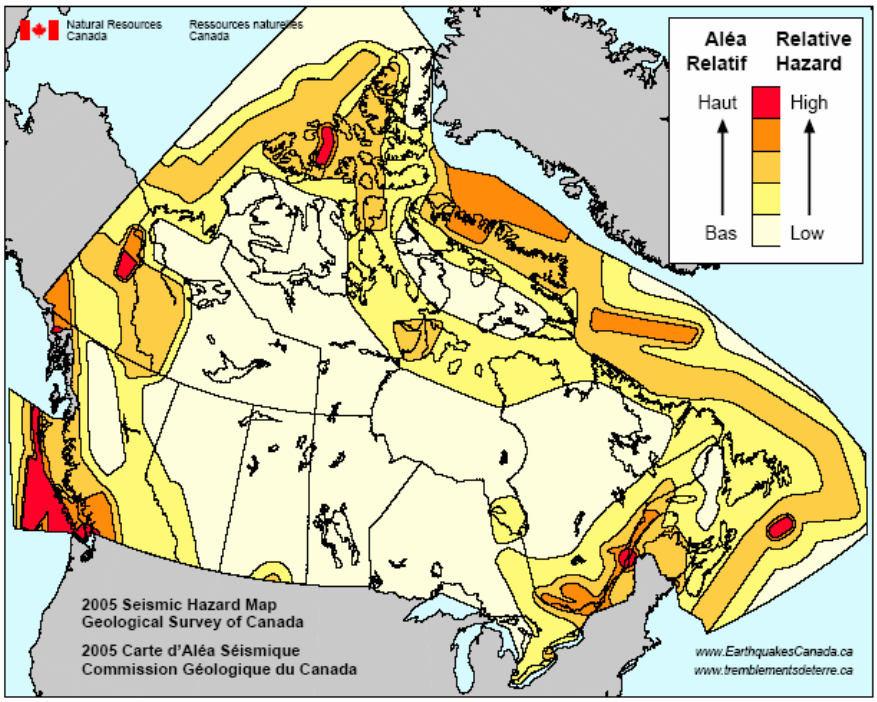

Figure 3.9. Simplified Seismic Hazard Map of Canada (NRCan 2006).

[2] This bulk of this section has been adapted from Natural Resources Canada website, found at http://earthquakescanada.nrcan.gc.ca/hazard/zoning/haz_e.php#calculation

3.1.4. Slope Stability[3]

The potential for large downslope sediment mass movement poses a hazard to offshore structures. Such movements can be classified on the basis of sediment type and strength[4]. The terms "slump" and "slide" are both used to describe failure along discrete surfaces. Slumping is a rotational failure that is generally associated with homogeneous deposits of fine cohesive material, such as clays, whereas sliding is a translational failure that usually follows sedimentary bedding planes and generally occurs within non-cohesive soils such as sands and silts.

The necessary condition for slumping on slopes less than 10 degrees is underconsolidation, where pore water pressures exceed hydrostatic levels. This may be caused by high rates of sedimentation, the presence of gas in sediment pore water, and residual pore pressures following repeated loading, as from storm waves. Slumping is typically initiated by some sort of trigger such as dynamic loads of earthquakes and sea ice, or oversteepening resulting from sediment deposition or erosion at the crest or toe of the slope, respectively.

Liquefaction will occur if the sediment structure breaks down as a result of temporarily high pore water pressures that reach the local lithostatic pressure. Liquefied sediment will flow rather than slump. Excess pore water pressures dissipate rapidly in coarse grained sediment. Therefore, flows in gravel would not last as long as flows involving finer grained sands and silts. Flows of fine grained cohesive sediment, or mudflows, dissipate excess pore water pressures very slowly and therefore are the most common mass flow material. Turbidity currents are flows of relatively high density and their destructive power is well known from the 1929 Grand Banks earthquake, where such currents caused a number of breaks in the Trans Atlantic cable. These are of greater concern along the lower part of the continental slope and continental rise than within the continental shelf or upper slope.

Although storm wave loading has been shown to trigger sediment instabilities in limited regions of the outer continental shelf, the most probable trigger for instabilities on shelf slopes is thought to be earthquake shaking, as on the continental slopes. Earthquake loading of sediments causes increased pore water pressures, which results in reduced sediment strength.

3.1.4.1. Oil Seeps

Based on satellite imagery, a number of potential oil seeps have been identified in and adjacent to the Laurentian Basin area (NPA, unpubl. confidential data *in* LGL 2005). While some of these may be anthropogenic (e.g., illegal dumping), their recurrence at the same latitudes and longitudes suggests that at least some of these may be of natural origin.

[3] Adapted from Moran et al. 1990.
[4] These have been described in some detail in the previous section regarding Quaternary Sediments.

3.2. Weather Conditions

3.2.1. General Description of Weather Systems

The earth's general circulation arises from the normal tropical to polar temperature gradient that typifies the upper level in the mid-latitudes. The temperature gradient generates pressure differences between the tropics and the poles, which create winds that transport the energy northward in the Northern Hemisphere. Due to the effects of the earth's rotation, these winds are deflected, creating a prevailing westerly flow in the upper atmosphere of the middle and high latitudes. In the summer, winds aloft are predominately from the west, with the jet stream lying between 45 and 60 degrees north latitude. Upper level winds in the winter months can be as much as 60 percent stronger than in the summer months due to the stronger temperature gradient that exists between the low and high latitudes. The strength of the jet stream, which is proportional to the temperature gradient, is stronger and much better defined during this period.

At any given time, the upper level 500 mb (about half way up in the atmosphere) flow pattern consists of large amplitude ridges and troughs. These ridges and troughs tend to act as a steering agent for surface features such that their positions in the upper atmosphere determine the weather at the earth's surface. Over Eastern Canada, upper ridges generally mean good weather, while upper troughs tend to bring poor weather.

On average, about eight low-pressure systems affect the area per month. These low-pressure systems tend to develop within troughs and travel along the flow pattern set up between a ridge and trough.

During the winter months, the upper trough tends to lie over Central Canada and an upper ridge over the North Atlantic. This results in three main storm tracks that generally affect the area; one from the Great Lakes Basin, one from Cape Hatteras, North Carolina and one from the Gulf of Mexico.

Lows that develop off Cape Hatteras move over the Gulf Stream, then track northeast, typically passing over Newfoundland, Canada. The warm Gulf Stream waters cause the lows to intensify and when conditions are favourable during the winter, very intense storms known as "weather bombs" may develop. Weather bombs possess characteristics similar to a tropical storm, such as hurricane force winds near the center, the outbreak of convective clouds to the north and east of the center during the explosive stage, and the presence of a clear area near its center in its mature stage (Rogers and Bosart 1986). Sanders and Gyakum (1980) showed that these storms deepen in baroclinic environments and defined a "bomb" as a storm that undergoes central pressure falls greater than 2.4 kPa over 24 hours.

The warm waters of the Gulf of Mexico are also favourable for storm development during the winter months. With the upper troughs lying east of the area, cold air over the southeastern United States

interacts with the warm moist Gulf of Mexico air. This interaction results in the development of a low that will follow the upper flow into Eastern Canada. The low may become even more intense if its track brings it over the Gulf Stream.

Great Lakes lows develop as a result of the warm moist air over the Great Lakes interacting with colder air from off the land. These lows tend to be less intense than those that develop off Cape Hatteras or even in the Gulf of Mexico. As the lows develop, they tend to follow two main tracks, with one bringing the lows over Quebec and into Labrador, and the other bringing lows off the east coast of the United States. The latter track will result in further intensification as the low moves over coastal waters. In the case where the upper level long wave trough lies well west of the region, the main storm track will lie through the Gulf of St. Lawrence or Newfoundland. Under this regime, an east to southeast flow ahead of a warm front associated with a low, will give way to winds from the south in the warm sector of the system. Typically, the periods of southerly winds and mild conditions will be of relatively long duration, and in general, the incidence of extended storm conditions is likely to be relatively infrequent. Strong frictional effects in the stable flow from the south results in a marked shear in the surface boundary layer and relatively lower winds at the sea surface. As a consequence, local wind wave development tends to be inhibited under such conditions. Precipitation types are more likely to be in the form of rain or drizzle, with relatively infrequent periods of continuous snow, although periods of snow showers prevail in the unstable air in the wake of cold fronts associated with the lows. Visibility will be reduced at times in frontal and advection fogs, in snow, and in snow shower activity.

At other times, with the upper long wave trough further to the east, the main storm track may lie through or to the east of the Grand Banks. With the lows passing closer to the site and frequent high potential for storm development, the incidence of strong gale and storm conditions is greater. Longer bouts of cold, west to northwest winds behind cold fronts occur more frequently, and because the flow is colder than the surface water temperatures, the surface layer is unstable. The shear in the boundary layer is lower, resulting in relatively higher wind speeds near the surface and, consequently, relatively higher sea state conditions. With cold air and sea surface temperatures coupled with high winds, the potential for freezing spray will occur quite frequently. In this synoptic situation, a greater incidence of precipitation in the form of snow is likely to occur. Freezing precipitation, either as rain or drizzle, occurs rather infrequently on the Grand Banks. Visibility will be reduced in frontal and advection fogs, and relatively more frequently, by snow.

Frequently, intense low-pressure systems become ‘captured’ and slow down or stall under an upper air low pressure centre as they move through the Newfoundland region or across the Labrador Sea. This may result in an extended period of little change in conditions that may range, depending on the position, overall intensity and size of the system, from the relatively benign to heavy weather conditions. By summer, the main storm tracks have moved further north than in winter so that low-pressure systems are less frequent and much weaker. With increasing solar radiation during the spring, there is a general warming of the atmosphere. This warming is relatively greater at higher latitudes. This decreases the north-south temperature contrast, lowering the kinetic energy of the westerly flow aloft, and decreasing the potential energy available for storm development. At the same time, there is a northward shift of the

main band of westerly winds at upper levels in the atmosphere, and a marked development of the Bermuda-Azores sub-tropical high-pressure area to the south. This warm-core high-pressure cell extends from the surface upwards through the entire troposphere. The main track of the weaker low-pressure systems typically lies through the Labrador region and tends to be oriented from the west-southwest to the east-northeast.

With low pressure systems normally passing to the north of the region in combination with the northwest shoulder of the sub-tropical high to the south, the prevailing flow across Newfoundland and the Grand Banks is from the southwest during the summer season. Wind speeds are lower during the summer and the incidence of gale or storm force winds are relatively infrequent. There is also a corresponding decrease in significant wave heights.

The prevailing southwesterly flow during the late spring and early summer tends to be moist and relatively warmer than the underlying surface waters on the Grand Banks. Cooling of the air from below coupled with mixing in the near-surface layer frequently results in the saturation of the air, the condensation of water vapour, and the development of fog. This type of fog is termed Advection Fog and may persist for days at a time if there is little or no change in the wind direction. The incidence of advection fog and the frequency of poor visibility increases during the spring and are normally highest during July.

On occasion, when an upper level high pressure circulation centre forms and persists over the southern portion of the United States as a westward extension of the sub-tropical high, an upper level trough tends to become established over the east coast region of Canada. While this upper pattern prevails, low pressure systems will tend to develop further south and track through the Grand Banks region.

3.2.2. Tropical Cyclones

Tropical cyclones account for the strongest sustained surface winds observed anywhere on earth. These systems develop in the tropics during the warm season; typically from June through November in the Atlantic Ocean. In some years, tropical cyclones have been known to form as early as April and as late as December.

Conditions off Newfoundland associated with tropical cyclones and their remnants vary widely from relatively minor events to major storms producing windy wet weather and high waves. Figure 3.10 shows the historical track of tropical cyclones which passed within 65 nautical miles of 45.00ºN; 55.83ºW. Table 3.1 gives the statistical data on these hurricanes.

Development and maintaining of these systems require that a number of environmental conditions be met. Once formed, a tropical cyclone will maintain its energy as long as a sufficient supply of warm, moist air is available. Tropical cyclones obtain their energy from the latent heat of vapourization that is released during the condensation process. Since the capacity of the air to hold water vapour is dependent on temperature, as tropical cyclones move north over colder waters, they begin to lose their

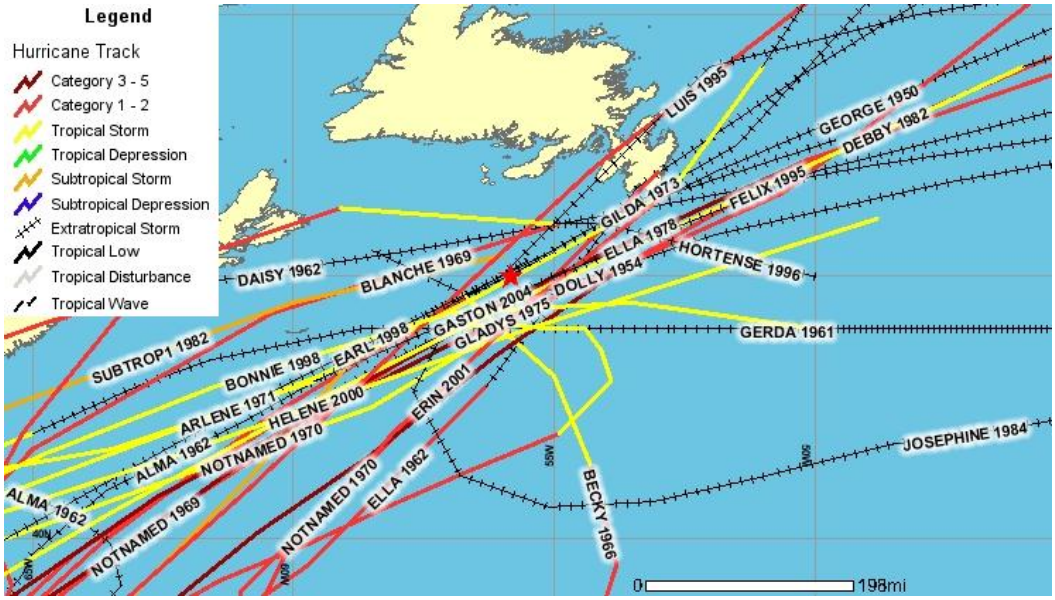

Figure 3.10. Historical Tropical Cyclone Tracks passing within 65nm of Grid Point 5400. 45.00 °N; 55.83 °W 1950 to 2004.

Source: NOAA Coastal Services Center Archive.

Table 3.1. Statistics on Tropical Cyclones passing within 65 nm of Grid Point 5400 at location 45.00ºN, 55.83ºW (1950 to 2004).

Record	Year	Month	Day	Storm Name	Wind Speed (kts)	Pressure (mb)
1	1950	10	5	George	85	N/A
2	1954	9	2	Dolly	70	N/A
3	1961	10	22	Gerda	30	N/A
4	1962	9	2	Alma	15	N/A
5	1962	10	9	Daisy	50	N/A
6	1962	10	22	Ella	60	N/A
7	1966	7	3	Becky	55	N/A
8	1969	8	12	Blanch	65	998
9	1969	9	25	NotNamed	65	N/A
10	1970	8	18	NotNamed	60	992
11	1970	10	17	NotNamed	70	980
12	1971	7	7	Arlene	45	1002
13	1973	10	27	Gilda	55	980
14	1975	10	3	Gladys	85	960
15	1978	9	4	Ella	115	956
16	1982	6	20	SubTrop1	60	984
17	1982	9	18	Debby	100	960
18	1984	10	18	Josephine	50	994
19	1995	8	22	Felix	50	987
20	1995	9	11	Luis	80	965
21	1996	9	15	Hortense	60	982
22	1998	8	30	Bonnie	45	1000
23	1998	9	5	Earl	50	990
24	2000	9	25	Helene	60	986
25	2001	9	14	Erin	65	987
26	2004	9	1	Gaston	45	999

Note: Wind speed refers to the maximum sustained1 minute mean wind recorded during the life of the tropical cyclone and not the wind speed at the time it passed near the Laurentian Sub-basin

Source: NOAA Coastal Services Center Archive.

tropical characteristics, often transforming into vigorous, fast moving extra-tropical cyclones. For this reason, it is rare for a tropical cyclone to maintain hurricane strength over the colder waters of the Laurentian Sub-basin. The greatest risk of occurrence for the Laurentian Sub-basin is during the months of August through October, however the frequency of occurrence in any particular year is low, and varies from none to a few.

3.2.3. Wind Conditions

The AES-40 data set consists of 54 continuous years of hindcast wind and wave data from a project completed by Oceanweather Inc. for the Meteorological Service of Canada. In an effort to provide high quality data for researchers, the National Centers for Environmental Prediction (NCEP) and the National Center for Atmospheric Research (NCAR) reanalyzed all available meteorological data. The winds were first modified by adding measured winds from buoys and platforms. Cyclone wind fields were then generated and added to the background winds. The wind fields were then refined using Oceanweather's Interactive Objective Kinematic Analysis System. The model grid spacing was 0.625º latitude by 0.833º longitude. The model output data represents hourly wind data at a reference height of 10 metres above sea level in six-hour intervals. This is a valuable data set for climate studies because the data is continuous over a long time period.

The AES 40 data set contains climatology data for a number of points in the Laurentian Sub-basin. The Location of Grid Point 5400 in the Laurentian Sub-basin (Figure 3.11) was deemed to be the most representative for this study.

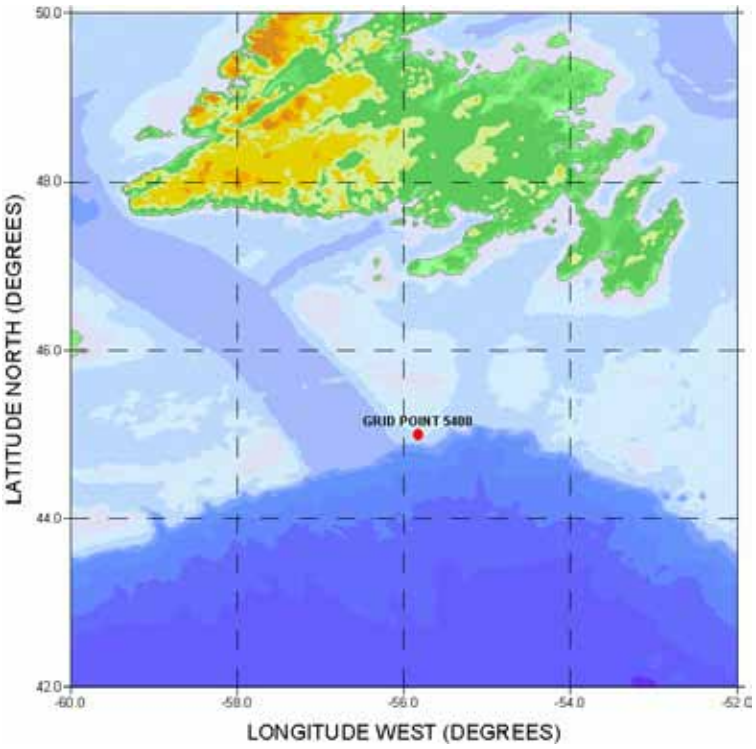

Figure 3.11. The Location of Grid Point 5400 in the Laurentian Sub-basin.

The percentage of observations of wind speed by direction is shown in Table 3.2. Directions are binned in 45-degree intervals centered on the directions shown. The table shows that during the colder months, winds are mainly from the northwest to west. As summer approaches, the predominant wind direction begins to shift such that wind directions for May and June show a mainly southwest to west flow. For the month of July, south to southwest winds are prevalent. As the colder months approach, the predominant wind direction begins to veer, becoming southwest to west in July and August, then west to northwest for the months of October, November and December.

Table 3.2. Percentage of Wind by Direction for AES Grid Point 5400.

	Direction								Total
Month	NE	E	SE	S	SW	W	NW	N	Reports
January	6.3	6.5	7.5	8.6	12.3	28.4	21.1	9.2	6076.0
February	7.4	7.5	7.5	8.8	11.2	25.1	23.2	9.3	5536.0
March	10.4	8.0	8.5	9.0	13.0	21.7	17.9	11.5	6076.0
April	8.2	10.9	9.9	10.7	15.3	19.1	15.2	10.7	5880.0
May	8.1	9.8	9.8	14.0	20.1	17.4	12.2	8.4	6076.0
June	6.7	6.7	8.9	16.3	29.6	17.0	8.7	6.1	5880.0
July	2.7	4.4	7.5	20.6	36.8	17.5	6.6	3.8	6076.0
August	4.5	5.2	7.5	16.1	31.3	20.9	9.3	5.3	6076.0
September	7.4	6.7	8.0	13.6	20.1	19.8	15.0	9.5	5880.0
October	6.8	5.6	9.5	11.5	15.9	22.5	17.3	10.8	6076.0
November	7.1	7.3	8.6	12.6	13.5	22.6	18.3	10.0	5880.0
December	6.6	6.0	8.8	9.6	12.1	27.0	20.3	9.5	6076.0
Years Mean	6.9	7.1	8.5	12.6	19.3	21.6	15.4	8.7	

Table 3.3 shows the highest 10 m winds that occur by month in each of the eight directions. The highest wind of 30 m/sec occurred in January from the northwest, while winds of 29 m/sec occurred in March from the northwest and north. The lowest maximum winds of 19 m/sec are in August; however Table 3.3 shows that gale force winds can occur in any month. Winds are classified as gale force when the wind speeds vary from 17.5 m/sec to less than 24.7 m/sec for 10-minute averaged winds.

Table 3.3. Monthly Highest 10 Metre Wind Speed (in units of m/sec) from each direction at Grid Point 5400.

	Direction								Monthly	
Month	NE	E	SE	S	SW	W	NW	N	Min	Max
January	22	24	22	24	27	25	30	22	22	30
February	24	22	23	23	26	26	24	26	22	26
March	24	26	25	21	27	24	29	29	21	29
April	20	21	24	20	21	23	21	21	20	24
May	19	22	18	19	18	20	19	17	17	22
June	17	16	17	16	20	17	19	19	16	20
July	11	14	14	20	16	14	16	12	11	20
August	19	18	17	17	18	18	17	14	14	19
September	22	19	16	23	21	21	21	18	16	23
October	28	25	23	25	24	23	24	20	20	28
November	22	26	22	21	20	24	24	21	20	26
December	24	23	24	22	24	27	25	24	22	27
Years Max	28	26	25	25	27	27	30	29		

Table 3.4 gives the monthly mean wind speed, standard deviation and maximum wind speeds. Gale force winds occurred in all months while storm force winds only occurred from October to March. Hurricane force winds did not occur at the grid point. Winds are classified as storm force when the wind speed varies from 24.7 m/sec to less than 32.5 m/sec. Winds are hurricane force when they exceed 32.5 m/sec. The data in Table 3.4 are for hourly mean wind speeds. The conversion factor is usually taken as 1.06 to convert from hourly mean values to 10-minute averaged winds.

Table 3.4. Monthly Statistics, Mean Wind Speed (m/sec), Maximum Wind Speed (m/s) and Standard Deviation at Grid Point 5400.

Month	Mean Speed	Standard Deviation	Maximum Speed
January	10.5	4.4	29.8
February	10.3	4.3	26.4
March	9.6	4.3	28.9
April	8.2	3.9	23.5
May	6.6	3.4	21.7
June	6.1	3.0	20.2
July	5.7	2.7	19.5
August	6.1	2.8	18.8
September	7.2	3.3	22.8
October	8.4	3.8	28.0
November	9.4	4.0	26.4
December	10.4	4.3	26.8

Wind roses that show the annual distribution of wind speed and direction for the grid point are plotted in Figure 3.12, and the data presented in the plots is given in Table 3.5. The wind roses for each month together with bivariate histograms are contained in Appendix 1 of Oceans (2006). The wind roses clearly show that the dominant directions are from the northwest, west, southwest and south and that there is a strong annual cycle in the wind direction. West to northwest winds in winter become summer south to southwest winds. In the transition month of April winds are distributed throughout all directions.

The bivariate histograms of the wind speeds versus directions in Oceans (2006) (Appendix 1) show that the wind speeds are much lower in summer than in winter (Appendix 1 *in* Oceans 2006). In general, November, December, and January are the months with the highest occurrence of higher wind speeds. High wind speeds can also occur in late summer and fall due to the passage of tropical systems but the frequency of high winds is lower.

The percentage exceedance of wind speeds at the grid point is shown in Figure 3.13. The percentage exceedance plots for individual months are contained in Appendix 2 of Oceans (2006).

Table 3.5. Percentage of Observations of Wind, Speed and Direction.

		Annual Wind Direction (from)								
		NE	E	SE	S	SW	W	NW	N	Total
Wind Speed (m/s)	0.00 - 4.99	1.82	1.91	2.53	3.57	4.73	4.02	2.63	2.06	23.26
	5.00 - 9.99	2.93	3.10	3.64	5.95	10.48	9.34	6.88	4.21	46.54
	10.00 - 14.99	1.54	1.58	1.75	2.42	3.40	5.98	4.79	2.08	23.53
	15.00 - 19.99	0.45	0.40	0.50	0.60	0.56	1.95	1.08	0.40	5.95
	20.00 - 24.99	0.06	0.05	0.05	0.05	0.06	0.26	0.10	0.04	0.69
	25.00 - 29.99	0.00	0.00	0.00	0.00	0.01	0.01	0.01	0.00	0.03
	Total	6.80	7.04	8.47	12.59	19.24	21.56	15.49	8.79	100.00
							Total	Observations:		6076

Source: AES grid point 5400. Lat 45.00, Long 55.83W, 1954 to 2003.

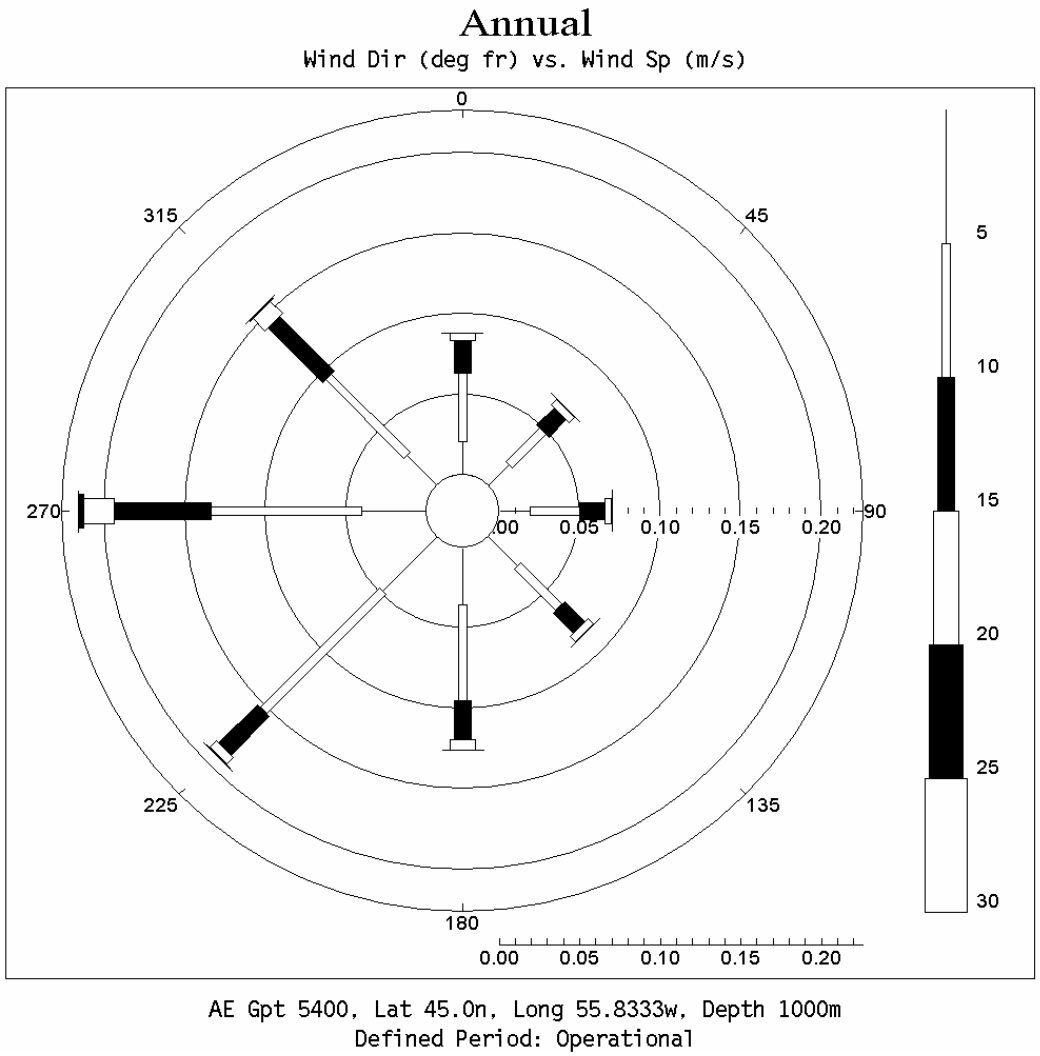

Figure 3.12. Wind Rose showing the Annual Distribution of Wind Speeds and Directions.

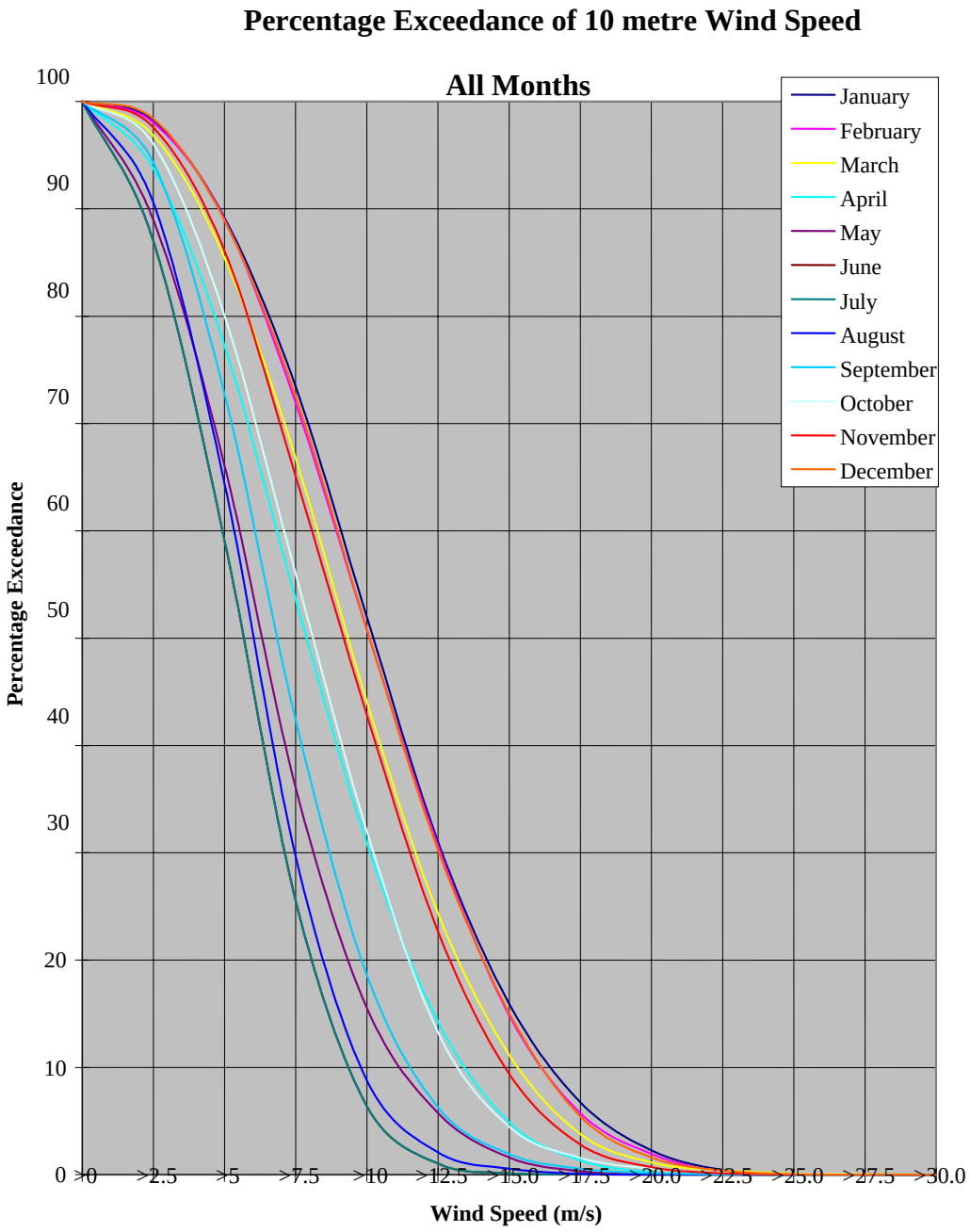

Source: AES grid point 5400. Lat 45.00, Long 55.83W, 1954 to 2003.

Figure 3.13. Percentage Exceedance of 10 m Wind Speed at Grid Point 5400.

3.2.4. Wave Climate

The AES-40 data set was used to generate the wave climate information. Wind data as described in the previous section was inputted into a third generation deep water wave model by Oceansweather Inc. This data set was used for the wave climate analysis.

A grid point is "iced out" when ice coverage is greater than or equal to 50%. The AES-40 hindcast uses mean monthly average ice. Consequently, when ice occurs a grid point gets "iced out" for an entire month at a time. When a point gets "iced out" there is no hindcast wave data for the entire month.

The main parameters for describing wave conditions are the significant wave height, the maximum wave height, the spectral peak period, and the characteristic period. The significant wave height is defined as the average height of the 1/3 highest waves, and its value roughly approximates the characteristic height observed visually. The maximum height is the greatest vertical distance between a wave crest and adjacent trough. The spectral peak period is the period of the waves with the largest energy levels, and the characteristic period is the period of the 1/3 highest waves. The characteristic period is the wave period reported in ship observations, and the spectral period is reported in the AES-40 data set.

A swell is a wave system not produced by the local wind blowing at the time of observation. Swells are created at some distance away and propagate to the vicinity of the observation area. Swell waves travel out of a stormy or windy area and continue on in the direction of the winds that originally formed them as wind waves. The swell may travel for thousands of miles before dying away. As the swell advances, its crest becomes rounded and its surface smooth.

Swell wave energy reaching a point may have been generated within the local weather system, or from within distant weather systems. Therefore, the swell energy may reach a point from more than two directions at a particular time. The former situation typically arises when a front, trough, or ridge crosses the point of concern, resulting in a marked wind shift.

A sea state may be composed of the wind wave alone, swell alone, or the wind wave in combination with one or more swell groups. Standard synoptic marine weather observations allow for the inclusion of a wind wave group and up to two swell groups.

The wave climate of the Laurentian Sub-basin is dominated by extra-tropical storms, primarily during October through March, however severe storms may, on occasion, occur outside these months. Storms of tropical origin may occur during the early summer, but most often between late August through October. Hurricanes are usually reduced to tropical storm strength or evolve into extra-tropical storms by the time they reach the area. However, they are still capable of producing storm force winds and high waves.

Swell energy derived from within the local weather circulation system affecting the Laurentian Sub-basin may arrive from essentially any direction, in accordance with the orientation of the surface

pressure and wind fields. The frequency of occurrence of such swell directions follows, to a large degree, the frequency of occurrence of wind directions at the point of concern. The direction of swell arriving from remote sources is governed by the synoptic climatology of the North Atlantic Ocean. Swell from distant sources is frequently reported to be from the south-southeast through southwest, and from the northeast. Less frequently, a swell generated at a distance reaches the Laurentian Sub-basin from the east to southeast. Also, due to the proximity of the Laurentian Sub-basin to the Island of Newfoundland, any swell coming from 320° to 050° would be short in duration and attributed to local weather systems.

Figure 3.14 shows the annual frequency of occurrence of the vector mean directions (VMD) of the combined significant wave heights, wind wave and swell and Table 3.6 presents a bivariate histogram of the significant wave heights and mean wave directions. The monthly wave roses and frequency of occurrence tables are contained in Appendix 3 of Oceans (2006). The plots show that the vector mean direction of the combined significant wave heights during the late fall and winter is from the west. This corresponds with a higher frequency of occurrence of the wind waves during these months, suggesting that during the late fall and winter, wind waves are the main contributor to the combined significant wave heights. During the months of March and April, wind waves remain predominantly from the west, while the swells are from the south, resulting in the vector mean direction of the combined significant wave heights being from the southwest. A mean southwesterly direction of the combined significant wave heights during the summer months is the result of a predominant southwesterly wind wave and a south to southwest swell. As winter approaches, during the months of September and October, the wind waves will veer to being from the west and become the more dominant component of the combined significant wave heights. This will result in the frequency of occurrence of the combined significant wave heights being higher for waves from a westerly direction.

The monthly maximum, mean and standard deviation of significant wave heights are presented in Table 3.7. The table shows that significant wave heights of 11.0 m or more occurred in each month between October and March, with the highest waves of 13.0 m occurring during the month of January. October had a maximum significant wave height of 12.5 m; however, its mean value was only 2.4 m, compared with 3.5 m in January. This peak in maximum wave heights in October may be attributed to tropical systems moving into the area. Figure 3.15 shows percentage exceedance curves of significant wave heights for each month of the year. During the month of March, the point was iced-out for 2% of the time resulting in no forecast data being generated. Percentage exceedance curves of the significant wave heights for each month of the year are contained in Appendix 4 of Oceans (2006).

The spectral peak period of the waves vary with season. The most common peak period during summer is approximately seven seconds (Table 3.8). In winter, the most common peak period is approximately nine seconds. The percentage occurrence of spectral peak period for each month is shown in Table 3.8 and Figure 3.16. A scatter diagram of the significant wave height versus spectral peak period is presented in Table 3.9.

Table 3.6. Bivariate Histogram of Significant Wave Height and Mean Wave Directions.

		Annual Mean Wave Direction (deg to)																
Significant Wave Height (m)	Sig Wave Ht (m)	22.5	45.0	67.5	90.0	112.5	135.0	157.5	180.0	202.5	225.0	247.5	270.0	292.5	315.0	337.5	360.0	Total
	0.00 - 0.99	0.91	0.66	0.31	0.23	0.15	0.14	0.09	0.08	0.09	0.13	0.17	0.15	0.23	0.26	0.49	0.69	4.76
	1.00 - 1.99	6.81	7.04	3.90	2.37	1.84	1.45	1.03	0.78	0.80	0.88	1.17	1.39	1.74	2.25	3.04	4.79	41.27
	2.00 - 2.99	3.07	3.51	3.12	2.49	2.09	1.41	0.97	0.64	0.62	0.78	0.98	1.15	1.24	1.23	1.69	2.47	27.47
	3.00 - 3.99	1.54	1.53	1.64	1.82	1.39	0.75	0.38	0.31	0.36	0.44	0.49	0.52	0.50	0.54	0.83	1.26	14.30
	4.00 - 4.99	0.72	0.73	0.83	1.04	0.75	0.33	0.13	0.13	0.16	0.23	0.20	0.19	0.23	0.23	0.39	0.57	6.87
	5.00 - 5.99	0.27	0.28	0.44	0.54	0.34	0.11	0.06	0.04	0.08	0.06	0.08	0.08	0.08	0.11	0.18	0.24	3.00
	6.00 - 6.99	0.10	0.12	0.20	0.25	0.12	0.04	0.02	0.01	0.02	0.02	0.03	0.03	0.03	0.03	0.07	0.10	1.18
	7.00 - 7.99	0.05	0.04	0.10	0.12	0.09	0.02	0.01	0.01	0.02	0.02	0.02	0.02	0.01	0.01	0.01	0.04	0.57
	8.00 - 8.99	0.01	0.03	0.05	0.09	0.04	0.01	0.01	0.00	0.00	0.01	0.01	0.00	0.00	0.01	0.01	0.01	0.31
	9.00 - 9.99	0.01	0.00	0.04	0.07	0.02	0.01	0.00	0.00	0.00	0.01	0.00	0.00	0.00	0.00	0.00	0.00	0.17
	10.00 - 10.99	0.00	0.01	0.02	0.03	0.00	0.00	0.00	0.00	0.00	0.00	0.00	0.00	0.00	0.00	0.00	0.00	0.07
	11.00 - 11.99	0.00	0.00	0.01	0.00	0.00	0.00	0.00	0.00	0.00	0.00	0.00	0.00	0.00	0.00	0.00	0.00	0.02
	Total	13.48	13.95	10.67	9.06	6.83	4.28	2.71	2.01	2.14	2.58	3.15	3.53	4.06	4.66	6.70	10.18	100.00

Source: AES grid point 5400. Lat 45.00, Long 55.83W, 1954 to 2003.

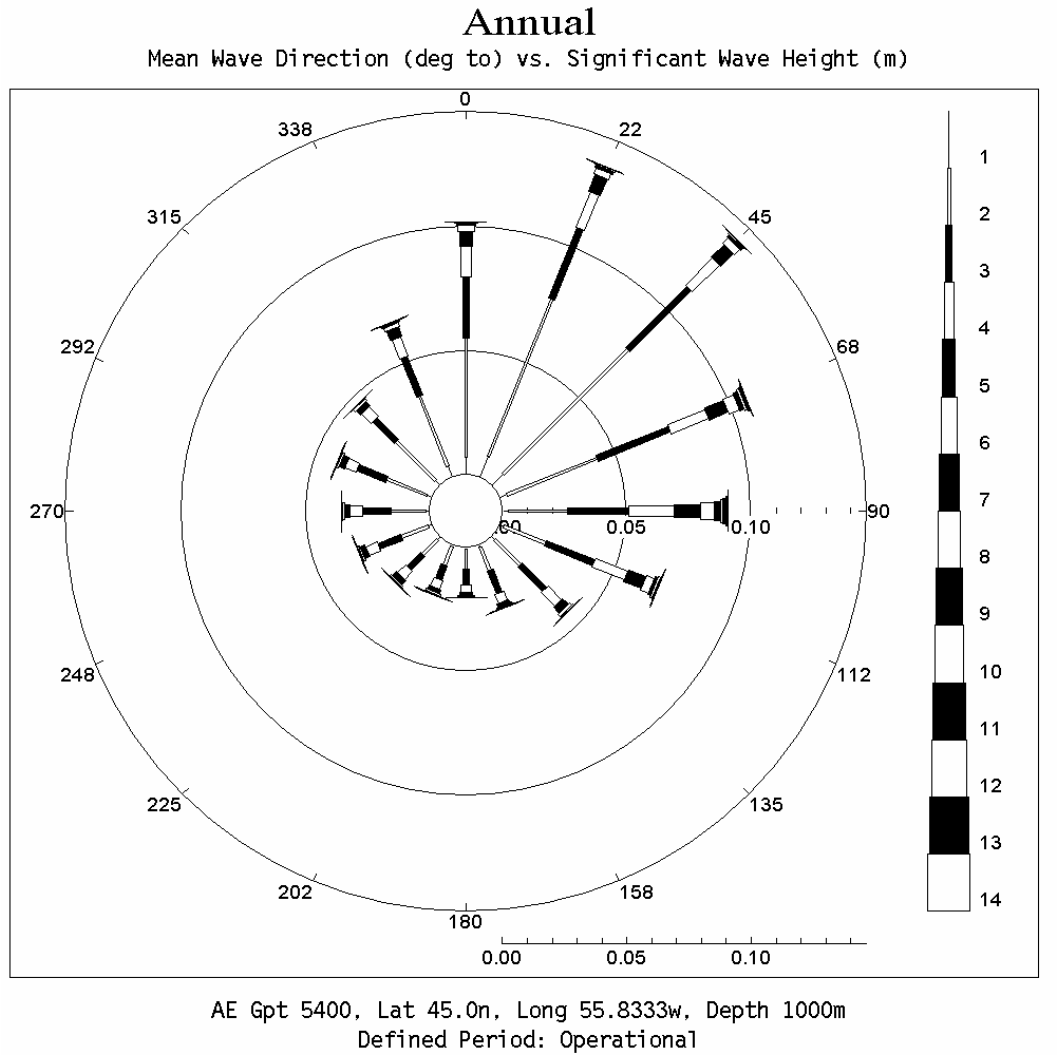

Figure 3.14. Wave Rose Showing the Annual Distribution of Significant Wave Heights and Wave Directions.

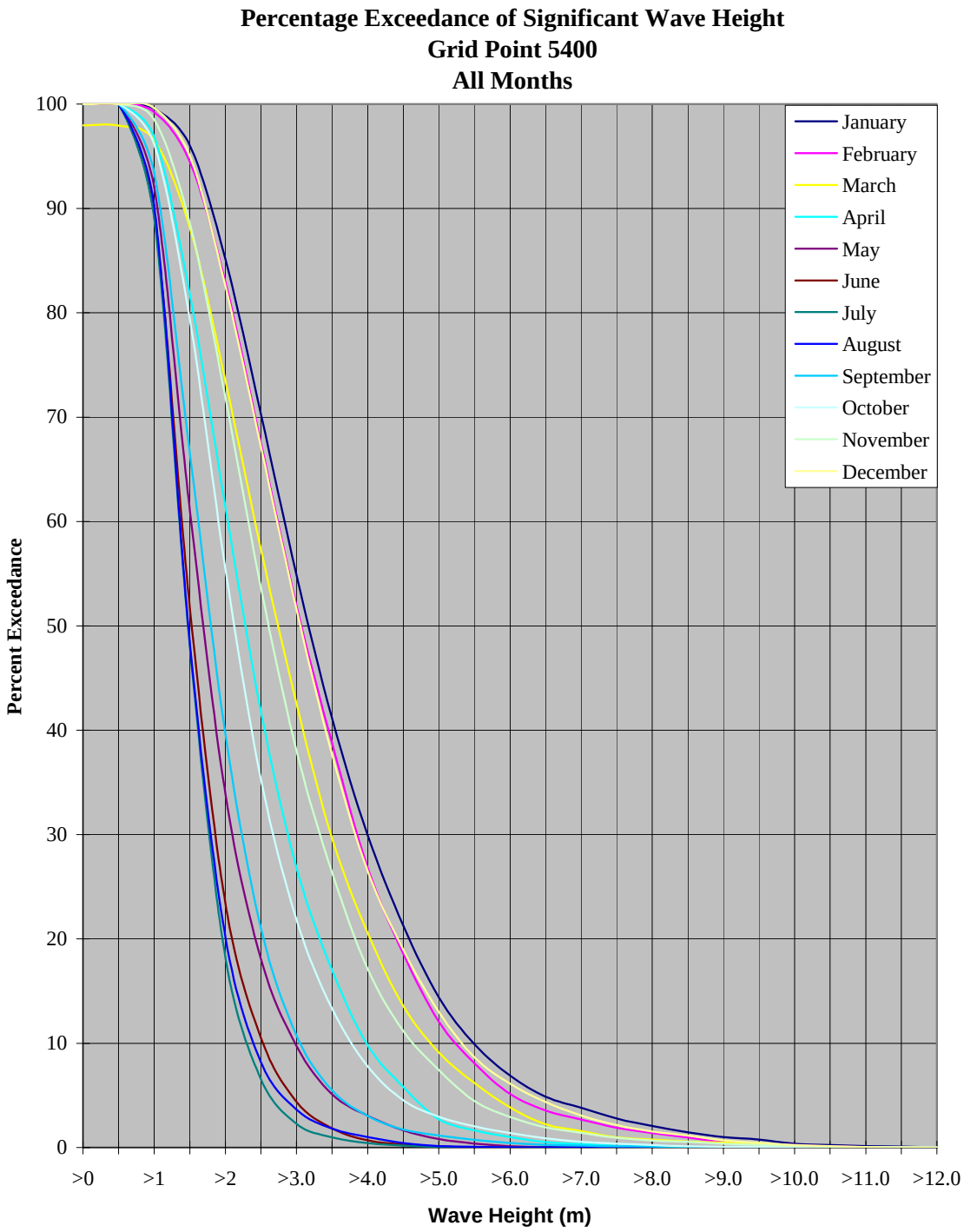

Source: AES grid point 5400. Lat 45.00N, Long 55.83W , 1954 to 2003.

Figure 3.15. Percentage Exceedance of Significant Combined Wave Heights at Grid Point 5400.

Table 3.7. Monthly Maximum, Mean and Standard Deviation of Significant Wave Height at Grid Point 5400.

Month	Mean Height (m)	Maximum Height (m)	Standard Deviation (m)
January	3.5	13.0	1.6
February	3.3	11.4	1.5
March	3.0	11.2	1.5
April	2.5	9.3	1.1
May	1.9	8.7	0.9
June	1.7	5.5	0.7
July	1.6	5.4	0.6
August	1.6	7.0	0.6
September	2.0	9.0	0.9
October	2.4	12.5	1.1
November	2.9	11.0	1.4
December	3.4	11.5	1.5

Table 3.8. Percentage Occurrence of Peak Spectral of the Total Spectrum at Grid Point 5400.

	Peak Spectral Period (seconds)															
Month	1	2	3	4	5	6	7	8	9	10	11	12	13	14	15	16
January	0.0	0.0	0.0	0.2	1.7	5.0	12.4	14.4	16.7	**16.6**	14.7	10.5	5.8	1.6	0.4	0.0
February	0.0	0.0	0.0	0.2	2.3	6.6	13.1	15.0	**16.9**	16.7	13.8	7.9	5.1	2.0	0.3	0.2
March	0.0	0.0	0.0	0.5	2.8	7.7	14.1	13.3	16.8	**18.5**	12.5	7.3	4.4	1.5	0.4	0.1
April	0.0	0.0	0.0	0.8	3.9	9.5	17.2	18.0	**18.8**	16.1	9.3	4.5	1.3	0.5	0.1	0.0
May	0.0	0.0	0.0	0.9	6.8	12.1	23.0	**23.8**	17.3	9.0	4.2	1.9	0.4	0.3	0.1	0.1
June	0.0	0.0	0.0	0.9	6.9	16.3	**30.1**	22.0	13.3	5.4	1.8	1.1	1.1	0.8	0.3	0.0
July	0.0	0.0	0.0	0.8	6.2	16.9	**32.9**	22.6	12.2	4.6	1.5	0.9	0.8	0.3	0.2	0.3
August	0.0	0.0	0.0	0.7	7.9	20.7	**32.9**	16.6	9.3	3.9	3.7	2.1	1.2	0.7	0.2	0.1
September	0.0	0.0	0.0	0.8	6.6	16.2	**24.5**	17.1	13.0	8.0	5.3	3.8	2.9	1.2	0.3	0.1
October	0.0	0.0	0.0	0.7	5.5	11.5	**23.6**	20.8	16.3	10.2	5.9	3.3	1.4	0.6	0.1	0.1
November	0.0	0.0	0.0	0.4	3.3	8.5	16.5	17.8	**20.0**	16.8	9.4	4.1	2.1	1.1	0.2	0.0
December	0.0	0.0	0.0	0.3	1.8	5.7	12.8	15.1	**19.1**	17.5	12.8	8.4	4.5	1.6	0.2	0.1

Figures highlighted in bold are the highest monthly percentage.

Source: AES grid point 5400. Lat 45.00º, Long 55.83ºW, 1954 to 2003.

.

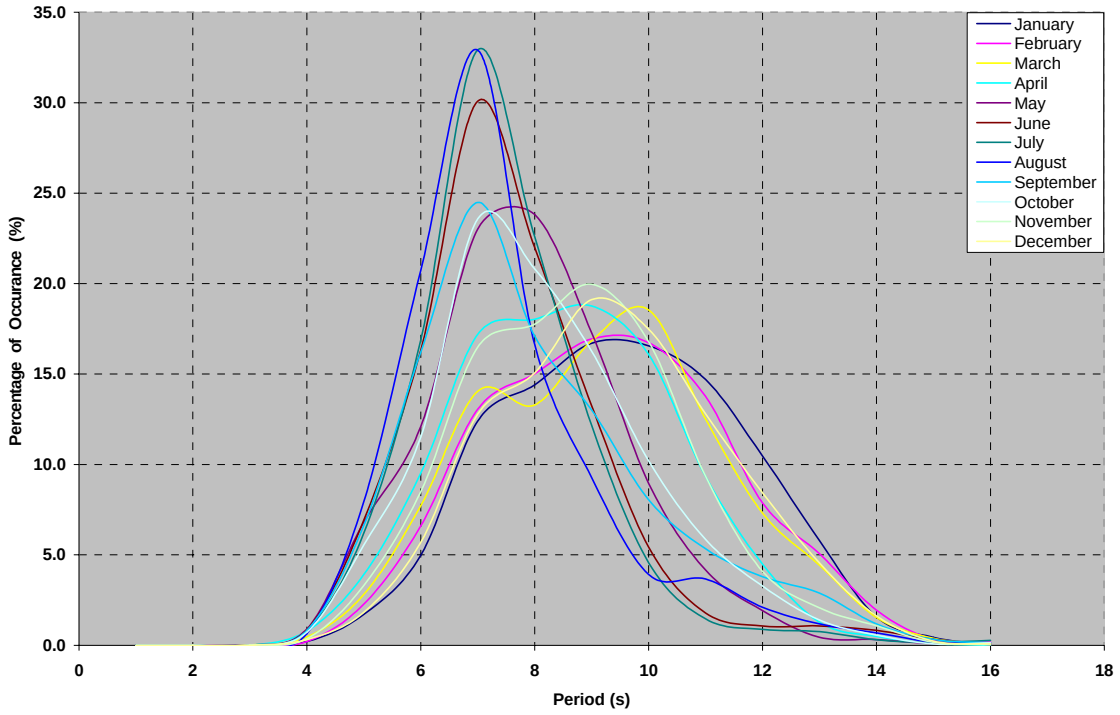

Figure 3.16. Percentage of Occurrence of Peak Wave Periods for each Month at Grid Point 5400.

Table 3.9. Percent Frequency of Occurrence of Significant Combined Wave Height and Peak Spectral Period at Grid Point 5400.

	Wave Height (m)												
	1	2	3	4	5	6	7	8	9	10	11	12	13
0													
1													
2													
3	0.004												
4	0.514	0.082											
5	3.171	1.443	0.042										
6	4.646	6.363	0.393	0.007									
7	7.278	9.668	4.020	0.131	0.003								
8	4.305	6.849	5.189	1.616	0.066	0.001							
9	2.185	5.771	3.621	3.347	0.786	0.036							
10	1.094	3.390	2.921	2.164	1.838	0.437	0.025	0.003					
11	0.731	1.576	2.127	1.326	0.941	0.803	0.284	0.054	0.003				
12	0.464	0.827	0.943	0.940	0.532	0.332	0.275	0.212	0.084	0.008			
13	0.332	0.490	0.360	0.387	0.337	0.226	0.119	0.075	0.115	0.102	0.013		
14	0.154	0.236	0.135	0.112	0.122	0.101	0.050	0.024	0.018	0.021	0.029	0.008	
15	0.054	0.078	0.041	0.015	0.011	0.011	0.017	0.006			0.003	0.001	
16	0.052	0.028	0.018			0.003	0.003						
17	0.015	0.008	0.003										
18	0.003	0.003											
19													
20													

Source: AES grid point 5400. Lat 45.00º, Long 55.83ºW, 1954 to 2003.

3.2.5. Interannual Variability and Short Term Climate Trends

Changes in weather conditions over the Laurentian Sub-basin vary from short-term, to seasonally, to longer time scales. Short-term changes are a consequence of the passage of synoptic scale weather systems (e.g., lows, highs, troughs, and ridges), whereas seasonal and long-term changes are due to larger planetary-scale features.

The north-south temperature gradient, which changes seasonally, affects the upper level circulation pattern usually resulting in more intense winter systems than one would expect to see in the summer (Figure 3.17). A time-series of seasonally averaged mean wind speeds and wave heights show that wind speeds and wave heights are higher during the winter months, and the seasonal variability is also greater during the winter due to the more intense weather systems.

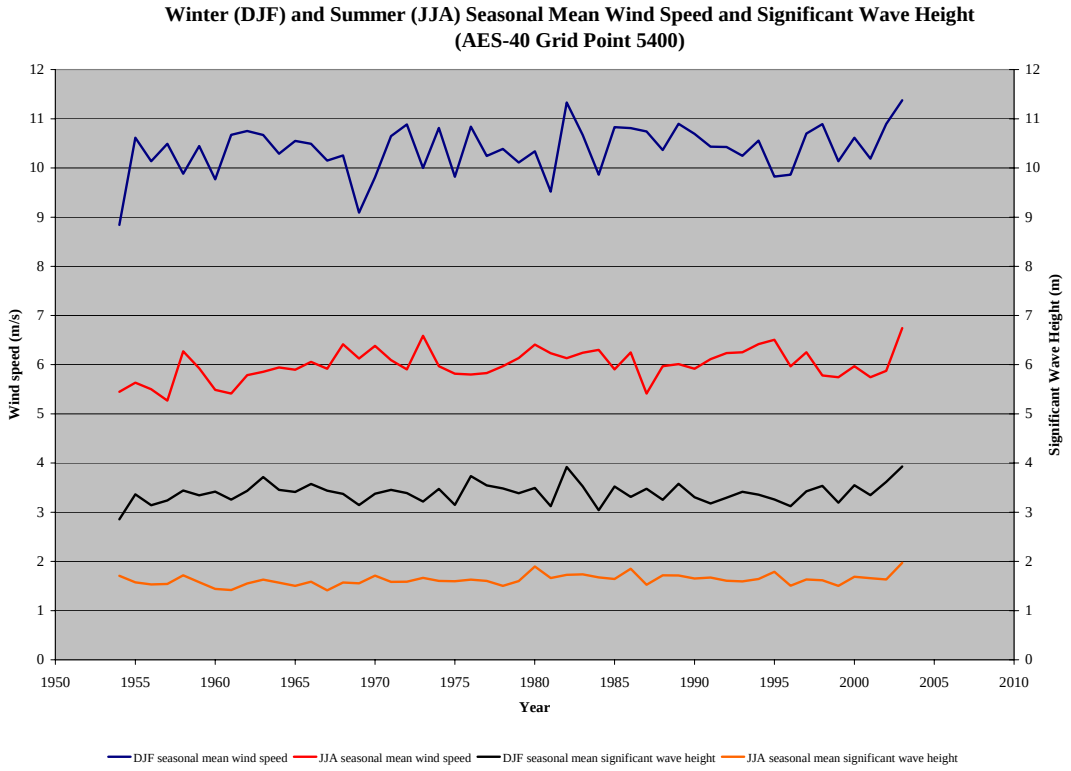

Figure 3.17. Winter and Summer Seasonal Variability of Mean Wind Speed and Mean Significant Wave Height at AES-40 Grid Point 5400.

The AES-40 hindcast dataset is of sufficient length to carry out investigations of short-term wind and wave climate variability studies over the North Atlantic Basin (e.g., Wang and Swail 2002) but validations must be made to ensure that the hindcast results accurately reflect true climatic conditions. Swail et al. (2003) investigated several wind statistic trends for the Sable Island area using two hindcast datasets (including AES-40), measured wind data, and pressure field computed wind data. The results

show trends varying from slowly decreasing, to no change, and to slowly increasing with time over the 40-year period. The authors suggest that wind and wave hindcast datasets may be affected by a "creeping inhomogeneity" as a consequence of the increased data density and increasing anemometer heights on board ships with time, but that the AES-40 hindcast 'should be a truer indication of the more tangible creeping inhomogeneties in the reanalysis process', … They conclude that 'trends are generally consistent with the analysis measurements from weather ships, transient ships, and …', and suggest that 'hindcasts may provide a good upper bound to true trends in the wind and wave climate'.

The North Atlantic Oscillation (NAO) is one of the most important indicators of the climate of the North Atlantic Ocean. It is characterized by an area of relatively low pressure near Iceland, and a Sub-tropical high near the Azores. The NAO Index is a measure of the difference of normalized sea-level pressure between these two features and serves as a means to determine the marine climate variability over the North Atlantic Ocean. A positive NAO Index is the result of a stronger than normal subtropical high and a deeper than normal Icelandic low, which brings stronger winds and colder temperatures over the Northwest Atlantic. Conversely, a weak subtropical high and a weak Icelandic low will give a negative NAO Index, resulting in weaker storms following a more west-east trajectory.

Figure 3.18 and Figure 3.19 shows the seasonally averaged NAO Index for the summer and winter months respectively, along with their associated trend lines for the period of 1954-2004. In the summer the trend is seen to have had a positive slope at the beginning of the period, and a negative slope towards the end of the period, indicating that the strength of the Azores High and the Icelandic Low is currently weakening. This weakening trend also corresponds with a slight weakening of wind speeds during the summer over the Laurentian Sub-basin towards the latter part of the period (Figure 3.17), as would be expected from the weaker pressure between the two features. Significant wave heights in Figure 3.17 show a continuous positive trend throughout the period of 1954-2004, which would seem to contradict the negative trend in wind speeds during the latter part of the period. The continuous positive trend however may be due to increased swells arising from another point; however, this is not investigated here.

Larger variability is evident in the winter NAO Index data and the trend is positive throughout the period, with some leveling off towards the latter years. This positive trend would indicate a strengthening of the Icelandic Low and Azores High, resulting in an increasing pressure gradient, and consequently an increase in wind speeds, as indicated by the positive trend of the winter wind speeds in Figure 3.17.

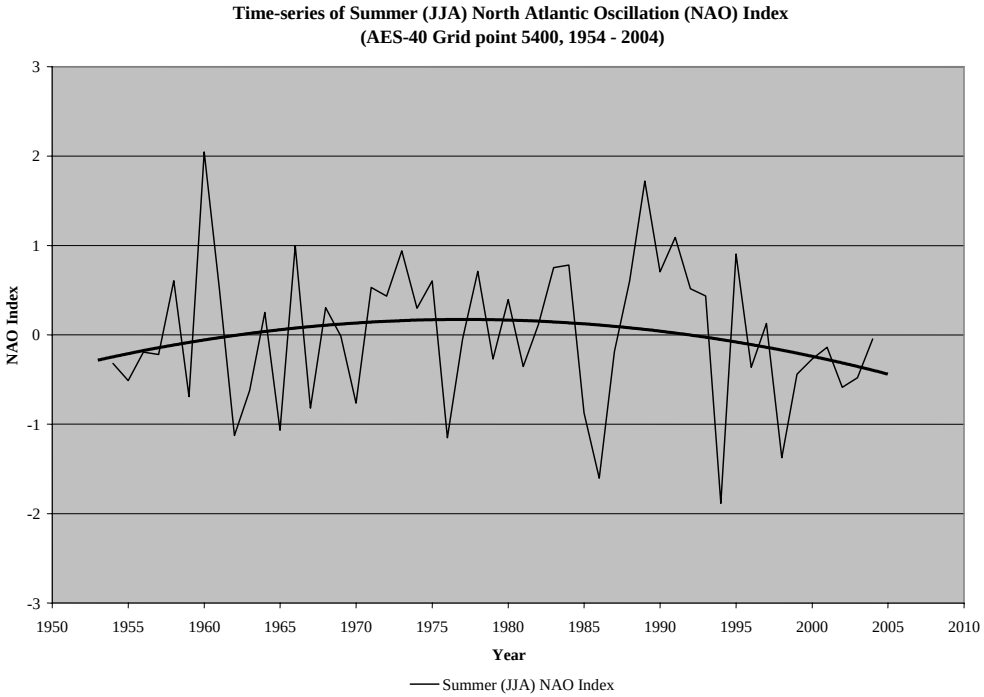

Figure 3.18. Average Summer NAO Index.

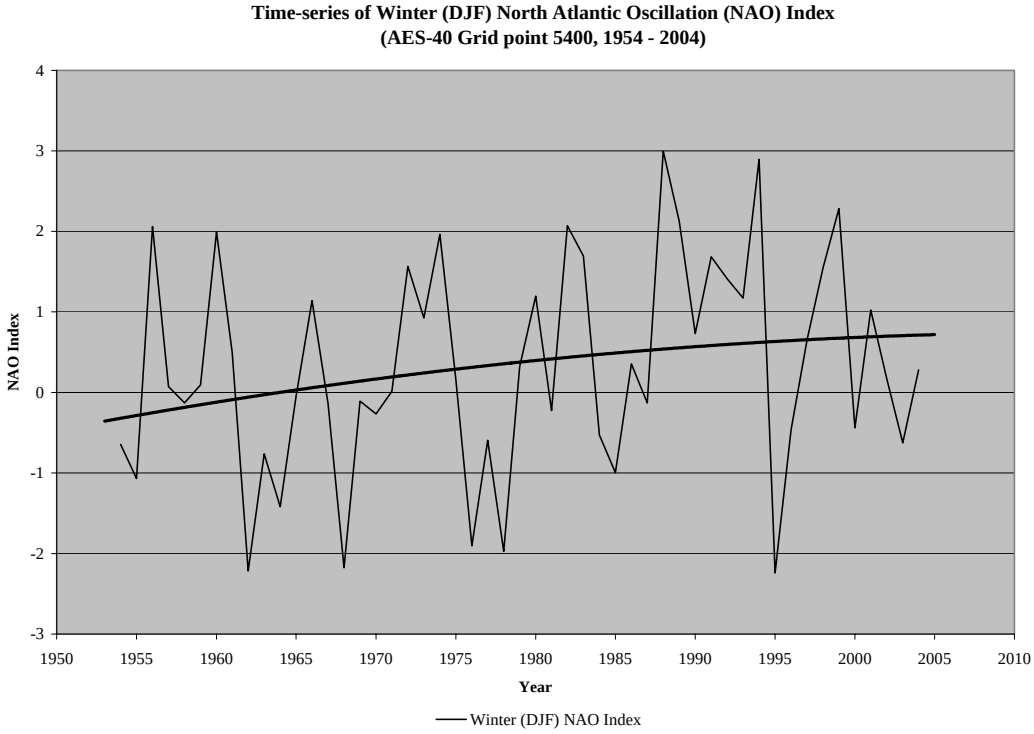

Figure 3.19. Average Winter NAO Index.

3.2.6. Air and Sea Surface Temperatures

The moderating influence of the ocean serves to limit both the diurnal and the annual temperature variation in the Laurentian Sub-basin, in common with all marine locations. Diurnal temperature variations due to the day/night cycles are very small. Short-term, random temperature changes are due mainly to a change of air mass following a warm or cold frontal passage. In general, air mass temperature contrasts across frontal zones are greater during the winter than during the summer season.

Air and sea surface temperatures for the area were extracted from the COADS ship and rig marine synoptic observations for years 1954 through 2003 for the area 44.0N to 46.0N and 55.0W to 57.0W. Temperature statistics presented in Table 3.10 show that the atmosphere is coldest in February with a mean temperature of –0.4°C, and warmest in August with a mean temperature of 16.8°C. The sea surface temperature is warmest in August with a mean temperature of 15.8°C and coldest in March with a mean temperature of 1.3°C. Figure 3.20 shows that the mean sea surface temperature is 0 - 2°C colder than the mean air temperature from April to September, and 0 - 2°C warmer than the mean air temperature from October to March. Bivariate histograms of the number of observations in specific degree intervals during each month are presented in Tables 3.11 and 3.12 for air and sea surface temperatures, respectively. These tables clearly show that there are more observations during August, September and October than any other month for both air and sea temperatures. The least number of air and sea surface temperatures are in January. Statistics were calculated on a monthly basis to avoid the bias that would be created by calculating overall statistics from a varying number of observations.

Table 3.10. Monthly Air and Sea Surface Temperature Means and Standard Deviations.

	Air Temperature			Sea Temperature		
Month	Mean	Standard Deviation	Total Observations	Mean	Standard Deviation	Total Observations
January	0.7	4	2587	2.9	2.9	2150
February	-0.4	4.3	3108	1.6	2.5	2765
March	0.6	3.6	3607	1.3	2.7	3248
April	2.9	3.1	2975	2.4	2.6	2624
May	5.6	2.9	3232	4.3	2.6	2961
June	9.6	3.1	3238	7.9	2.7	3168
July	14.5	3	3482	12.9	3	3095
August	16.8	2.9	4163	15.8	2.5	3916
September	14.8	2.8	4165	14.7	2.5	3725
October	10.7	3.2	4125	11.3	2.7	3606
November	7	3.5	3226	8.1	2.6	2857
December	3.3	3.8	3115	5.4	2.7	2707

Source: COADS Data for 44.0N to 46.0N; 55.0W to 57.0W (1954-2003)

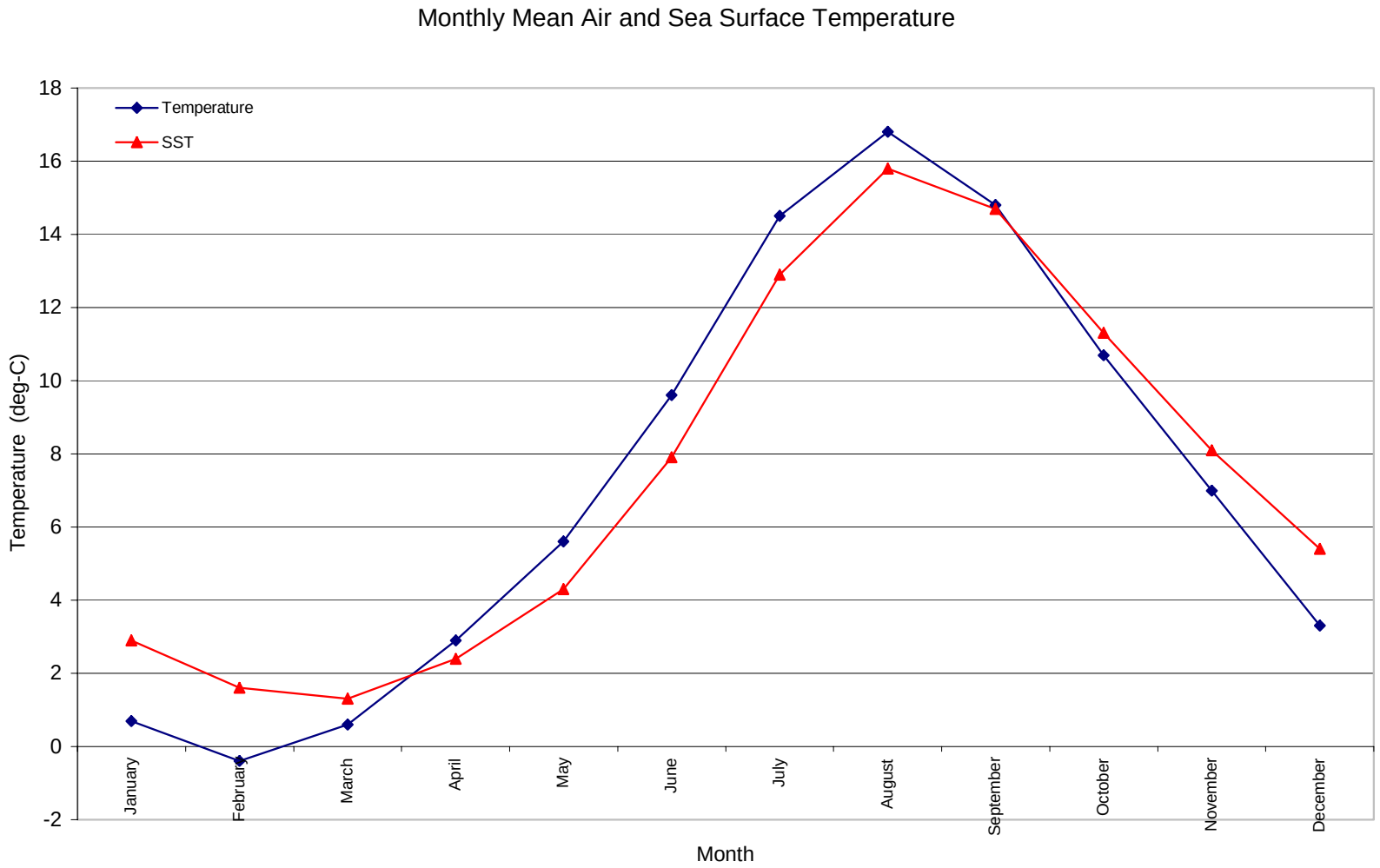

Figure 3.20. Monthly Mean Air and Sea Surface Temperature.

Table 3.11. Bivariate Histogram of the Number of Observation of Air Temperatures in Specific Centrigrade Degree Intervals by Month.

	Jan	Feb	Mar	Apr	May	Jun	Jul	Aug	Sep	Oct	Nov	Dec
-13		1										
-12		5										
-11	1	3										
-10	1	15	2									
-9	4	10	8									
-8	11	20	12									2
-7	21	57	20									1
-6	43	78	44									7
-5	46	112	67									14
-4	96	151	83	11								35
-3	119	200	137	6	1						1	44
-2	160	256	195	14	1						2	71
-1	214	292	274	44	3						7	120
0	251	331	364	120	2						9	164
1	240	365	430	259	26						32	212
2	334	362	603	415	103	2				6	54	296
3	330	307	485	558	200	3				13	118	343
4	269	206	368	505	405	12				33	196	403
5	156	135	246	393	517	54				37	327	350
6	140	109	153	271	536	119	2			108	370	310
7	95	77	102	188	501	237	6		4	152	416	258
8	47	42	66	132	379	371	5		9	253	419	161
9	39	34	37	68	275	431	14	2	25	359	380	167
10	20	9	15	39	173	456	54	3	50	477	337	99
11	13	14	11	15	107	444	117	18	90	482	208	89
12	9	10		12	57	371	232	33	186	541	185	50
13					41	308	345	79	376	502	120	25
14					28	176	460	176	515	430	70	8
15						109	530	317	627	308	48	
16						81	495	503	620	195	20	
17						45	415	673	570	138	15	
18						22	338	712	465	61		
19							187	585	293	29		
20							114	474	187	20		
21							74	266	66			
22							33	156	36			
23							22	77	17			
24								24				
25								26				

Table 3.12. Bivariate Histogram of the Number of Observations of Sea Surface Temperature in Specific Centigrade Degree Intervals by Month.

	Jan	Feb	Mar	Apr	May	Jun	Jul	Aug	Sep	Oct	Nov	Dec
-5		1	1									
-4												
-3	1	3	6									
-2	17	67	179	18	1							4
-1	62	285	541	100	9							5
0	193	570	588	362	63	10						29
1	374	624	684	581	227	7					15	71
2	470	526	505	524	400	19					17	199
3	337	273	269	418	498	48					42	319
4	273	162	205	245	544	144	2			8	96	457
5	149	93	104	121	398	270	5			11	170	356
6	123	61	52	111	351	490	13			41	306	372
7	53	34	40	58	182	503	43			100	456	320
8	32	15	10	28	124	507	100		10	276	566	256
9	19	14	14	14	64	373	144	9	34	382	416	115
10	12			8	45	296	248	95	53	507	279	95
11	4				9	212	347	52	129	562	208	61
12					18	118	443	118	249	587	172	21
13						63	443	222	471	443	49	11
14						55	435	473	650	326	17	
15						15	254	582	584	134	14	
16						19	278	830	690	89		
17							186	663	459	56		
18							75	425	233	34		
19							20	222	58	11		
20							9	118	40			
21							9	37	10			
22								22	11			
23								12				

3.2.7. Precipitation

The migratory high and low pressure systems transiting the temperate middle latitude of the Northern Hemisphere cause a variety of precipitation types to occur in the Laurentian Sub-basin. According to the COADS's ship observations, the occurrence of precipitation is lowest in July (3.6 percent) and highest in February (13.7 percent). Figure 3.21 shows the precipitation types for each month and the percentage occurrence of each type. The precipitation types during the summer season are largely limited to rain and drizzle with some reports of hail in June and August, and a few reports of freezing precipitation and snow in June. Reports of hail occurred in every month, with the exception of May and July as shown by the COADS observations. Rainfall is most likely to occur in autumn, with moderate to heavy rainfall occurring most frequently in September and October. The months with the most precipitation are January and February. The months with the most snow are December, January,

February and March. Snow is likely to occur any time between September and June, ranging form 0.05 percent in June to 9.4 percent in February. Freezing precipitation, either freezing rain or freezing drizzle is most likely to occur in February and March with a reported percent occurrence of approximately 0.16 percent for each month.

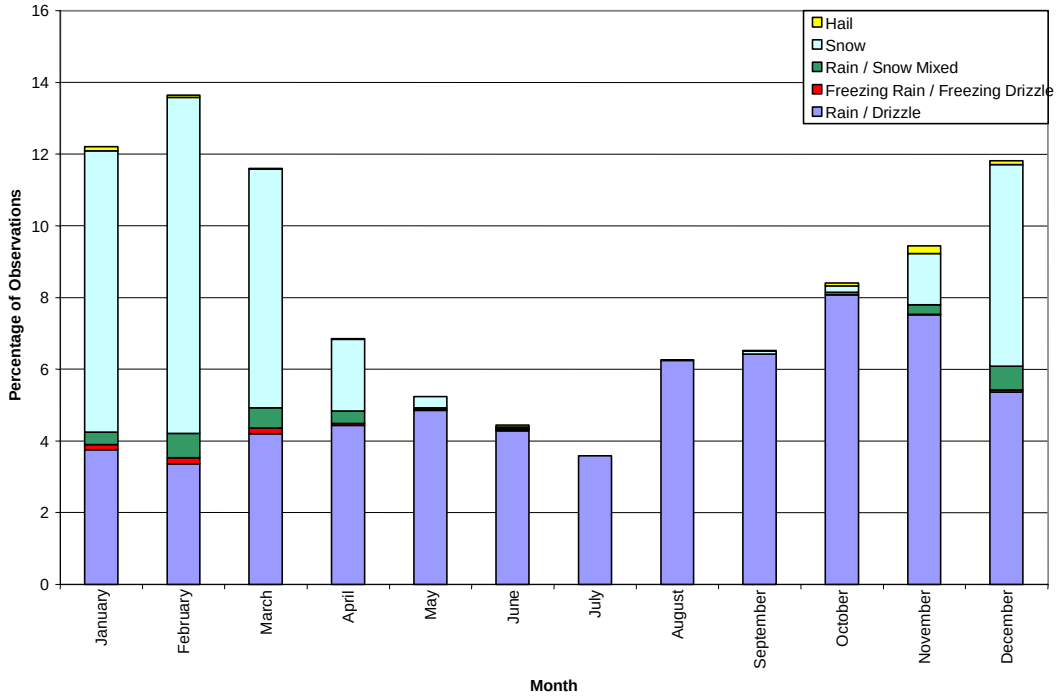

Figure 3.21. Percentage Occurrence of Precipitation Types.
Source: COADS Data for 44.0ºN to 46.0ºN; 55.0ºW to 57.0ºW (1954-2003).

3.2.8. Visibility

Reduction in visibility can be attributed to the occurrence of snow or mist/fog. As can be seen from Figure 3.21 rain and drizzle may occur within the Laurentian Sub-basin in any month and typically accompanying these rain/drizzle events is a reduction in visibility due to mist/fog. During the winter months, while some of the reduction in visibility may be attributed to mist/fog, snow tends to cause the greatest occurrence in reduction of visibility. In April as the snow tends to turn to rain the reduced visibilities will become the result of advection fog. Advection fog forms when warm moist air moves over the cooler waters of the Laurentian Sub-basin. The air is cooled from below and becomes saturated resulting in fog forming. Figure 3.21 shows that in April the mean air temperature rises above the mean sea surface temperature. Advection fog increases during May, June and July (Figure 3.22). In August the temperature difference between the air and the sea begins to narrow and by September, the air temperature falls below the sea surface temperature. As the air temperature drops, the occurrence of fog decreases. Reduction in visibility during autumn and winter is relatively low and is mainly attributed to the passage of low-pressure systems, with mist/fog mainly being the attributed to the poor visibility in

autumn and snow mainly being attributed to poor visibility in the winter. September has the lowest occurrence of visibility less than five nautical miles since air temperature has, on average, decreased below the sea surface temperature and the winter snow has yet to arrive.

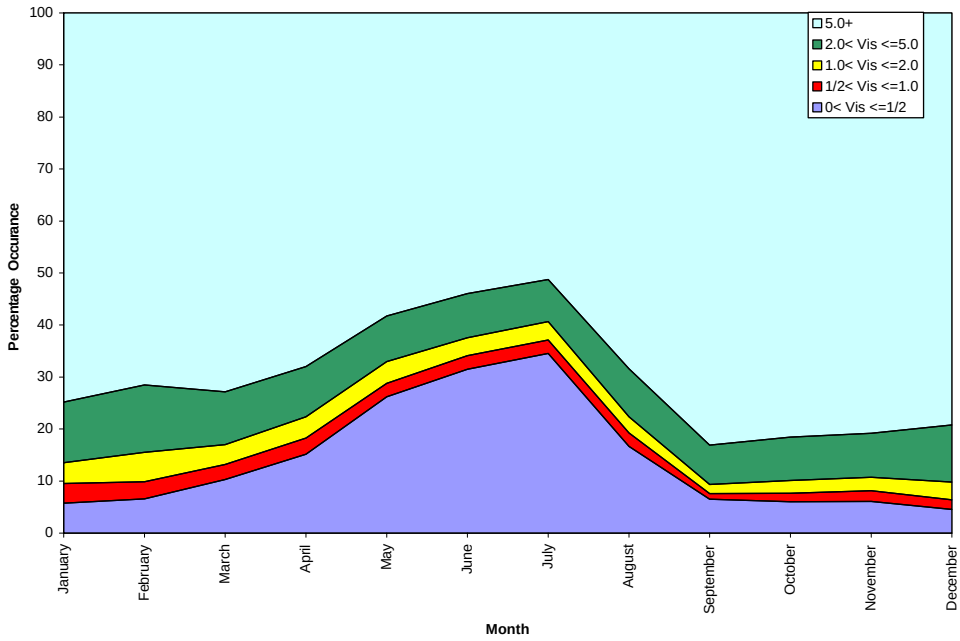

Figure 3.22. Percentage Occurrence of Visibility for each Month near Grid Point 5400.
Source: COADS Data for 44.0ºN to 46.0ºN; 55.0ºW to 57.0ºW (1954-2003).

3.3. Water Properties

Temperature and salinity data from historical measurements were extracted from the Bedford Institute of Oceanography (BIO) archive. This archive in addition to BIO and Department of Fisheries and Oceans (DFO) data also contains data collected by Marine Environmental Data Service (MEDS) in Ottawa, the National Oceanographic Data Center (NODC) in Washington, and from universities, consulting firms, and other groups. The geographic limits for the database are from 35 °N to 90 °N and 40 °W to 90°W (Petrie et al. 1999), thus incorporating the region for this study. The geographic limits used for this study are 43.5°N to 46.5°N, and 58°W to 54°W (Figure 3.23). There is considerable temperature and salinity data available for the Study Area. The data were divided into different depth ranges from 5 to 100 m in steps of 10 $\pm$5 m, from 125 to 500 m in steps of 50 $\pm$25 m, and from 600 to 3,500 m in steps of 100 $\pm$25 m. Since the Study Area has complex bathometry regions that may have different water properties in different areas, the data were also split into three regions; the Shelf with a maximum depth of 200 m, the Laurentian Channel with a maximum depth of 500 m, and the Slope with a depth of 500 m to 3,500 m. The southwestern Newfoundland Shelf includes the St. Pierre and Green Banks. The Laurentian Channel divides the Scotian and Newfoundland shelf. The Slope which incorporates the Laurentian Fan begins at the edge of the Channel marked by the 500 m bathymetry contour and extends into deep water. The monthly statistics are contained in Appendix 5 of Oceans (2006) for depths 0, 25,

55, 125, 175, 225, 475, 800, 1,000, 2,000 and 3,000. The locations of the data collection and histograms of the data distribution according to month and depth are also shown in Appendix 5 of Oceans (2006). Monthly contour and line plots of temperature and salinity by depth are shown in Figure 3.24 to Figure 3.29, T-S diagrams in Figure 3.31 to Figure 3.35, and seasonal T-S diagrams in Figure 3.38 to Figure 3.40.

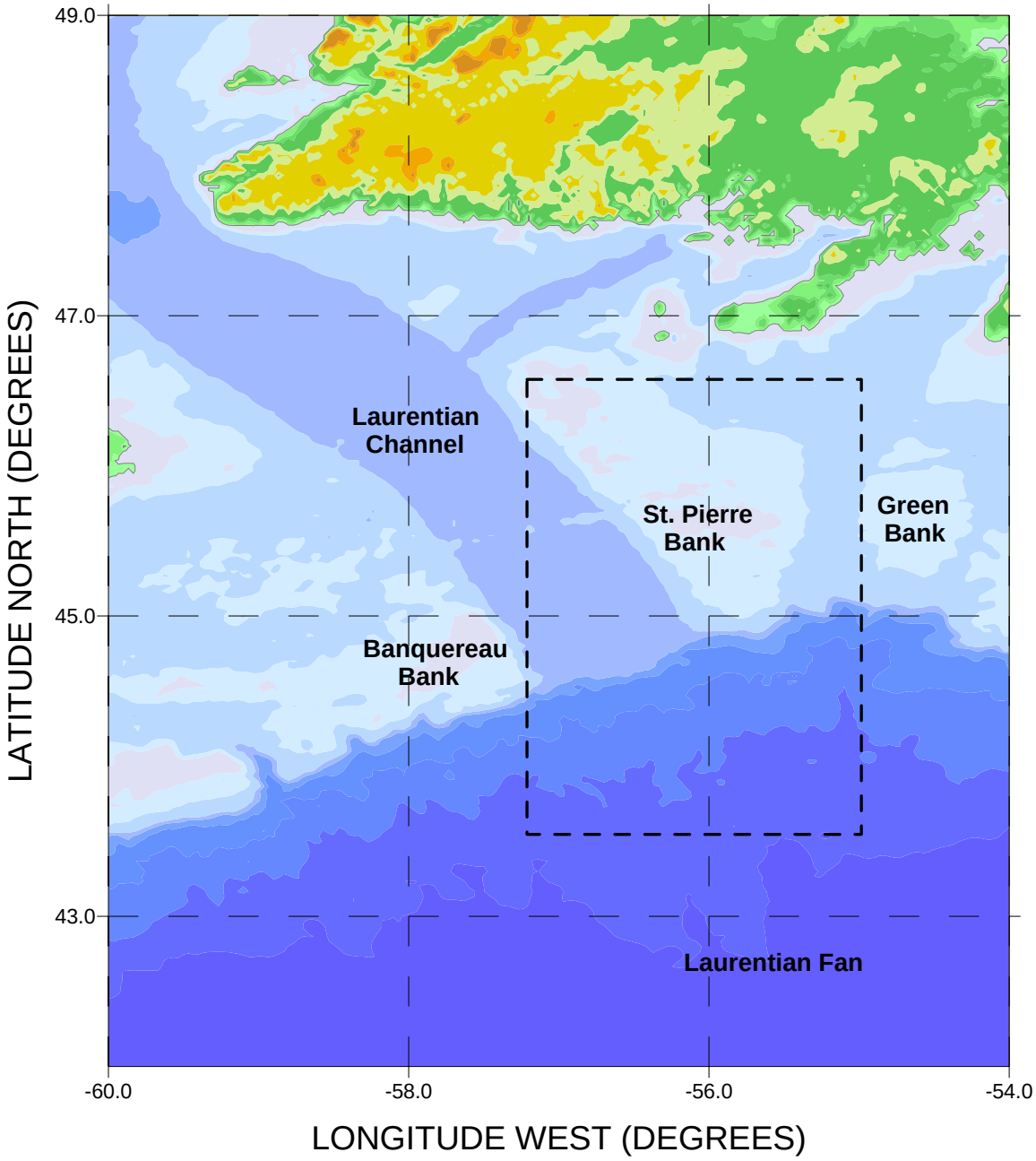

Figure 3.23. Location of Study Region.

3.3.1. Newfoundland Shelf Region

The waters on the southwestern Newfoundland Shelf are mixed waters from different sources and show some seasonal changes. From May to December the water structure has three layers, a warm surface stratified layer (in summer) overlaying a colder intermediate layer, below which is a warmer, saltier layer. The stratified surface layer extends to a depth of about 50 m with monthly mean surface temperatures and salinities ranging from 15.53ºC to -0.51°C and 31.47 ‰ to 32.29 ‰, respectively. In winter, with colder air temperatures and intense wave action the surface layer mixes and deepens to the level of the bottom of the intermediate cold layer such that the water column becomes almost uniform with little stratification. The cold layer has a temperature ranging from just below 0ºC to just above 2ºC (Figure 3.24). Between 150 and 200 m, the water is slightly warmer and more saline (Figure 3.25) which indicates that the bottom water originates from the warmer, more saline waters of the Channel and Continental Slope.

The range of temperatures and salinities with depth are given in Appendix 5 of Oceans (2006). The surface temperature is highly variable and ranges from –1.27ºC in winter to 19.16ºC in August. The monthly mean surface temperature varies from 15.53ºC in August to -0.51ºC in February. At 25 m, the highest monthly mean temperature is 8.54°C in October and the coldest mean temperature is -0.27°C in February. The warmer temperatures in October indicate seasonal mixing. The mean temperature range at 55 m is from -0.45ºC in February to 1.70ºC in November. Below the mixed layer at 125 m, the monthly mean temperature ranges from -1.05°C in October to 1.31°C in June.

The monthly mean salinity increases with depth from a minimum surface value of 31.5 ‰ to 34.0 ‰ at 175 m. The surface salinity ranges from 30.0 ‰ to 33.2 ‰. At 25 m, the mean monthly salinity ranges between 31.6 ‰ in October, during the time of surface mixing and breakdown of the thermocline to 32.4 ‰ in May. Below the mixed layer at 125 m, the monthly mean salinity ranges between 32.6 ‰ in May to 33.1 ‰ in August.

3.3.2. Laurentian Channel

The waters of the Laurentian Channel are mixed waters from different sources. Similar to the waters on the Shelf, seasonal variations (Lauzier and Trites 1957; Lauzier 1958) are also present. In spring, summer and fall there is a four layer structure; a warm low salinity stratified surface layer, an intermediate cold water layer, a warm stratified higher salinity layer, and a deep high salinity warm layer. The top three layers resemble those of the Shelf in depth, seasonal cycle and water properties. The monthly mean temperature data shows a distinct upper stratified layer to about 50 m and an

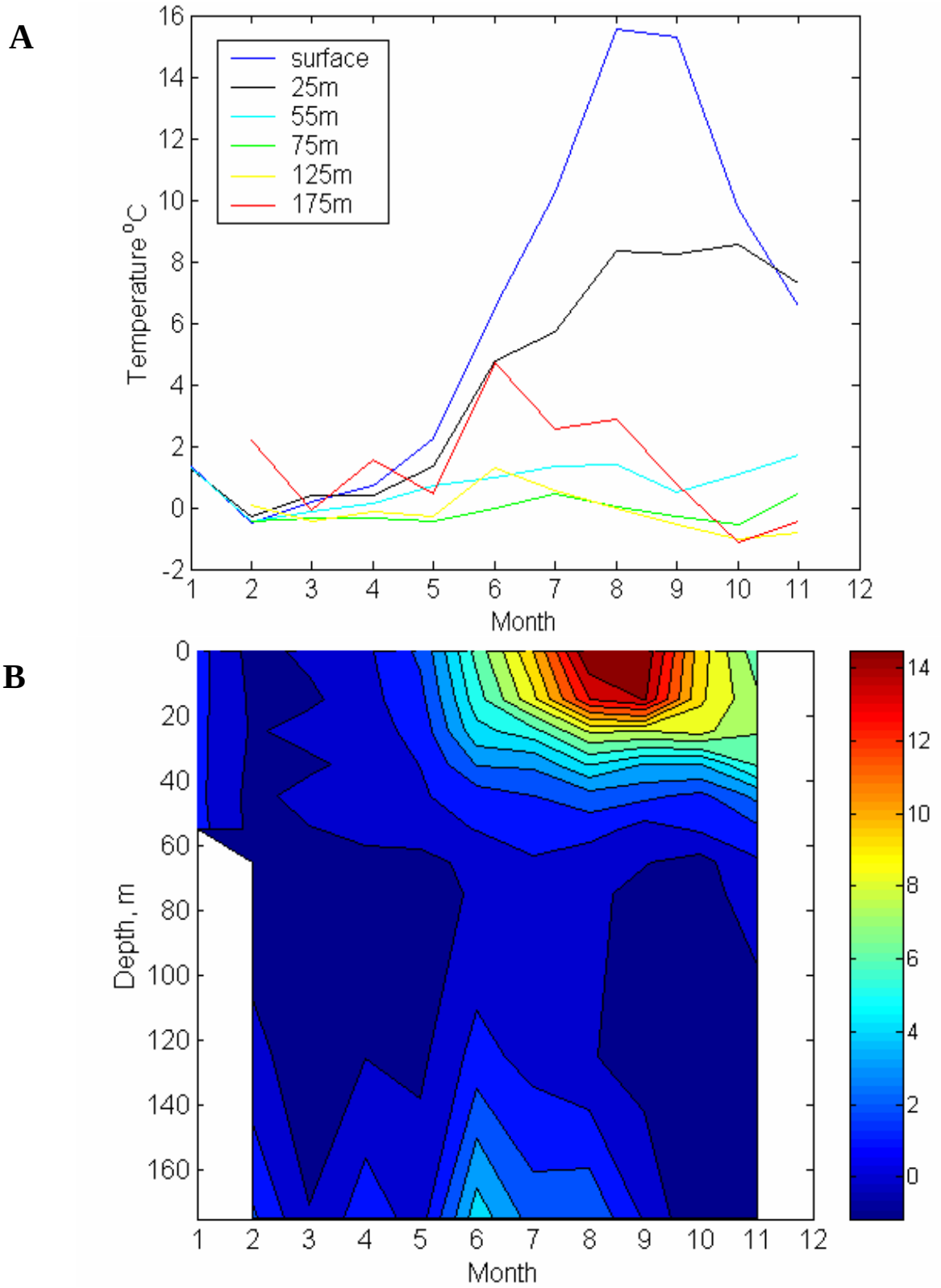

Figure 3.24 Monthly Mean Temperature from BIO Database, 1900-2004, for the Shelf Surrounding the Southern Laurentian Channel from the Surface to 180 m.

Note: A) Lines depict depths in metres. B) Contour plot contours depict temperature in °C.

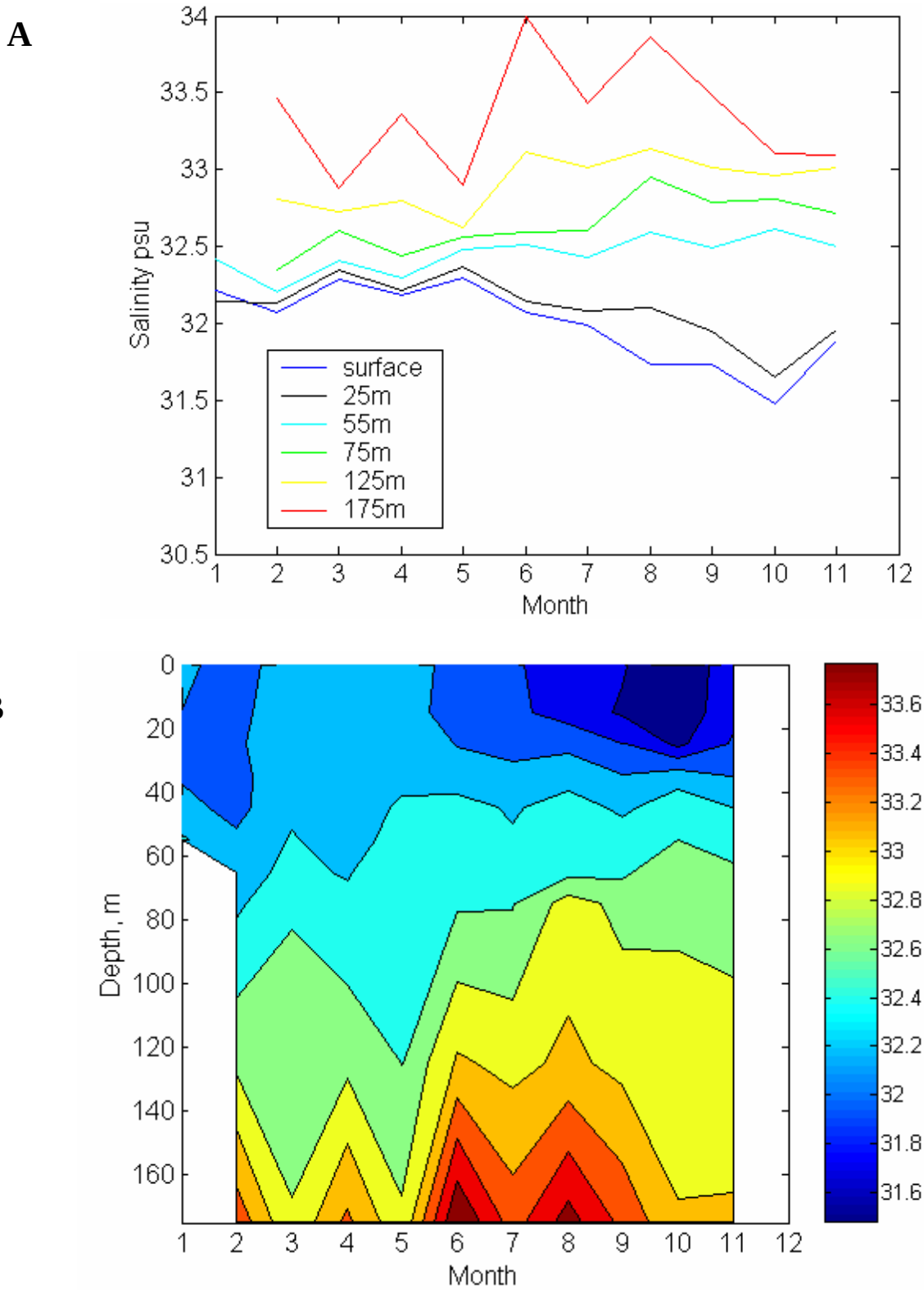

Figure 3.25 Monthly Mean salinity from BIO Database, 1900-2004, for the Shelf from the Surface to 180 m.

Note: A) Lines depict depths in metres. B) Contour plot contours depict salinity in ‰.

intermediate cold layer from about 50 to 125 m from April to December (Figure 3.26). During autumn the surface layer thickens due to heat loss at the surface and the subsequent breakdown of the vertical structure of temperature and salinity in the upper water column. As winter approaches, the mixed layer deepens to the level of the intermediate layer now forming a three layer stratification structure; the surface layer, the stratified higher salinity layer, and the deep warm layer. This is evident from January to April where the surface layer extends to about 125 m (Figure 3.26). According to the study by Lauzier and Trites (1957), which summarized data from 1914 to 1957, the deep warm layer was formed by waters of salinity generally greater than 34 ‰ and temperature greater than 4°C. Also, they identified a boundary zone between the intermediate layer and the deep layer with salinity between 33 ‰ and 34 ‰ and temperature between 1°C and 4°C. This is the layer, referred to in this report as the warm, stratified higher salinity layer. The temperature and salinity gradients in the boundary zone and deep layer were found to be independent of seasons but did have long term variations. This is consistent with this data summary in which the deep layer (> 300 m) has a monthly mean salinity between 34.50 ‰ and 34.9 ‰ and mean temperatures between 4.0°C and 6.2°C (Figure 3.26 and Figure 3.27). The boundary zone occurs from about 125 m to 250 m with a mean monthly salinity between 33 ‰ and 34.5 ‰, and a mean temperature between 2°C and 6°C.

The range of temperatures and salinity with depth are given in Appendix 5 of Oceans (2006). The surface temperature reaches a minimum of –1.56ºC in winter and a maximum of 21.14ºC in August. The mean surface temperature varies from 17.68°C in August to -0.17°C in March. At 25 m, the highest mean temperature is 11.72°C in September and the coldest is -0.06°C in March. The maximum mean temperature at 55 m occurs later in October at 2.27°C and the minimum is in March at 0.23°C. At 125 m, the mean temperature ranges from 0.77°C to 2.56°C. At 225 m, the mean monthly temperature varies slightly between 4.17°C and 6.66°C with a range of 0.2°C to 10.3°C.

The monthly mean salinity increases with depth from a minimum surface value of 30.69 ‰ to 34.91 ‰ at 475 m. At the surface the mean salinity ranges from 30.69 ‰ in October to 32.18 ‰ in April. In the top 30 m the salinity minimum occurs in October. Figure 3.27 shows that in general the salinity is lower from June to December in the surface waters. The cold layer has a salinity range from 32.2 ‰ to 33.34 ‰. The deep layer has a characteristic range of salinity with monthly means between 34.2 ‰ and 34.6‰.

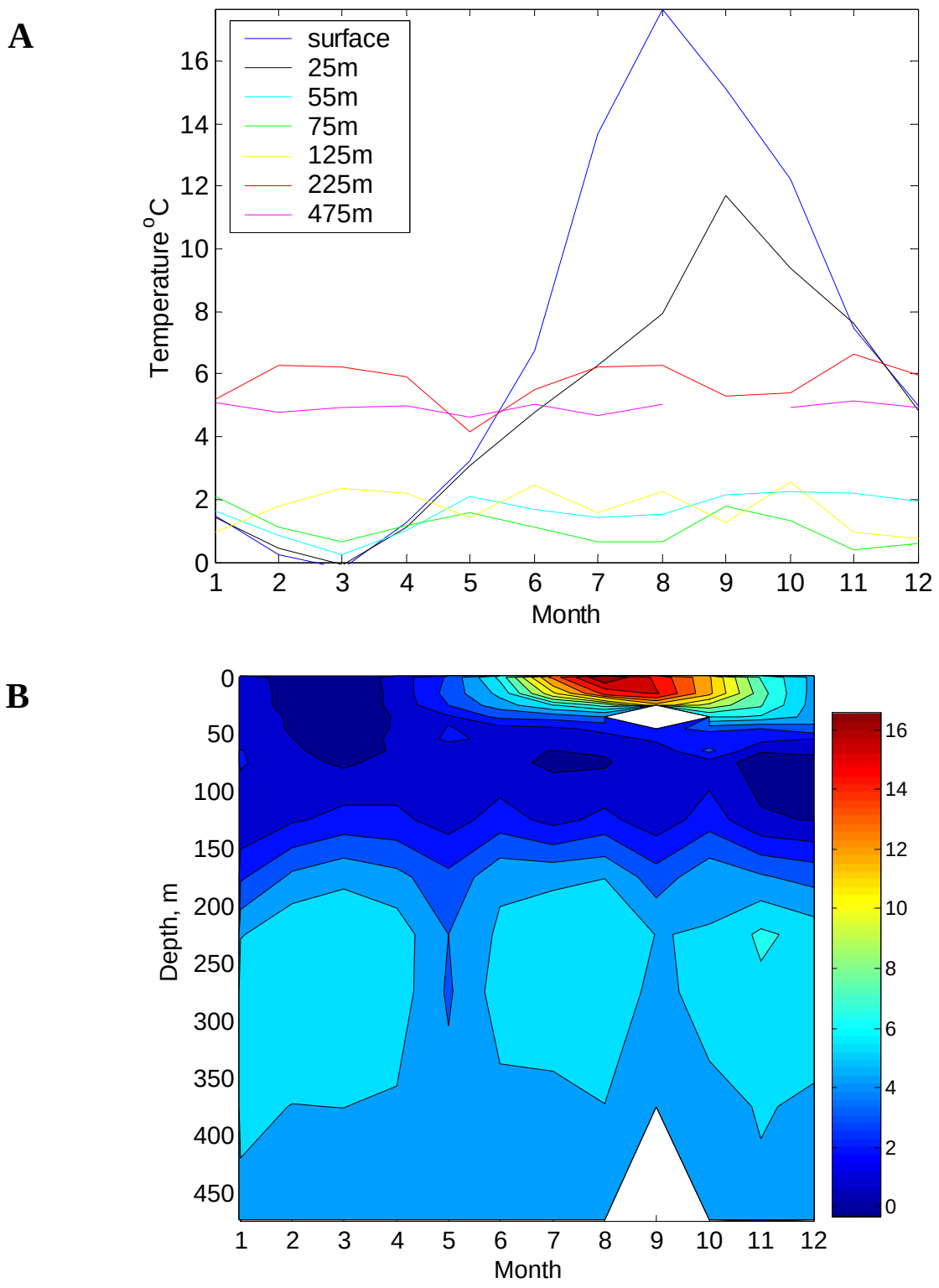

Figure 3.26 Monthly Mean Temperature from BIO Database, 1900-2004, for the Southern Laurentian Channel from the Surface to 500 m.

Note: A) Lines depict depths in metres. B) Contour plot contours depict temperature in ºC.

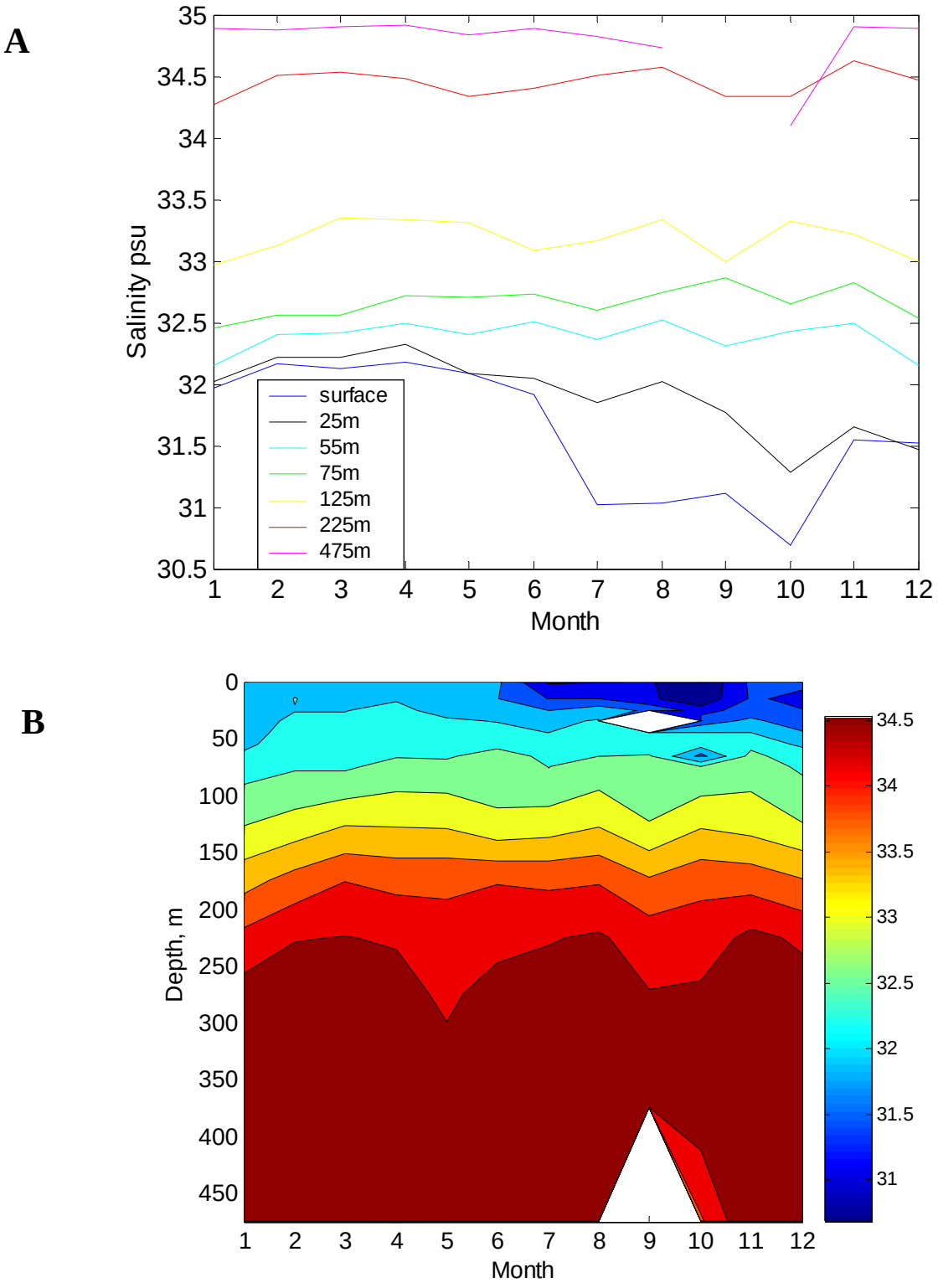

Figure 3.27 Monthly Mean Salinity from BIO Database, 1900-2004, for the Southern Laurentian Channel from the Surface to 500 m.

Note: A) Lines depict depths in metres. B) Contour plot contours depict salinity in ‰.

3.3.3. Slope (Laurentian Fan)

There are fewer data for the Slope than for the other two regions. There are no data in January or December and at depths greater than 800 m there is an increasing number of missing data. At 1,000 m there are no data in February and October and at 2,000 m and 3,000 m there are only data for three and two months of the year, respectively. In spring, summer and fall the structure is in layers; a warm surface stratified layer, an intermediate cold water layer, a warm, stratified higher salinity layer, a deep warm layer and a colder bottom layer. The monthly mean temperature data show that there is a distinct upper surface layer to about 50 m and an intermediate cold layer from about 50 to 125 m during April to December (Figure 3.28). These two layers vary seasonally while the lower layers show little if any seasonal variations. In autumn, the surface layer begins to thicken and by winter the surface layer extends to the level of the intermediate layer forming a four layer stratification; the surface layer, the stratified higher salinity layer (boundary layer), the deep warm layer and the bottom cold layer. The upper waters above 450 m are similar in structure to those of the Channel, but have slightly different water properties. The cold intermediate layer is slightly warmer than the Channel with a minimum temperature around 2°C. The mean temperature and salinity of the warm deep layer is also greater with values between 6°C and 10°C, and 34.55 ‰ and 34.95 ‰, respectively. The bottom layer is slightly colder and more saline with mean temperatures from 3.5°C to 4.5°C, and with salinities from 34.90 ‰ to 35.0 ‰, respectively (Figure 3.29).

The range of temperatures and salinity with depth are given in Appendix 5 of Oceans (2006). The surface properties are the most variable with temperature ranging from –1.43ºC in winter to 19.95ºC in August. Since there is no data in December and January and few data in February and March it is difficult to determine the trend in winter. The surface is warmest in August with a mean temperature of 17.21°C and coldest in February with a mean temperature of 0.89°C. At 25 m, it is warmest in September at 13.06°C and the coldest in February at 1.21°C. At 125 m, 225 m and 475 m the monthly mean temperature varies between 4.35°C in July to 9.03°C in March, between 5.91°C in May to 9.19°C in March, and between 4.66°C in July to 6.23°C in March, respectively. There is no seasonal trend below 475 m and the mean monthly temperature varies slightly around 4.3°C (at 800 m) and around 2.7°C at 3,000 m.

The monthly mean salinity increases with depth from a minimum surface value of 31.56 ‰ to 35 ‰ at 3,000 m. At the surface, the monthly mean salinity varies between 31.56 ‰ and 32.79 ‰. The minimum mean salinity occurs between August and October at the surface, and in October at 25 m. At 125 m, 225 m, and 475 m, the monthly mean salinity varies between 33.25 ‰ and 34.59 ‰, between 34.55 ‰ and 34.95 ‰, and between 34.86 ‰ and 35.03 ‰, respectively. Below 475 m, the mean salinity is 34.95 ‰ at all depths with only slight temporal variations.

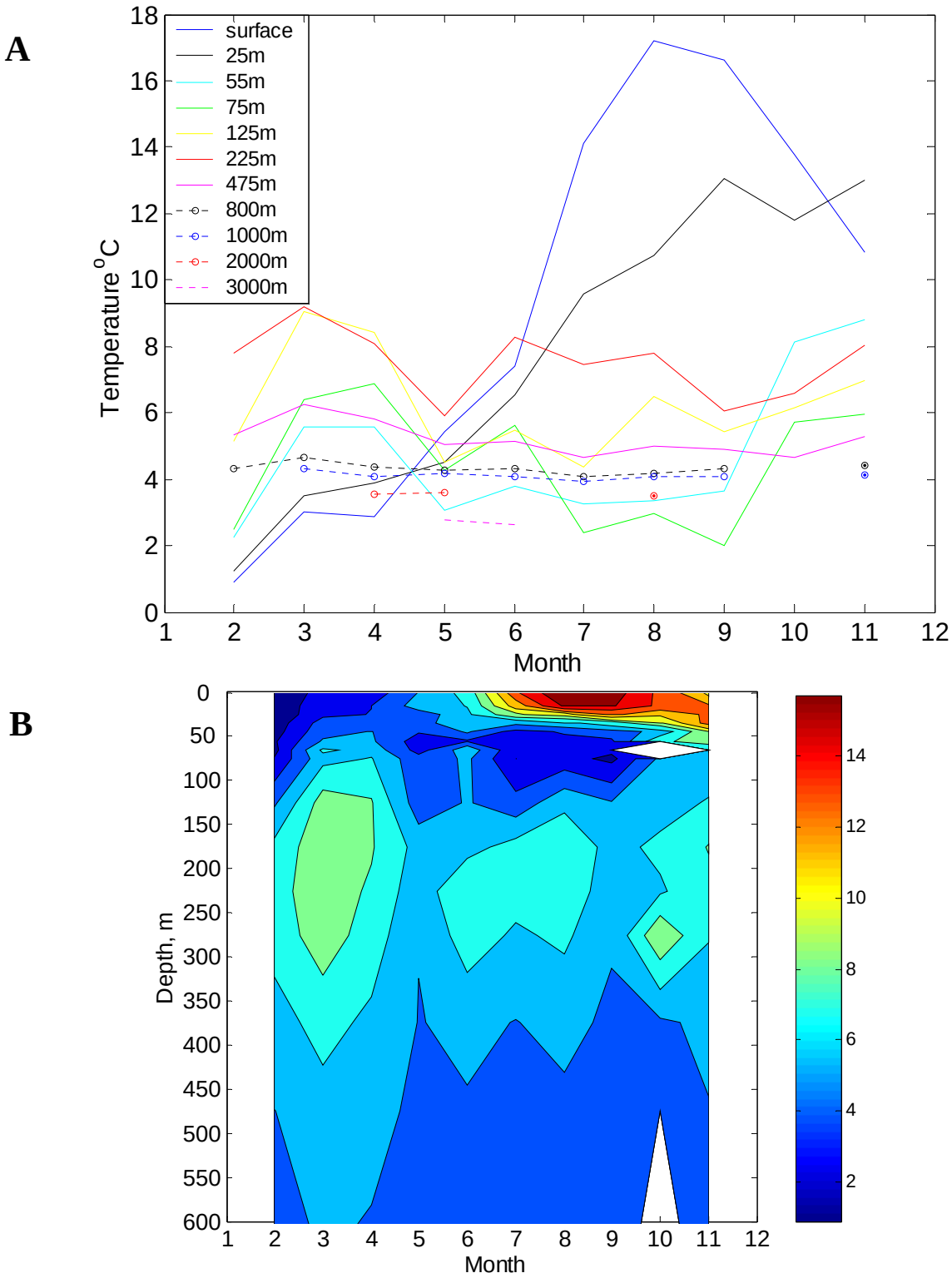

Figure 3.28 Monthly Mean Temperature from BIO Database, 1900-2004, for the Laurentian Fan.

Note: A) From the surface to 3,500 m, lines depict depths in metres. B) From surface to 500 m, contours depict temperature in ºC.

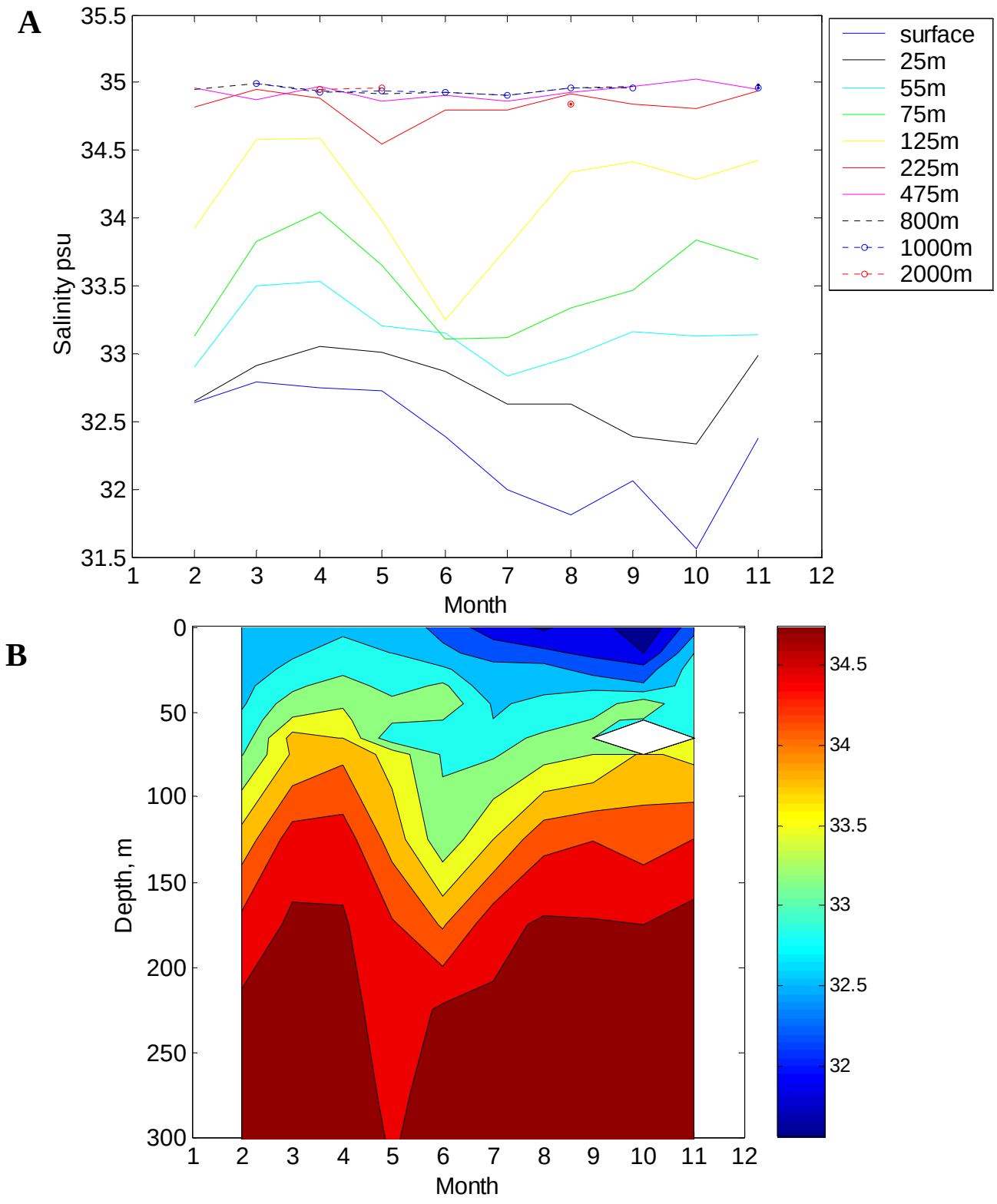

Figure 3.29 Monthly Mean Salinity from BIO Database, 1900-2004, for the Laurentian Fan.
Note: A) From the surface to 3,500 m, lines depict depths in metres. B) From surface to 300 m, contours depict salinity in ‰.

3.3.4. Water Properties Variability

In addition to seasonal cycles, and density differences, water properties are also characterized by long term variation due to atmospheric fluxes which can result in changes from transport from upstream sources, sea-ice dynamics, and exchange with adjacent offshore waters. Colbourne (1996, 2000) and Drinkwater et al. (2002) examined and compared oceanographic data during the 1990s to the long-term (1961-1990) average on the Nova Scotia and southern Newfoundland Shelves, respectively. The temperature anomalies on the St. Pierre bank from 1950 to 1999 in the upper 100 m had amplitudes generally less than $\pm$ 1°C with periods between five to 10 years. During the mid-1980s an uncharacteristic cold period started on the Shelf, reaching a minimum in the early 1990s and gradually warming to above normal temperatures by the end of the decade (Colbourne 1996, 2000; Drinkwater et al. 2002). The colder temperatures were accompanied by lower salinities (Colbourne 2000; Drinkwater et al. 2002). Colbourne (1996) indicated that the cold period moderated in some areas during the early 1990s, but large areas with below normal temperatures continued into 1995, particularly on the eastern portions of St. Pierre Bank. On the St. Pierre and Green Banks during 1985 the aerial extent of sub 0ºC bottom water increased from a 20 % average to 100 % and persisted at about 94 % until 1994, decreasing to 10 % by 1998. This area with a mean temperature range from 0ºC to 1ºC on the Newfoundland Shelf had large fluctuations during the 1970s, 1988 and 1996 (Colbourne 2000). Generally during the cold period the temperatures decreased by 2ºC in the upper water column and 1ºC in the lower (Colbourne 2000). The temperatures in the 200 to 400 m depth range, along the edges of the Laurentian Channel and southwestern Grand Bank, did not reveal any significant interannual variations, however, the region experiences large spatial variations of the order of 2.5ºC at 200 m depth (Colbourne 1996).

These variations are consistent with the periods of cold fresh water events in the Labrador Sea and North Atlantic in the early 1970s, mid-1980s, and early 1990s during peaks in the NAO index (Colbourne et al. 2002; Yashayaev 2002) (Figure 3.30). The NAO measures the wintertime sea level pressure difference between Iceland and the Azores. When the NAO index is high, it indicates that there is a greater cyclonic flow over the North Atlantic resulting in a greater circulation of cold Arctic air and stronger storms. This results in more heat loss from the sea surface, increased ice cover and fresher than normal water over the shelf. When the NAO index is low, the opposite is true with an expected reduced heat loss from the sea surface.

Lauzier and Trites (1957) summarized data in the deep waters of the Laurentian Channel from 1914 to 1951. They found that the maximum temperature in the deep layer varied annually. In years with a lower temperature maxima, the deep layer was thinner than in other years when the temperature was warmer.

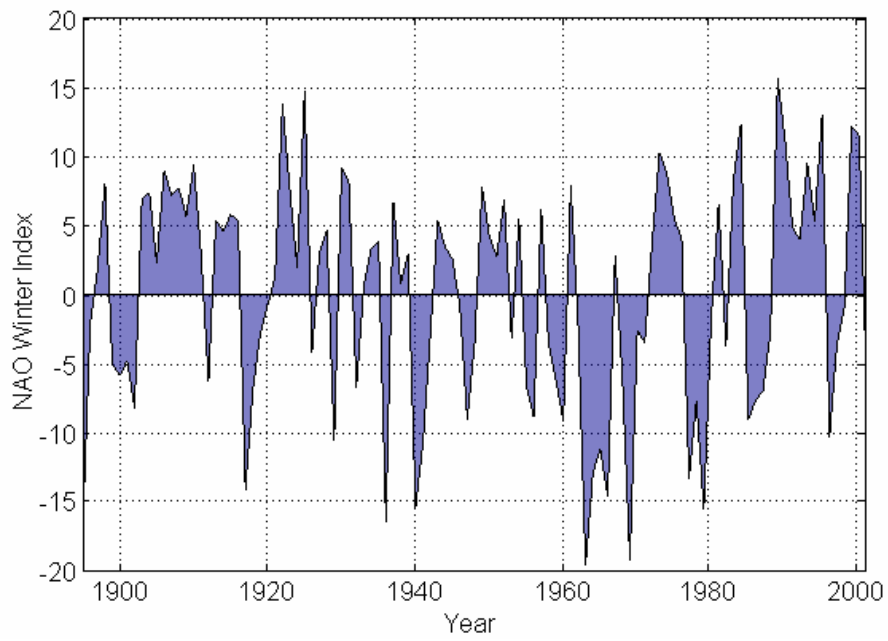

Figure 3.30. Time Series of the NAO Index, Winter Mean.
Note: During the 1960s the NAO index is highly negative, whereas in the 1970s the index is slightly negative. From the 1980s to the 1990s the index is positive and increases. The greatest contrast in the NAO index is between the negative values in the 1960s and the high positive index in the 1990s.

3.3.5. Water Masses

The major features of the general circulation in the study region consists of; a southwest flow along the Shelf comprised of Gulf of St Lawrence water, a Labrador Current inshore branch which divides into two parts one flowing west around the north of St. Pierre Bank and the other flowing south between Whale Bank and Green Bank, a Labrador Current offshore branch flowing westward along the Shelf to the Laurentian Channel, and the Gulf Stream further south (Colbourne 2000).

There are four water masses in the study region: three on the Shelf and an additional water mass in the deeper water along the Slope. The water masses on the Shelf consist of Coastal water due to a mixture of local run-off and waters from the Gulf of St. Lawrence, Labrador Current water, and some mixed water near the bottom transported from the Slope region. Figure 3.31 shows that the coastal waters are located in the top 50 m above the Labrador Current Water. The characteristics of this water match the water properties identified as coastal water, by McLellan (1957) (Figure 3.32). In the Laurentian Channel (Figure 3.33) there are four water masses, Coastal Water, Labrador Current Water with properties similar to those on the Shelf, warm Slope Water below a depth at 250 m, and some mixed Slope and Atlantic water near the bottom. On the Slope in the area of the Laurentian Fan, there are still four water masses (Figure 3.34). The surface water to a depth of 50 m is much warmer than found on the Shelf or in Laurentian Channel (Figure 3.35). These warmer temperatures were probably due to intrusion of the North Atlantic central water. Drinkwater et al. (2002) describe the Slope waters as

being a combination of the colder, fresher Labrador Current water and the warmer saltier North Atlantic Central Water. The slope water properties at a particular location depend upon whether the North Atlantic Central Water or the Labrador Current Water is dominant. Labrador Slope Water was defined as having a lower salinity and temperatures in the range of 34.3 ‰ to 35 ‰ and 4°C to 8°C, respectively. The warm Slope Water was defined as having water properties ranging from 34.7 ‰ to 35.5 ‰ and 8°C to 12°C (Drinkwater et al. 2002). Figure 3.36 show the distribution of the two offshore slope waters as presented by Drinkwater, et al. (2002).

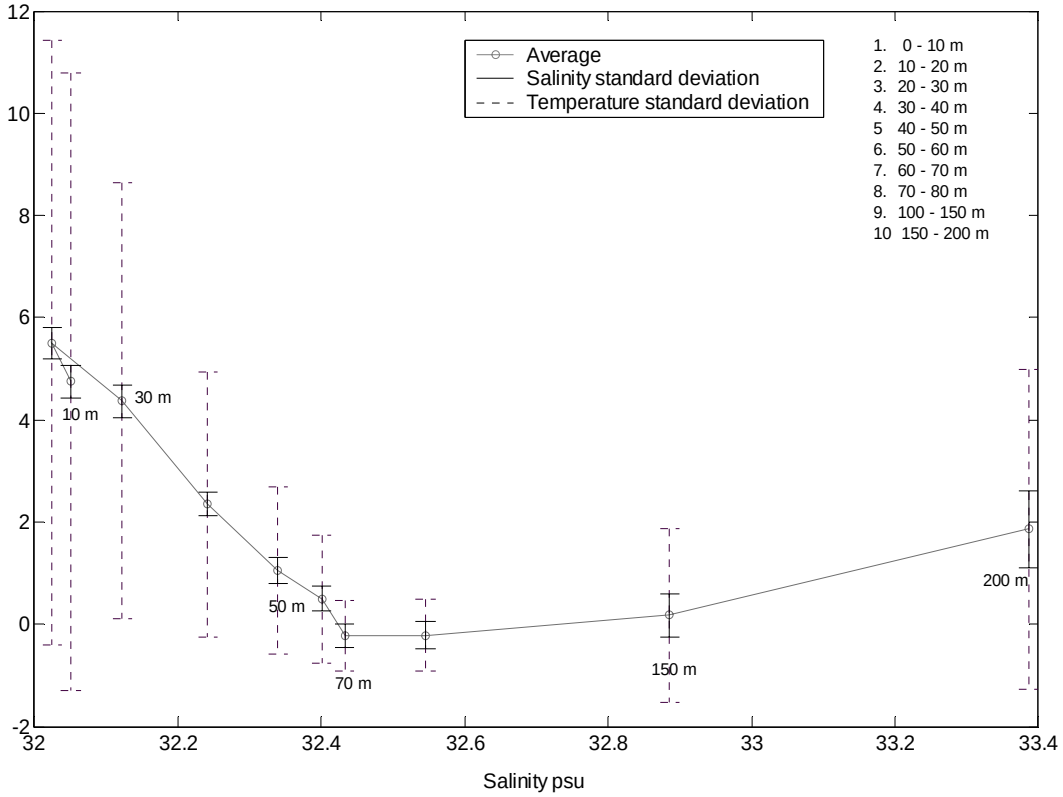

Figure 3.31. T-S Curve, for the Banks Surrounding the Southern Laurentian Channel from the Surface to 200 m, Data from BIO Database from 1900-2004.

Note: The solid grey line is the average value and the solid and dotted bars are the standard deviation for salinity and temperature, respectively.

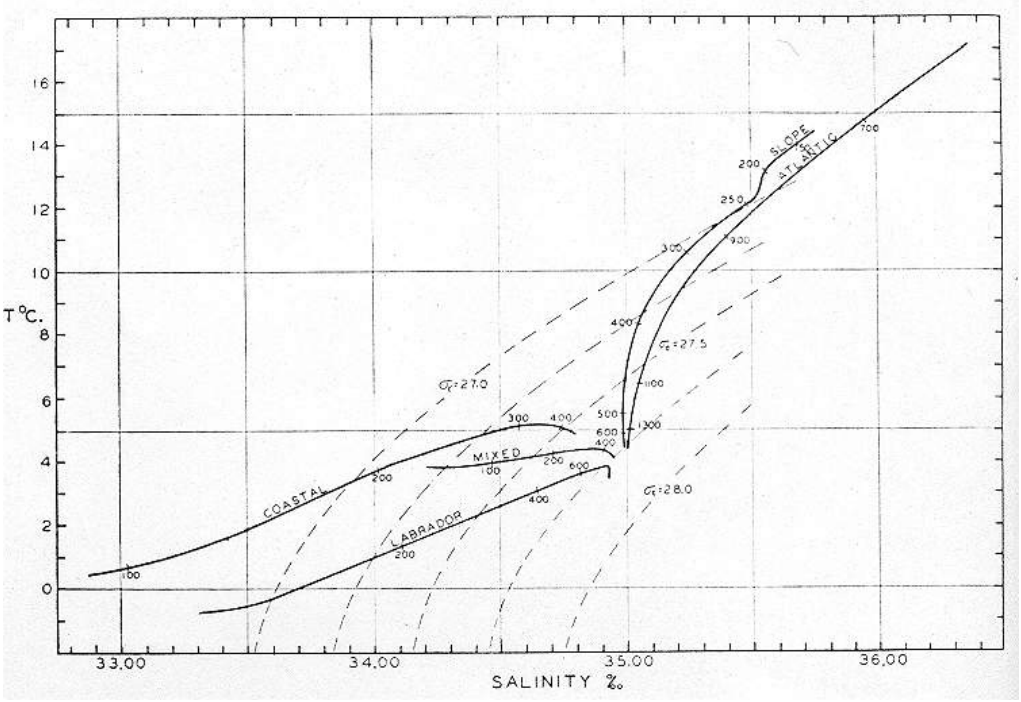

Figure 3.32 T-S Curves for Five Water Masses Found Between the Gulf Stream and the Continental Shelf West of 45 Degrees West.

Source: McLellan (1957).

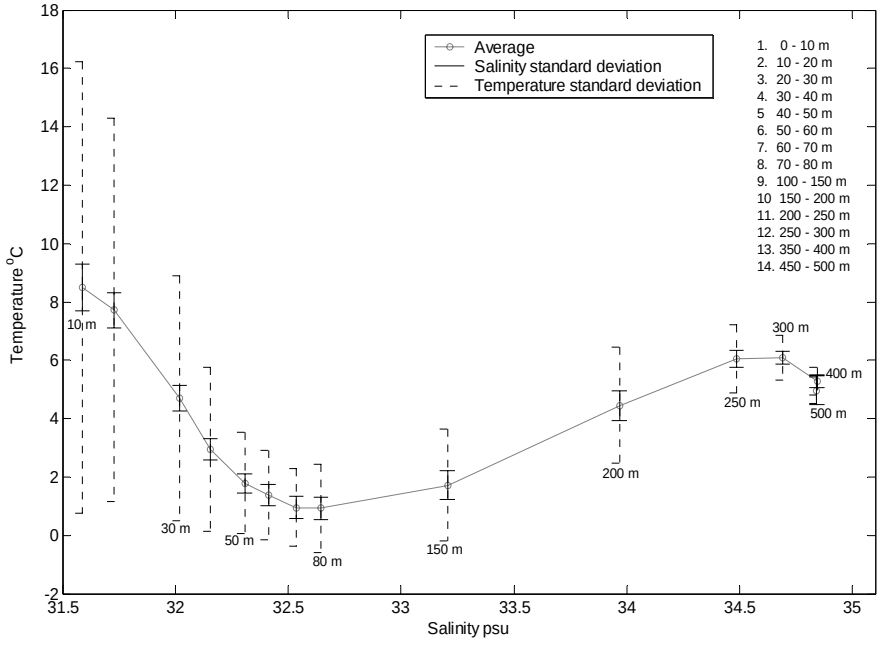

Figure 3.33. T-S Curve, for the Southern Laurentian Channel from the Surface to 500 m, Data from BIO Database from 1900-2004.

Note: The solid grey line is the average value and the solid and dotted bars are the standard deviation for salinity and temperature respectively**.**

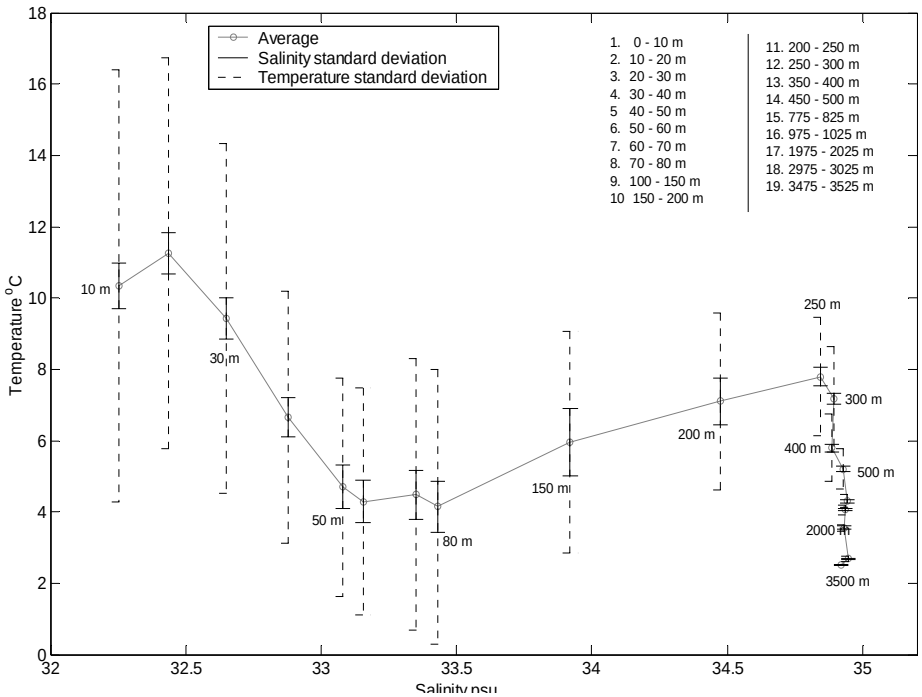

Figure 3.34. T-S Curve, for the Laurentian Fan from the Surface to 3,500 m, Data from BIO Database from 1900-2004.

Note: The solid grey line is the average value and the solid and dotted bars are the standard deviation for salinity and temperature, respectively.

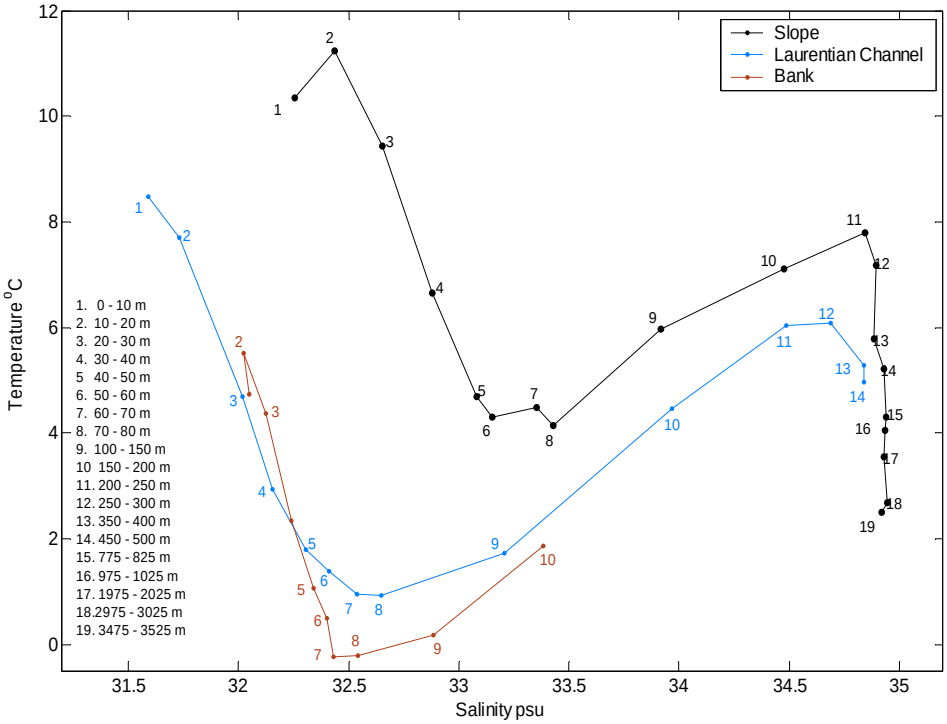

Figure 3.35. Comparison of T-S Curves Averaged by Depth for the Shelf (red), the Southern Laurentian Channel (blue) and the Laurentian Fan (black). Data from BIO database from 1900-2004.

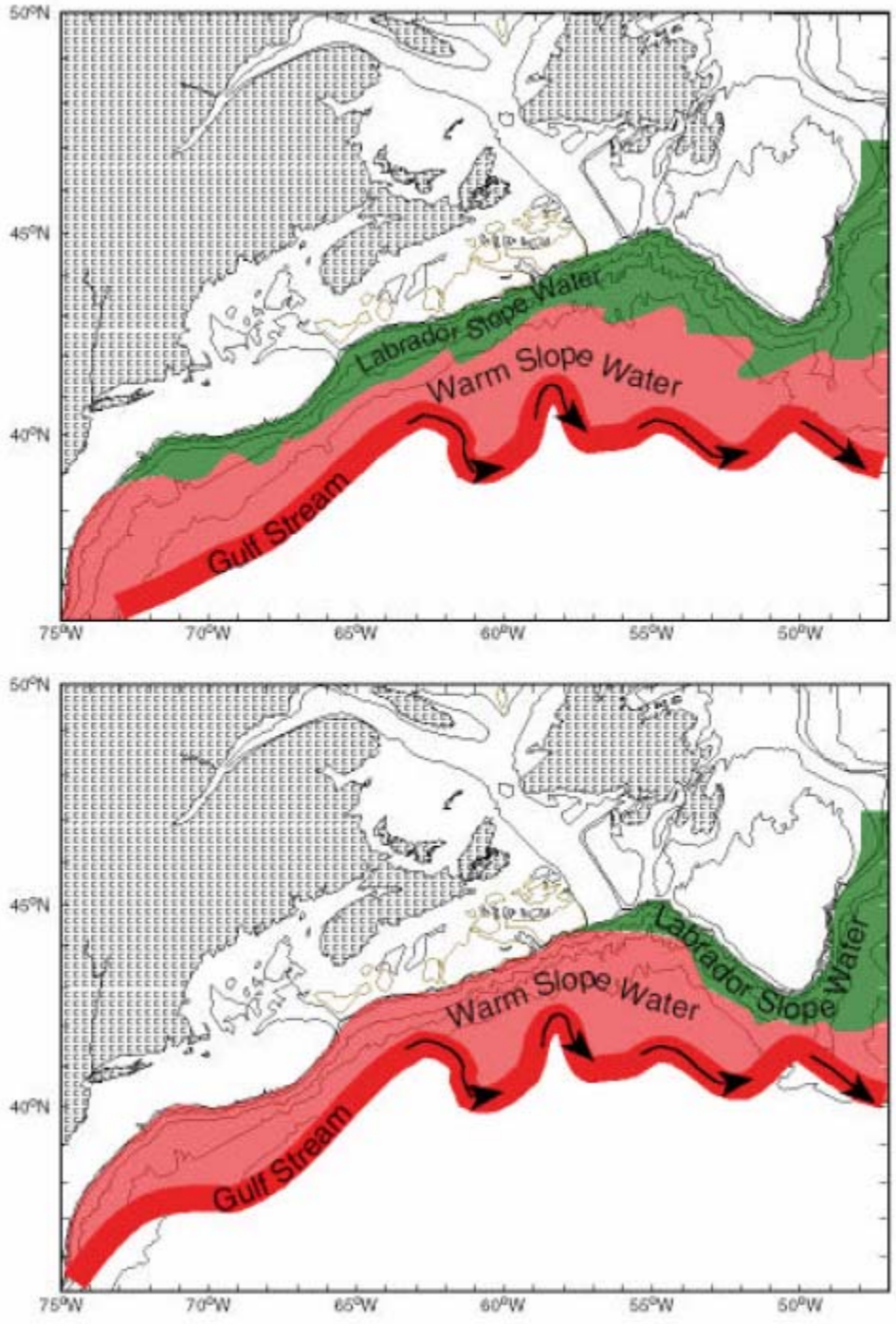

Figure 3.36. The Distribution of the Offshore Labrador Slope Water at Approximately 200 m during the Maximum Southward Extension in 1998 (top panel) and it's more Typical Distribution during most of the 1970s through the 1990s (Bottom Panel).

Source: Drinkwater et al. (2002).

A study by Lauzier and Trites (1957) investigated the water mass characteristics of the deep waters of the Laurentian Channel. They found variability in the water mass properties between the entrance of the Channel and Cabot Strait (Figure 3.37). They suggested that the coastal waters at the entrance to the Channel and their mixing with the Labrador Slope Water are an intermediate step in the formation of the deep waters of the Channel.

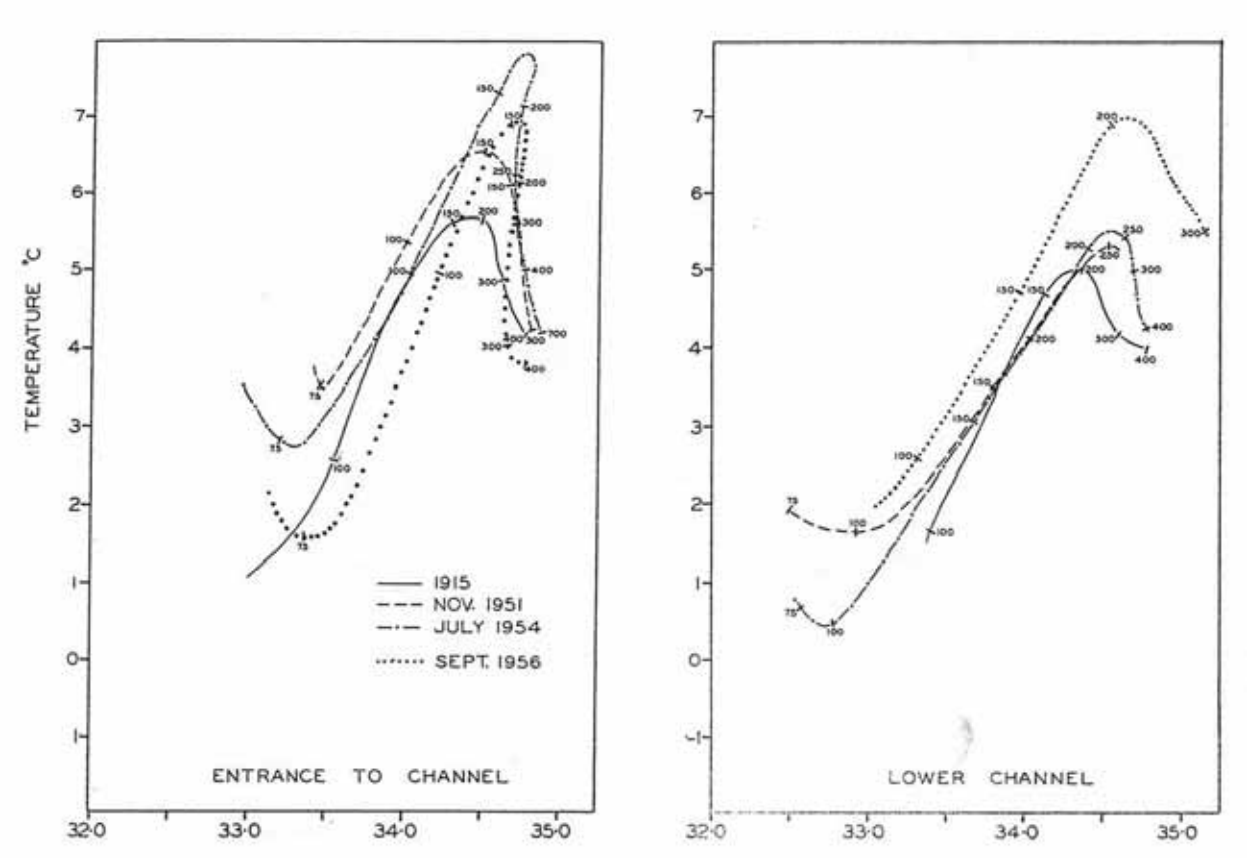

Figure 3.37. Temperature-Salinity Diagram from the Deep Waters of the Entrance and Lower Region of the Laurentian Channel.

Source: Lauzier and Trites 1957.

Figure 3.38 to Figure 3.40 show the seasonal variations in water properties. The monthly T-S curves for the Shelf (Figure 3.38) shows that there is a strong seasonal variability in the upper water mass in the top 50 m of the water column. The greatest difference is in temperature which fluctuates around 0°C throughout the 50 m depth in winter and spring and changes to a gradient in the surface depth in summer and fall with values varying between 10°C and 0°C in the surface layer.

The seasonal T-S curves for the Channel (Figure 3.39) reveal that there is the same type of seasonal variability to about 50 m as found on the Shelf. Below 50 m there is little seasonal variation in either water mass.

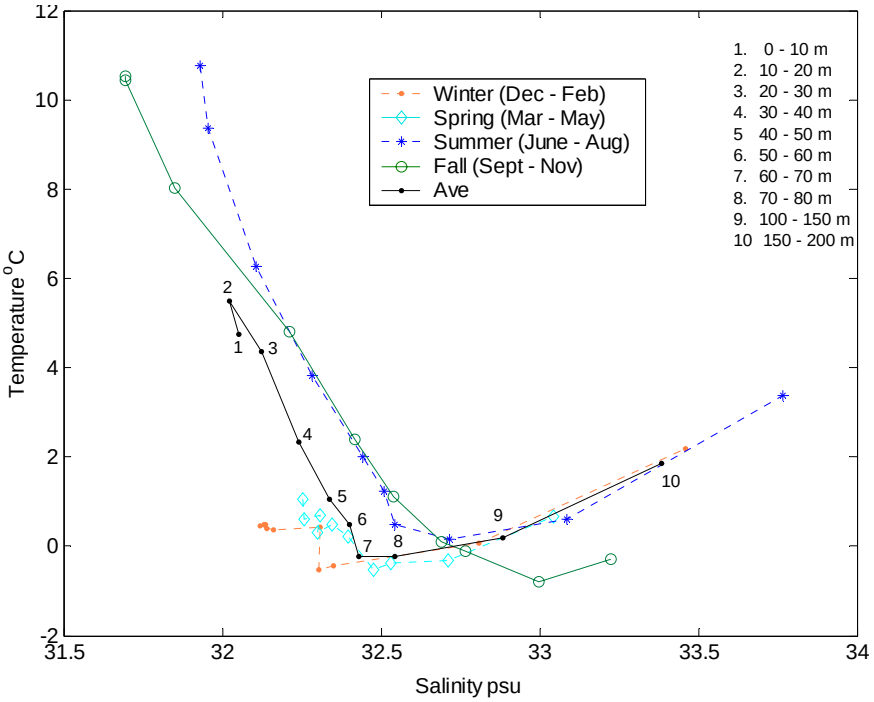

Figure 3.38. T-S Seasonal Depth Averaged Curve from BIO Database, 1900-2004, for the Shelf Area.

Note: Each colour line depicts a season and the black solid line is the yearly average.

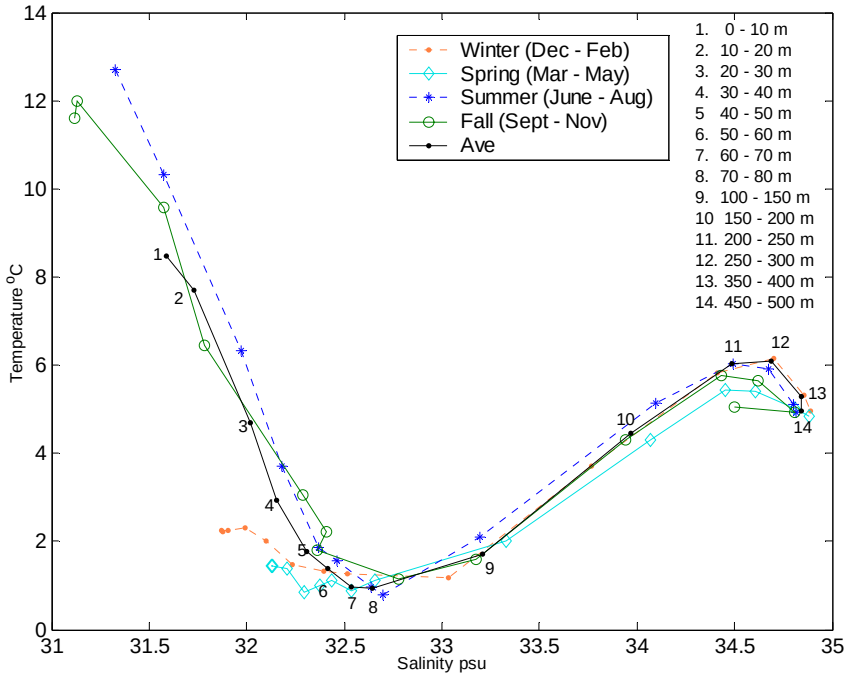

Figure 3.39. T-S Seasonal Depth Averaged Curve from the BIO Database for the Southern Laurentian Channel.

Note: Each colour line depicts a Season and the Black Line is the Yearly Average.

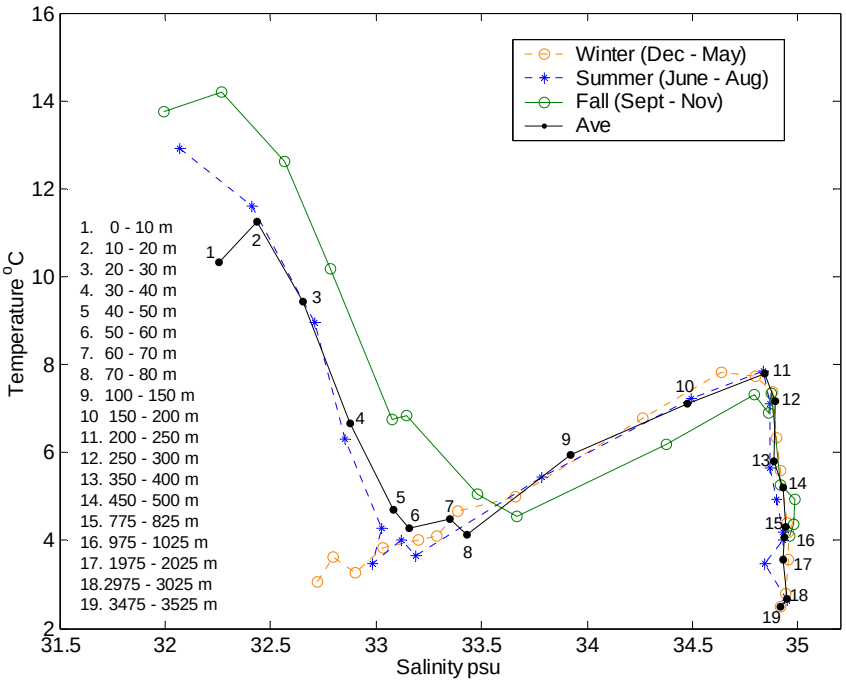

Figure 3.40. T-S Seasonal Depth Averaged Curve from BIO Database, 1900-2004 for the Laurentian Fan.

Note: Each colour line depicts a season and the black solid line is the total yearly average.

For the Slope water, unlike the Shelf and Laurentian Channel waters, the mean temperature does not drop below 4°C in the top 800 m of the water column (Figure 3.40). From 350 to 500 m (the maximum depth of the Channel) the average T-S curves are almost identical. The seasonal T-S curves for the Slope (Figure 3.40) reveal that the temperature during the fall is warmer in the top 70 m, and then colder between 70 m and 250 m as compared with the other three seasons.

3.4. Currents

3.4.1. Characteristics of the General Circulation

The general circulation in the region of interest features a remarkably complex picture of dynamic interactions, resulting from the interconnection between the North Atlantic Subpolar and Subtropical gyres, which meet off the Grand Banks of Newfoundland. A series of thermohaline and wind driven currents extend from the shelf break to the deep Continental Slope and from the Grand Banks of Newfoundland to the Scotian Shelf.

The Labrador Current is a cold, relatively fresh, buoyancy driven current with general equatorward flowing direction. This flow is intensified by strong winter cooling and freshening by rivers and ice melt along its way. This current extends across isobaths from the Labrador Continental Shelf over the Continental Slope and forms what is known as the Labrador Slope Water. When this water reaches the

Newfoundland Shelf, most of the flow is directed along the outer edge of the Grand Bank and a small fraction flows across the banks themselves (Townsend et al. 2002).

This cold and fresh mixture of shelf and slope waters continues to border the continental shelf break until it reaches the Scotian Shelf.

Another important factor in the system is the Gulf Stream and its associated eddies. Between 65 °W and 50 °W the Gulf Stream flows almost eastward and is located south of 40 °N, which is relatively far from our Study Area. However one of the inherent features of this current system is its meandering path. These meanders may be formed both in northward and southward directions. Northward forming meanders at certain stages of their development separate from the main stream and generate rings or eddies, which start moving independently from the Gulf Stream flow. These eddies contain a warm water core that makes them easily identifiable in sea surface temperature satellite images.

Once these eddies are born, they drift in different directions and can be sustained, for a considerable amount of time. Their size may be of 100 to 300 km in diameter and can reach considerable depths. The trajectory of these warm water rings, once they depart from the Gulf Steam jet together with their interaction with the bathymetry of the Continental Slope and with other current flows, influence the dynamic regime in the vicinity of the shelf break of the Grand Banks and the Scotian Shelf.

To further complicate the picture, some authors such as Pickart et al. (1999) report the existence of another water flow sandwiched between the eastward flowing Gulf Stream and the westward flowing Labrador Slope water, which flows to the east and northeast on its way along the border of the Continental Slope. This current according to Pickart et al. (1999) separates from the Gulf Stream somewhere around 60 °W and continues flowing eastward. Fratantoni and Pickart (2005) often refer to this current as the Slope Water Jet (Figure 3.41).

The interaction among these circulatory features is known to correlate with the behaviour of the North Atlantic Oscillation (NAO) Index. The NAO Index, as defined by Rogers (1984) is the difference in winter (December, January and February) sea level atmospheric pressures between the Azores and Iceland, and is a measure of the strength of the winter westerly winds over the northern North Atlantic. A high NAO index corresponds to an intensification of the Icelandic Low and Azores High which creates strong northwest winds, cold air and sea temperatures and heavy ice in the Labrador Sea and Newfoundland Shelf regions (Colbourne et al. 1994; Drinkwater 1996). In Low Index years, the north wall of the Gulf Stream is displaced to the south and the southward transport associated with the Labrador Current is intensified. As a consequence of these north-south displacements of the shelf/slope front, the area is subject to thermal anomaly oscillations (Petrie and Mason 2000; Drinkwater et al. 2000; DFO 2002a)

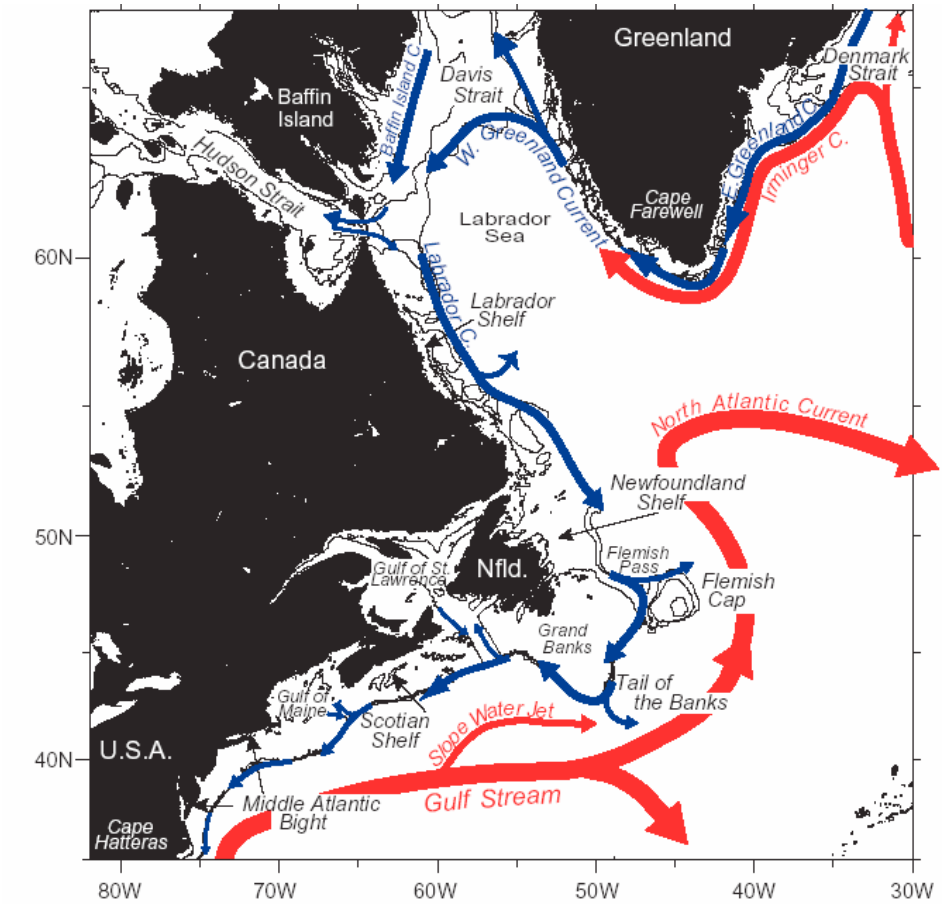

Figure 3.41. Schematic Diagram of the Main Features of the Surface Circulation in the Western Atlantic Ocean.

Note: Cold shelf break waters are shown in blue while warm Gulf Stream waters are shown in red.
Source: Fratantoni and Pickart 2005.

The shelves off southeastern Newfoundland and Nova Scotia are exceptionally broad and support extensive and productive fisheries. The biological productivity of these shelves results from a number of factors and processes. They include cross-isobath fluxes of deep water nutrients and winter convective mixing which annually replenishes surface nutrient concentrations. The winter corrective mixing is followed by strong vertical stratification in the warmer months created both by fresh water run-off and spring warming of the upper layers. The winter period is often followed by intense winter-spring plankton blooms that commence in very cold water temperatures. Vertical mixing by tides in a number of areas further stimulates nutrient fluxes that promote high levels of plankton production throughout much of the year.

South of western Newfoundland, the Laurentian Channel displays a two-layer current structure, with fresher water leaving the gulf near the surface and saltier, heavier water entering the gulf at deeper levels. Currents reach over 40 cm/sec in both directions year around (El-Sahb 1976).

Han et al. (1999) found that the bimonthly mean currents along the shelf break around the mouth of the Laurentian Channel are oriented towards the west-southwest (Figure 3.42) although, due to the limited amount of data available, this fact is less evident in the upper 30 m surface than in the rest of the water column.

Model output reported in the same study show consistency with these measured mean currents (Figure 3.43). The transport across a section to the east of the Study Area was estimated to be 2.6 Sv, which is consistent with the findings of Fratantoni and Pickart (2005) who reported that the total transport associated with this system, in the vicinity of the Laurentian Channel, is in the order of 2 Sv. According to Fratantoni and Pickart (2005), in the area south of the Grand Banks the speed of the currents associated with the shelf break current system decreases, and the jet itself is confined to the shallower levels.

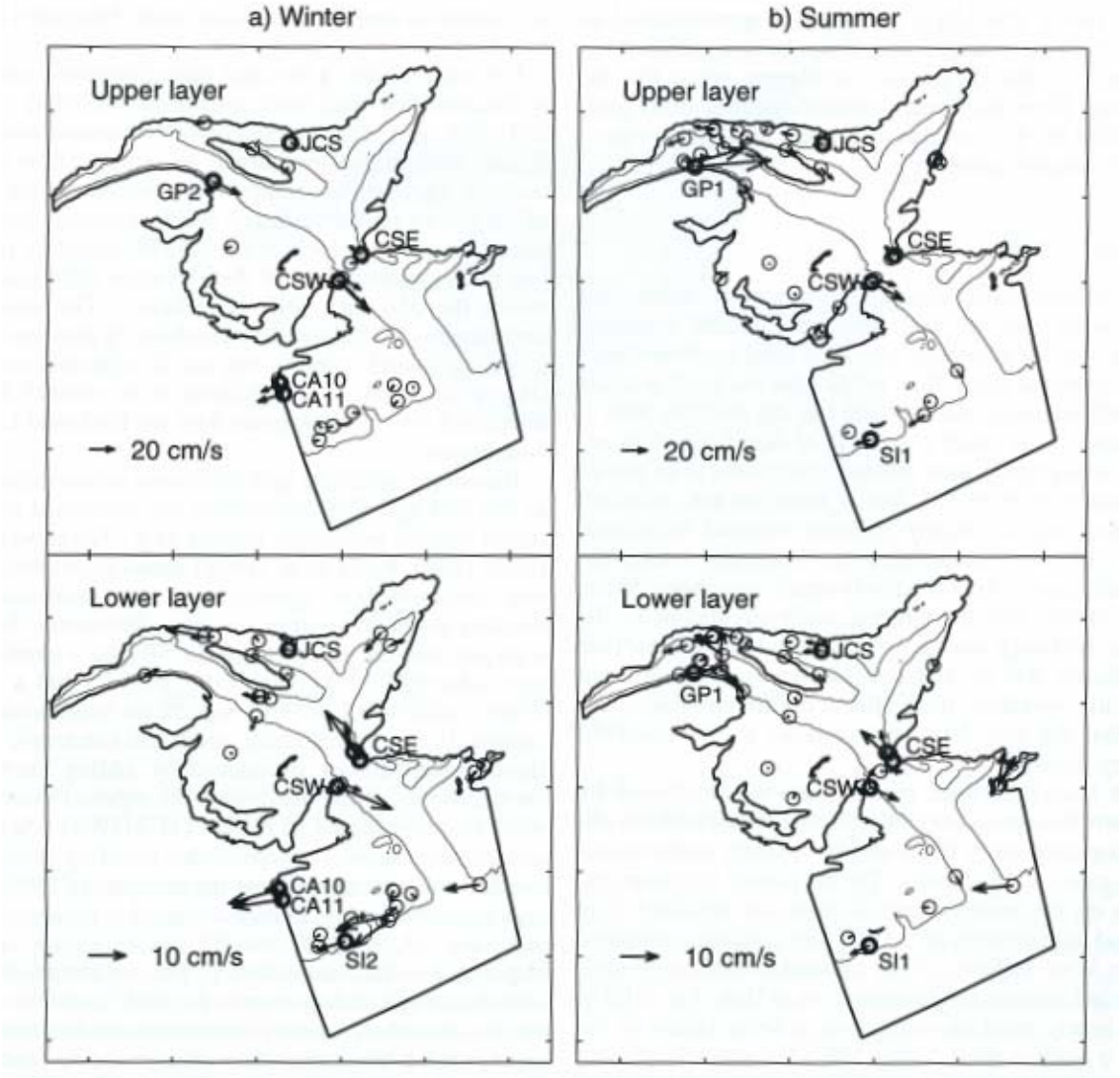

Figure 3.42. Bimonthly Mean Currents from Moored Measurements for the Upper Layer (Upper 30 m) and Lower Layer (Remainder of the Water Column) for Winter and Summer.

Source: Han et al. (1999).

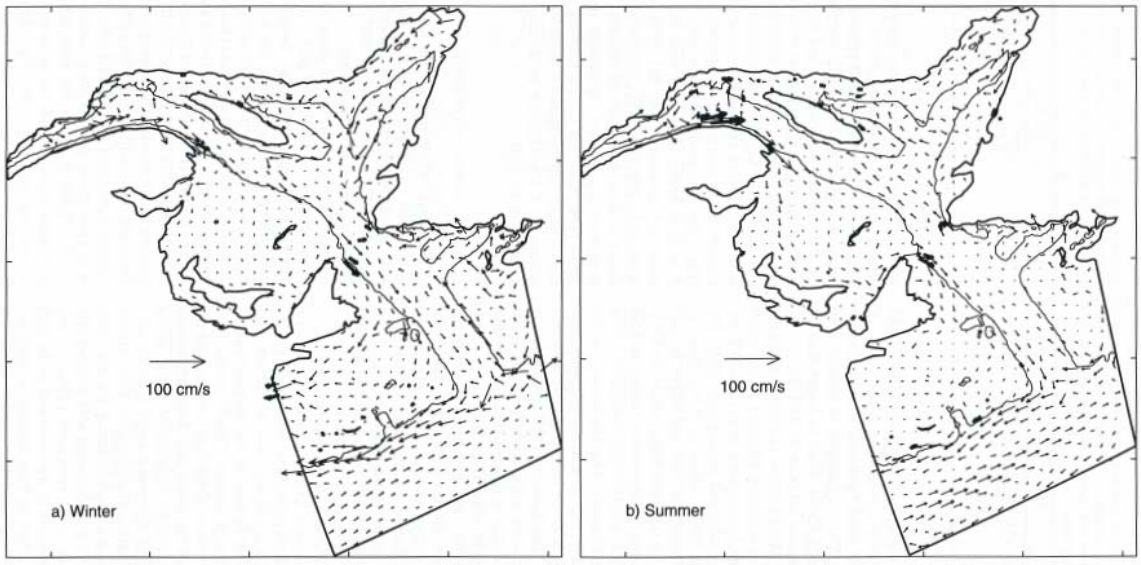

Figure 3.43. Near-Surface Mean Currents for Winter and Summer in the Gulf of St. Lawrence and the Laurentian Channel.

Source: Han et al. (1999).

3.4.2. Current Data Available

Current metre data sets for the area were found in the BIO Ocean Data Inventory. Additionally a set of instruments deployed by the Bedford Institute of Oceanography on request from Conoco-Phillips during 2003 and 2004 was made available for this report.

The analyzed material includes:

- A mooring deployed between April and December 1975 with metres at four depths.
- A series of current data covering the period from June 1996 to April 2000. This mooring contained instruments at four levels and was recorded almost continually during the entire 5-year period.
- A set of four metres deployed between July 2003 and June 2004
- A current data series from an upward-looking Acoustic Doppler Current Profiler (ADCP) which covered the upper 60 metres of the water column.

Table 3.13 summarizes information relevant to these current metre moorings. Figure 3.44 shows the geographic locations of the moored metres.

Most of these data sets cover a lengthy period of time. This was accomplished by replacing the metres after a period of time that ranged between five and 10 months. Consequently, there were small differences in geographic coordinates upon redeployment. These differences had a maximum of around 1.5 miles though typically were below 0.3 miles.

Table 3.13. Data Record.

Period	Coordinates	Depths	Filled records (%)	Notes
June 1996 – April 2000	44.84 ° N 55.83 ° W	56 m 153 m 400 m 680 m	17 (0.05%) 17 (0.04%) 0 (0.0%) 17 (0.05%)	Two series at 400 m: June/96 to May/97 and December /97 to April/00
April 1975 – December 1975	44.03 ° N 56.96 ° W	140 m 450 m 1,000 m 2001 m	0 (0.0%) 45 (0.3%) 25 (0.4%) 25 (0.4 %)	Two series at 140 m: April-May and August-December, 1975
July 2003 – June 2004	44.83 ° N 56.18 ° W	121 m 196 m 296 m 371 m	0 (0.0%) 0 (0.0%) 0 (0.0%) 0 (0.0%)	Two series at 196 m: July – September 2003 and November 2003 to July 2004
July 2003 – June 2004	44.83 ° N 56.18 ° W	16 m 40 m 60 m	0 (0.0%) 0 (0.0%) 0 (0.0%)	Three depths were selected for processing

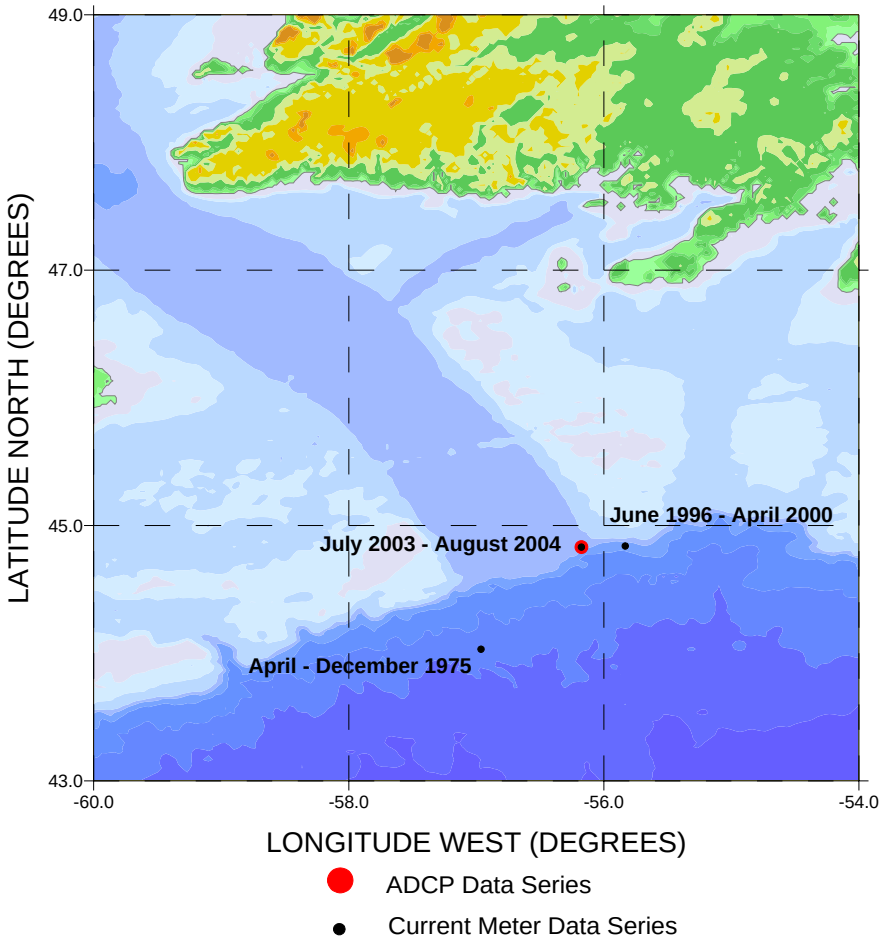

Figure 3.44. Geographic Location of the Survey Areas and the Current Data Sets.

Also, the gaps in the data were small due only to the time necessary to retrieve and redeploy the instruments. These maneuvers lasted from a few hours to a little less than a day. When the gap was shorter than half a semidiurnal tide cycle, the missing values were filled with linearly interpolated values of current speed and direction. On several occasions the gaps lasted from 12 to 22 hours. In these cases, the linear interpolation was considered inadequate to replace the values missing from the series. Instead, an analysis was done of the data series variability immediately before and after the gap, in order to select a segment of the series that most likely would correspond to the behaviour of the data in the missing fragment. Fortunately, the gaps occurred during periods of moderate changes in the character of the current variability so that the substitution was possible with realistic results.

Table 3.13 indicates the proportion that these filled gaps represent of the total length of the series. It does not go beyond 0.4 % of the total number of records in any of the data sets. In order to take advantage of the benefits of using long data series, these data sets were treated as single, uninterrupted data series. On occasions, some of the instruments stopped working days or weeks before the respective mooring were retrieved for replacement. For these times and depths, two data series resulted. The data from these locations were treated as separate series for purposes of creating progressive vector diagrams and performing harmonic analysis of tidal constituents. For the calculations of statistics and bivariate histograms the data was processed jointly.

The current data series come from three moorings grouped in two areas: the shelf break outside St. Pierre Bank at a depth ranging between 400 and 700 m, and the Slope outside the Laurentian Channel (Figure 3.44). These two locations represent different regions of the regional topography and thus, should show a different current pattern.

The discussion of the data analysis will be focused in these two areas. There is enough data in each area to develop a relatively detailed picture of the current character and variability.

3.4.3. Currents on the Continental Slope

The Continental Slope area was represented by a mooring that was in the water from April to December 1975 and had four instruments placed at depths of 140 m, 450 m, 1,000 m, and 2,001 m.

This location (to the south of the western side of the Laurentian Channel) is expected to be exposed to the exchange of waters with the Gulf of St. Lawrence and at the same time to the effects of the Slope Water Jet described by Fratantoni and Pickard (2005). As a result, it is reasonable to expect some degree of variability.

The information in the progressive vector diagrams for this location (Figure 3.45) are consistent with this idea and show currents to the north and northeast between April and May for depths of 140 m and 450 m and then a succession of direction shifts, after which a final southwest flow is established. The currents at 1,000 m and 2,001 m show a similar pattern except at these depths the currents are flowing

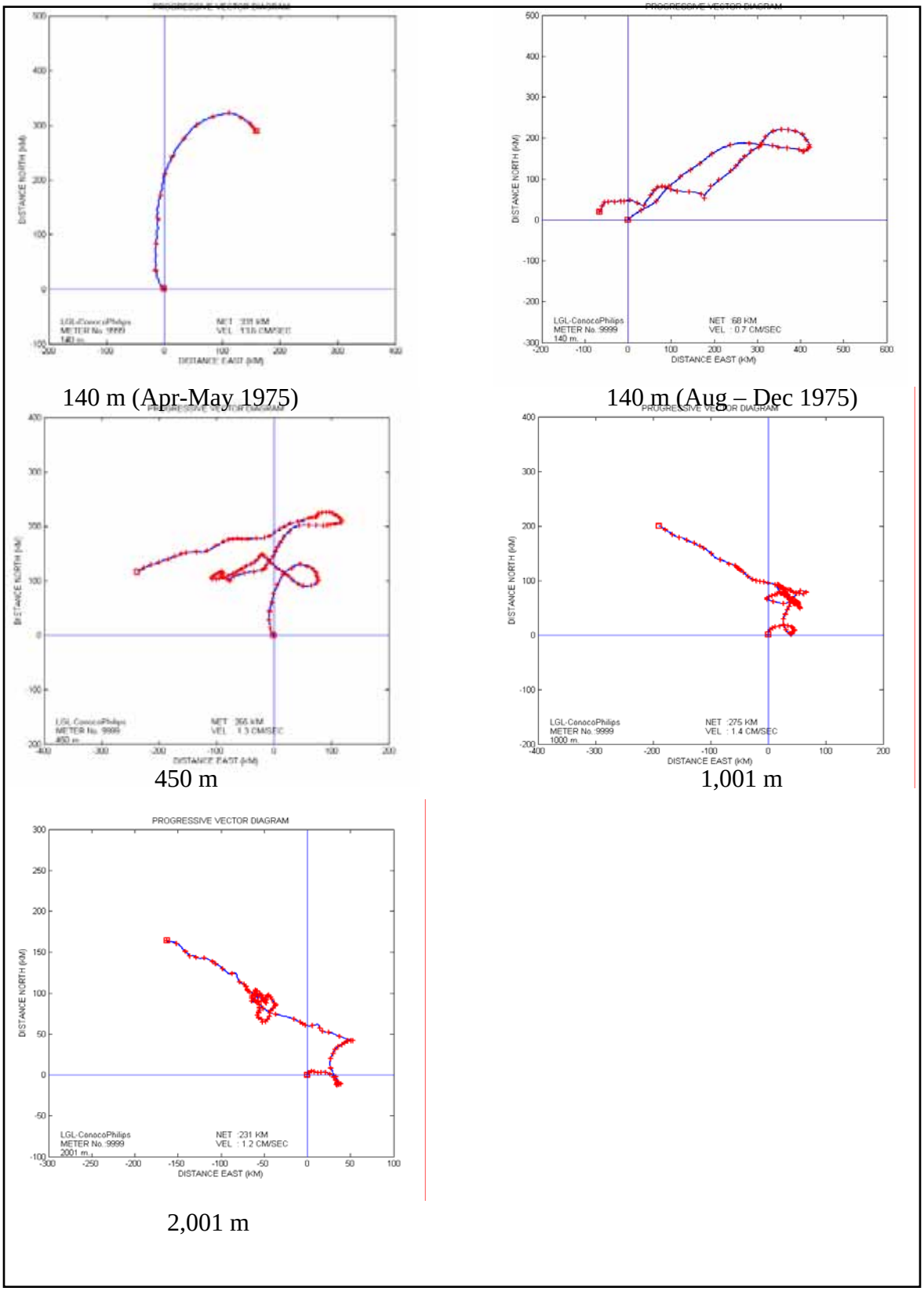

Figure 3.45. Progressive Vector Diagrams for the Continental Slope (April - December 1975).

northwest when the current at 140 m and 450 m are flowing southwest. The variability in the circulation at this location is more clearly demonstrated in the rose plots contained in Appendix 6 of Oceans (2006).

The monthly rose plots in Appendix 6 of Oceans (2006) show similarities in the currents at 140 m and 450 m. The dominant current direction was towards the north in April, northeast in August, and southwest from October to December. During the other months the currents were more evenly distributed among all directions.

Currents at 1,000 m and 2,001 m show some degree of analogy between them but differ from the upper layers of the water column. During the months of June, and October to December the currents tended to flow in a northwest direction at both depths. During April, the currents were northeast more often at 1,000 m and southeast more often at 2,001 m. During the remaining months the currents were more evenly distributed in all directions.

The magnitude of the tidal currents is relatively low at this location. At all observed levels the most important constituents (M_2, N_2, S_2, O_1, K_1) have low values and the most important constituents are those of long periods like SSA, MSM and MM indicating that the longer period oscillations are more important at this location. An amphidromic point for the lunisolar diurnal constituent K_1 is reported for the vicinity of the studied area (Dupont et al. 2002), but it does not explain the small values for the semidiurnal constituents. Current speed statistics are given in Table 3.14.

The maximum current speeds at this location were 46.6 cm/sec in April at 140 m; 26.1 cm/sec in May at 450 m; 16.5 cm/sec in November at 1,000 m and 17.1 cm/sec in July at 2,001 m. The average current speeds were 14.6 cm/sec at 140 m; 6.7 cm/sec at 450 m; 4.0 cm/sec at 1,000 m, and 3.5 cm/sec at 2,001 m.

3.4.4. Currents Outside St. Pierre Bank

The shelf break outside St. Pierre Bank is represented in this study by two datasets. The first dataset was collected between June 1996 and April 2000 and the second dataset was collected between July 2003 and June 2004. The multi-year deployment in the first dataset had instruments at four sampling depths: 56 m, 153 m, 400 m and 680 m. The data at 400 m had a gap from May to December, 1997. For that reason, two progressive vector diagrams are shown for this depth in Figure 3.46.

The progressive vector diagrams for the first location show a steady westerly flow at the first three levels and a northwest flow at 680 m, near the bottom. The westward flow is most likely to the Labrador Current waters flowing along the shelf break. The northwestward flow near the bottom appears to be part of the circulatory system of the Laurentian Channel, where waters enter the Gulf of St. Lawrence along the east margin of the channel and leaves the Gulf along the west margin. The difference in current directions between the upper layers of the water column and the near-bottom depths may be evidence of a deep-water topographic steering of the flows contributing to the mass balance of the Gulf of St. Lawrence.

Table 3.14. Current Speed (cm/sec) Statistics for the Continental Slope.

APRIL – DECEMBER 1975

SPEED STATISTICS 140 M

MONTH	MEAN	STD	MINIMUM	MAXIMUM	N.OBS.
APRIL	25.51	8.50	7.40	46.60	811
MAY	15.27	8.03	1.50	41.50	1218
JUNE	***	***	***	***	***
JULY	***	***	***	***	***
AUGUST	22.58	6.34	6.80	39.20	1320
SEPTEMBER	10.42	5.24	1.50	30.60	2160
OCTOBER	12.94	6.23	1.50	32.70	2232
NOVEMBER	11.47	5.10	1.50	29.40	2160
DECEMBER	11.30	5.02	1.50	22.20	196
TOTAL	**14.60**	**8.00**	**1.50**	**46.60**	**10097**

SPEED STATISTICS 450 M

MONTH	MEAN	STD	MINIMUM	MAXIMUM	N.OBS.
APRIL	10.37	5.09	1.50	25.50	805
MAY	8.39	5.07	1.50	26.10	2232
JUNE	6.07	3.14	1.50	18.70	2160
JULY	4.63	2.04	1.50	12.00	2232
AUGUST	7.62	3.59	1.50	20.20	2233
SEPTEMBER	4.89	2.88	0.92	15.80	2160
OCTOBER	5.74	3.06	1.44	14.40	2232
NOVEMBER	8.28	4.36	1.24	22.00	2160
DECEMBER	8.66	3.88	1.50	19.10	197
TOTAL	**6.73**	**4.02**	**0.92**	**26.10**	**16411**

SPEED STATISTICS 1000 M

MONTH	MEAN	STD	MINIMUM	MAXIMUM	N.OBS.
APRIL	4.13	2.46	0.00	14.80	272
MAY	3.89	2.37	0.00	12.80	744
JUNE	3.83	2.29	0.00	11.10	720
JULY	1.99	0.14	0.00	2.20	744
AUGUST	4.58	2.82	0.00	14.70	744
SEPTEMBER	2.38	1.01	0.00	7.50	720
OCTOBER	4.36	2.62	0.00	13.90	744
NOVEMBER	6.25	3.72	0.00	16.50	720
DECEMBER	9.42	2.76	3.20	15.20	57
TOTAL	**3.96**	**2.78**	**0.00**	**16.50**	**5465**

SPEED STATISTICS 2001 M

MONTH	MEAN	STD	MINIMUM	MAXIMUM	N.OBS.
APRIL	3.26	1.53	0.00	7.50	272
MAY	4.37	2.53	0.00	11.70	744
JUNE	3.84	2.50	0.00	12.80	720
JULY	3.98	3.48	0.00	17.10	744
AUGUST	2.44	1.23	0.00	8.00	744
SEPTEMBER	2.38	1.11	0.00	7.60	720
OCTOBER	2.58	1.39	0.00	9.90	744
NOVEMBER	4.86	3.05	0.00	16.50	720
DECEMBER	7.67	2.32	2.00	12.30	65
TOTAL	**3.53**	**2.53**	**0.00**	**17.10**	**5473**

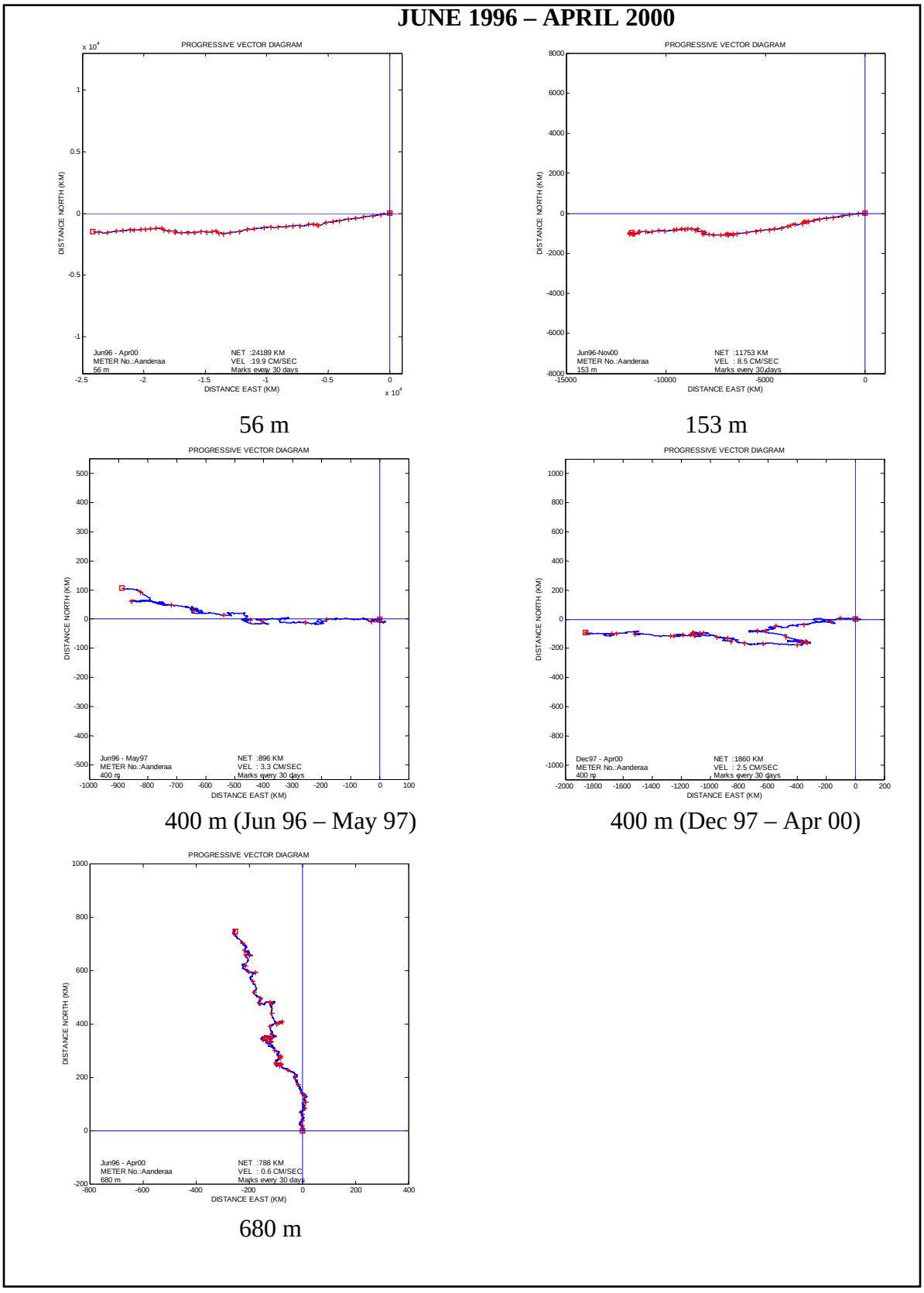

Figure 3.46. Progressive Vector Diagrams for the area outside of St. Pierre Bank.

The rose plots for this site show little variability from month to month. This is particularly true at 56 m and 153 m. At these two levels, all the monthly roses are almost identical and so are the overall plots (Appendix 6 *in* Oceans 2006). They show dominant westward currents similar to the progressive vector diagrams. At 400 m, the monthly rose plots show a similar picture with currents flowing in a westerly direction from January to May, in August, and from October to December. During June, July and September, the dominant current flow was in an opposite direction towards the east. This is consistent with the flow reversals observed in the progressive vector diagrams for this depth. Near the bottom, the current directions are well represented in all directions except southeast with the dominant currents oscillating between northeast and southwest.

The maximum currents (Table 3.15) were observed in January at 56 m (83.8 cm/sec), April at 153 m (55.2 cm/sec), December at 400 m (44.1 cm/sec) and October at 680 m (30.2 cm/sec). The average current speeds were 23.9 cm/sec at 56 m, 14.7 cm/sec at 153 m, 9.9 cm/sec at 400 m, and 4.8 cm/sec at 680 m.

The second location on the shelf break outside St. Pierre bank was surveyed during a year-long period starting in July 2003 and finishing in June 2004. These measurements were made by BIO on request of Conoco-Phillips and were designed to investigate the oceanographic conditions in the area of potential drilling programs.

This measurement program was accomplished in two stages. During the first stage the instruments were in the water from July 17 to November 5, 2003. During the second stage of the program, the instruments were deployed on the same day as the first instruments were retrieved and they stayed in the water until June 8, 2004. The mooring contained four current metres located at 121 m, 196 m, 296 m and 371 m. In addition, an ADCP was placed at 66 m looking upward. From the data delivered by the ADCP, three levels were selected for analysis and discussion; 16 m (the shallowest depth with acceptable data quality with 84% of good pings), 40 m, and 60 m (the deepest level for which the ADCP rendered information).

The residual currents as shown by the progressive vector diagrams (Figure 3.47) have well established west-northwest directions from 60 m to 296 m. The directions of the residual currents appear to rotate clockwise with depth. Between 60 m and 296 m the residual direction rotates from west to northwest. However at 371 m, the residual current flows to the southwest. The magnitude of the residual velocity is approximately 12.7 cm/sec at 16 m and 40 m, 11.7 cm/sec at 60 m, 8.1 cm/sec at 124 m, 3.5 cm/sec at 296 m, and 5.1 cm/sec at 371 m.

The rose plots show little change from 16 m to 296 m, with the most occurrences concentrated in the west to northwest directions. The maximum observed speeds were also in a westerly direction and has values of 100.7 cm/sec at 16 m, 17.2 cm/sec at 40 m, 55.3 cm/sec at 60 m, 49.6 cm/sec at 121 m, 49.3 cm/sec at 196 m and 42.4 cm/sec at 296 m (Table 3.16). The average current speeds were 21.0 cm/sec at 16 m, 19.0 cm/sec at 40 m, 17.3 cm/sec at 60 m, 14.9 cm/sec at 121 m, 13.1 cm/sec at 196 m, and

Table 3.15. Current Speed (cm/sec) Statistics for the Area outside St. Pierre Bank for June 1996 - April 2000.

JUNE 1996 – APRIL 2000

SPEED STATISTICS 56 M

MONTH	MEAN	STD	MINIMUM	MAXIMUM	N.OBS.
JANUARY	27.85	14.61	1.40	86.83	2976
FEBRUARY	25.28	13.75	1.68	71.70	2712
MARCH	25.61	12.08	1.40	68.80	2976
APRIL	20.97	11.83	1.10	60.40	2844
MAY	19.16	10.41	1.10	53.70	2232
JUNE	21.91	11.75	1.39	69.39	2283
JULY	22.48	11.21	1.10	70.26	2976
AUGUST	23.82	10.50	1.10	65.61	2976
SEPTEMBER	23.10	13.07	1.39	62.71	2881
OCTOBER	25.29	12.38	1.10	77.50	2976
NOVEMBER	24.03	11.58	1.70	67.94	2880
DECEMBER	25.98	13.85	1.40	82.18	2976
TOTAL	**23.93**	**12.56**	**1.10**	**86.83**	**33688**

SPEED STATISTICS 153 M

MONTH	MEAN	STD	MINIMUM	MAXIMUM	N.OBS.
JANUARY	16.95	11.69	1.10	53.12	2976
FEBRUARY	16.10	9.52	1.10	51.08	2712
MARCH	15.83	9.54	1.10	48.18	2976
APRIL	15.10	9.39	1.10	55.20	2880
MAY	12.48	8.05	1.10	38.30	2976
JUNE	14.38	8.00	1.10	44.98	3004
JULY	12.83	7.76	1.10	46.14	3720
AUGUST	13.51	8.37	1.10	48.76	3720
SEPTEMBER	12.45	7.74	1.10	53.12	3600
OCTOBER	17.11	10.05	1.10	52.54	3720
NOVEMBER	15.05	8.70	1.10	52.00	3332
DECEMBER	15.43	9.51	1.10	50.21	2976
TOTAL	**14.71**	**9.19**	**1.10**	**55.20**	**38592**

SPEED STATISTICS 400 M

MONTH	MEAN	STD	MINIMUM	MAXIMUM	N.OBS.
JANUARY	11.32	6.86	1.10	39.50	2976
FEBRUARY	11.46	7.47	1.10	41.78	2712
MARCH	10.04	5.72	1.10	38.30	2976
APRIL	10.92	6.93	1.10	35.70	2844
MAY	8.01	4.48	1.10	23.19	1526
JUNE	8.00	4.68	1.10	24.64	1563
JULY	8.47	5.41	1.10	25.80	2232
AUGUST	7.37	5.20	1.10	27.54	2232
SEPTEMBER	8.51	5.26	1.10	40.33	2161
OCTOBER	9.76	6.24	1.10	34.52	2232
NOVEMBER	9.17	5.62	1.10	32.80	2160
DECEMBER	9.58	5.87	1.10	44.11	2746
TOTAL	**9.59**	**6.15**	**1.10**	**44.11**	**28360**

Table 3.15 (cont'd)

SPEED STATISTICS 680 M

MONTH	MEAN	STD	MINIMUM	MAXIMUM	N.OBS.
JANUARY	5.70	4.09	1.00	24.93	2976
FEBRUARY	5.25	3.92	1.00	25.22	2712
MARCH	5.96	4.33	1.00	29.29	2976
APRIL	4.89	3.56	1.00	20.57	2844
MAY	3.88	2.92	1.00	16.79	2232
JUNE	4.05	3.10	1.10	21.73	2283
JULY	3.60	2.61	1.10	16.50	2976
AUGUST	3.74	2.68	1.10	14.18	2976
SEPTEMBER	4.55	3.40	1.10	27.25	2881
OCTOBER	4.80	3.61	1.10	30.20	2976
NOVEMBER	5.26	3.81	1.00	26.67	2880
DECEMBER	5.36	3.76	1.00	22.00	2976
TOTAL	**4.78**	**3.62**	**1.00**	**30.20**	**33688**

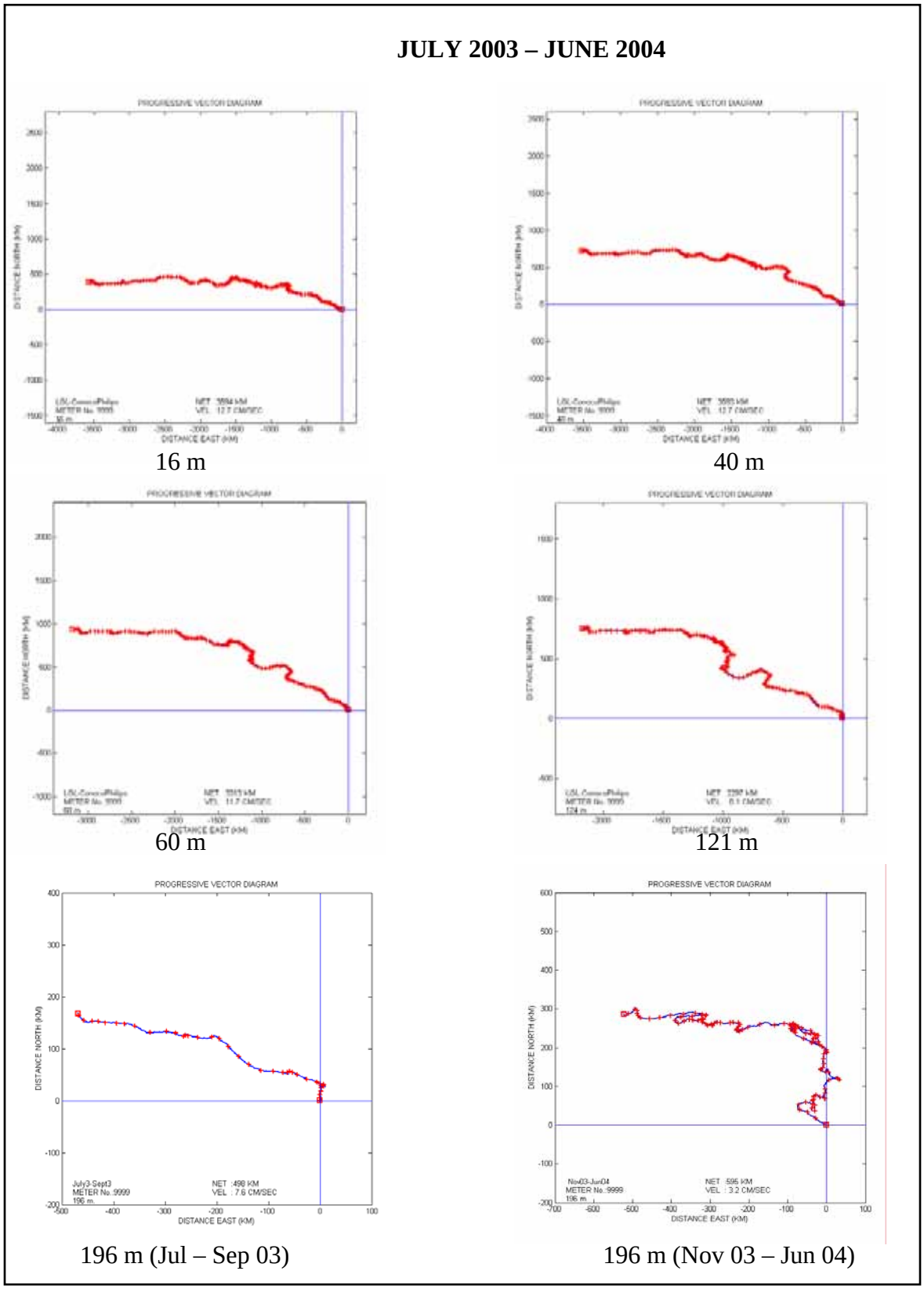

Figure 3.47. Progressive Vector Diagrams for the Area outside St. Pierre Bank.

JULY 2003 – JUNE 2004
(cont'd)

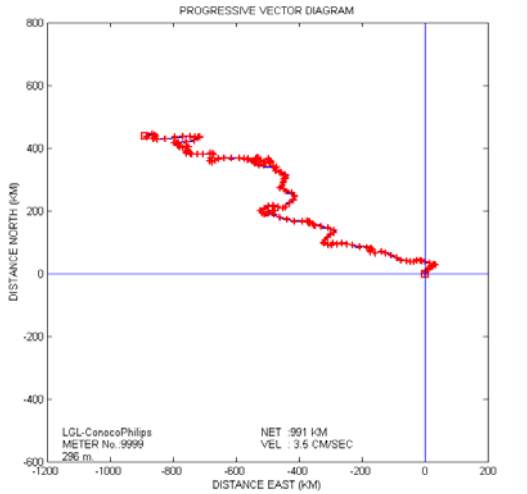

296 m

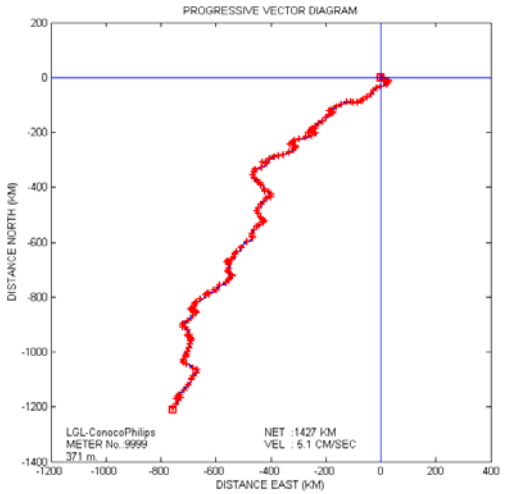

371 m

Figure 3.47 (cont'd) Progressive Vector Diagrams for the Area outside St. Pierre Bank.

Table 3.16. Current Speed (cm/sec) Statistics for the Area outside St. Pierre Bank for July 2003 - June 2004.

JULY 2003 – JUNE 2004

SPEED STATISTICS 16 M (ADCP DATA)

MONTH	MEAN	STD	MINIMUM	MAXIMUM	N.OBS.
JANUARY	20.12	10.19	1.30	64.88	744
FEBRUARY	23.03	10.96	0.94	76.82	696
MARCH	20.54	10.11	0.86	56.48	744
APRIL	28.48	12.13	1.10	67.88	720
MAY	23.14	11.95	0.32	55.35	744
JUNE	20.60	10.51	0.41	48.71	181
JULY	12.48	6.74	0.36	37.07	340
AUGUST	16.52	7.69	1.68	50.01	744
SEPTEMBER	21.73	11.16	0.85	58.47	720
OCTOBER	20.81	11.19	0.58	64.73	744
NOVEMBER	20.70	13.13	0.30	100.65	720
DECEMBER	19.18	10.90	0.82	64.72	744
TOTAL	**20.99**	**11.36**	**0.30**	**100.65**	**7841**

SPEED STATISTICS 40 M (ADCP DATA)

MONTH	MEAN	STD	MINIMUM	MAXIMUM	N.OBS.
JANUARY	17.34	9.81	0.42	57.30	744
FEBRUARY	20.89	10.24	0.50	61.44	696
MARCH	18.47	9.10	1.56	46.88	744
APRIL	27.80	9.89	4.21	63.24	720
MAY	20.62	11.27	0.80	55.14	744
JUNE	18.80	9.73	1.71	47.19	181
JULY	10.94	5.68	0.79	27.51	346
AUGUST	15.75	7.20	0.71	38.48	744
SEPTEMBER	19.99	9.43	0.61	46.27	720
OCTOBER	18.13	8.21	2.03	49.58	744
NOVEMBER	18.88	12.02	0.63	74.17	720
DECEMBER	16.53	9.81	0.09	57.34	744
TOTAL	**19.02**	**10.25**	**0.09**	**74.17**	**7847**

SPEED STATISTICS 60 M (ADCP DATA)

MONTH	MEAN	STD	MINIMUM	MAXIMUM	N.OBS.
JANUARY	15.20	8.58	0.09	49.76	744
FEBRUARY	19.27	9.61	0.42	52.01	696
MARCH	16.42	8.60	0.90	44.20	744
APRIL	25.04	9.43	3.53	54.29	720
MAY	19.93	11.98	1.51	50.38	744
JUNE	19.02	10.17	1.24	41.80	181
JULY	9.27	5.06	0.00	28.54	346
AUGUST	15.59	6.80	1.17	34.17	744
SEPTEMBER	18.34	8.57	1.07	47.45	720
OCTOBER	18.90	8.45	0.23	44.56	744
NOVEMBER	15.84	10.46	0.63	55.30	720
DECEMBER	13.24	7.85	0.30	38.92	744
TOTAL	**17.40**	**9.66**	**0.00**	**55.30**	**7847**

Table 3.16 (cont'd)

SPEED STATISTICS 121 M

MONTH	MEAN	STD	MINIMUM	MAXIMUM	N.OBS.
JANUARY	11.76	7.53	1.10	38.60	744
FEBRUARY	12.26	7.41	1.40	36.60	696
MARCH	14.36	8.15	1.40	44.40	744
APRIL	17.39	7.72	1.40	37.40	720
MAY	18.73	9.72	1.10	46.10	744
JUNE	15.50	7.70	1.40	40.30	181
JULY	8.64	4.27	1.10	24.10	347
AUGUST	15.58	7.08	1.10	31.60	744
SEPTEMBER	16.17	8.31	1.10	44.70	720
OCTOBER	15.97	7.44	1.70	40.90	744
NOVEMBER	16.04	9.55	1.10	49.60	720
DECEMBER	13.20	8.19	1.40	47.30	744
TOTAL	**14.87**	**8.37**	**1.10**	**49.60**	**7848**

SPEED STATISTICS 196 M

MONTH	MEAN	STD	MINIMUM	MAXIMUM	N.OBS.
JANUARY	12.80	7.41	1.10	49.30	744
FEBRUARY	11.65	6.60	1.40	41.20	696
MARCH	13.29	7.45	1.10	42.40	744
APRIL	12.31	5.73	1.40	31.90	720
MAY	15.38	7.02	1.40	42.10	744
JUNE	13.40	6.48	1.10	30.70	181
JULY	10.81	5.28	1.10	23.80	347
AUGUST	13.48	6.45	1.10	30.50	744
SEPTEMBER	13.73	7.50	1.10	38.00	718
OCTOBER	***	***	***	***	***
NOVEMBER	13.12	7.01	1.40	35.70	605
DECEMBER	13.31	7.23	1.10	47.00	744
TOTAL	**13.13**	**6.95**	**1.10**	**49.30**	**6987**

SPEED STATISTICS 296 M

MONTH	MEAN	STD	MINIMUM	MAXIMUM	N.OBS.
JANUARY	14.59	7.70	1.10	42.40	744
FEBRUARY	12.31	6.99	1.10	41.50	696
MARCH	13.03	6.31	1.10	37.70	744
APRIL	11.07	6.46	1.10	32.80	720
MAY	14.03	7.22	1.10	39.20	744
JUNE	13.56	7.00	1.40	29.90	181
JULY	8.30	4.51	1.10	28.40	360
AUGUST	12.67	6.11	1.10	27.50	744
SEPTEMBER	12.72	6.99	1.10	36.60	720
OCTOBER	11.71	6.67	1.10	37.40	744
NOVEMBER	14.68	6.84	1.10	34.80	720
DECEMBER	14.51	7.35	1.10	40.90	744
TOTAL	**12.94**	**6.96**	**1.10**	**42.40**	**7861**

Table 3.16 (cont'd)

SPEED STATISTICS 371 M

MONTH	MEAN	STD	MINIMUM	MAXIMUM	N.OBS.
JANUARY	16.65	10.57	1.10	60.40	744
FEBRUARY	14.86	8.99	1.10	44.70	696
MARCH	14.54	8.08	1.10	48.80	744
APRIL	15.13	9.64	1.10	54.60	720
MAY	16.30	9.97	1.40	52.20	744
JUNE	18.53	9.58	1.10	43.20	180
JULY	10.14	6.39	1.10	36.80	347
AUGUST	14.43	8.10	1.10	39.70	744
SEPTEMBER	14.47	8.04	1.10	48.20	720
OCTOBER	13.67	8.10	1.10	47.60	744
NOVEMBER	16.33	9.16	1.10	53.70	721
DECEMBER	16.58	11.73	1.10	69.70	744
TOTAL	**15.14**	**9.34**	**1.10**	**69.70**	**7848**

12.9 cm/sec at 296 m. At 371 m the overall rose plot shows dominant southward directions. This is also the direction associated with the highest speed values at this depth. At 371 m, the maximum speed was 69.7 cm/sec and the average speed was 15.1 cm/sec.

Unlike the other discussed location on the shelf break outside St. Pierre Bank, the tidal constituents at this location are well defined. The lunar and solar semidiurnal ellipses M_2 and S_2 have major axes with values that range between 5.5 cm/sec at 16 m and 12.6 cm/sec at 371 m for M_2 and 25.5 cm/sec and 3.7 cm/sec for S_2. Diurnal constituents O_1 and K_1 have values which range between approximately 1 cm/sec at 16 m to 4 cm/sec at 371 m.

3.5. Wind and Wave Extremal Analysis

The wind and wave extremal analysis was carried out for the Laurentian Sub-basin using the AES-40 data set at Grib Point 5400 (45 °N; 55.8 °W) for 54 years of data between 1950 and 2004. The AES-40 wind and wave hindcast data set for the North Atlantic Ocean was prepared by Oceanweather Inc. under contract to the Meteorological Service of Canada. The AES-40 data set is a hindcast data set using the National Center for Atmospheric Research (NCEP-CSAR) global re-analysis surface marine wind fields, and further re-analyzed by Oceanweather Inc. with corrections to the original data set. The corrections included adjusting all observed winds to the standard reference level of 10 m above the sea surface, intensifying extratropical storms as necessary and including tropical cyclone boundary layer winds. The waves were then hindcasted by Oceanweather using their third-generation wave model. The hindcast wind fields closely resembled the waves measured at offshore buoys and observations from offshore platforms, thus validating the data set. The data has been generated using time steps of six hours. In some storms, particularly those of short duration, the peak winds may get missed due to the length of the sampling period. A shorter sampling period would be more desirable. However, the AES-40 data set has been a major improvement over previous data sets because of the many years of continuous data.

The extreme values for wind and waves were calculated using the peak-over-threshold method; and after considering four different distributions, the Gumbel Distribution was chosen as the most appropriate because it gave the best fit to the data. A sensitivity analysis was carried out to determine how many storms to use in the analysis, because the extreme values can vary depending on how well the data fits the distribution function. The sensitivity analysis showed that the Gumbel Distribution had a good fit using 439 storms for winds and 241 storms for waves when all the data was considered in calculating the yearly extremes. For monthly extremes the top 95 storms were used for winds and the top 55 storms for waves.

3.5.1. Extreme Value Estimates for Winds

The extreme value estimates for wind were calculated using Oceanweather's software programs for return periods of 1-year, 10-years, 25-years, 50-years and 100-years. The values calculated for each month and all months combined are given in Table 3.17. The extreme value analysis used hourly wind values for the reference height of 10 metres above sea level. The 10-minute and 1-minute winds were calculated from the 1-hour mean values using a constant ratio of 1.06 and 1.22 respectively. The 100-year extreme wind speed was 29.8 m/s. The 1-year, 10-year, 25-year, and 50-year extreme wind speeds were 23.2 m/s, 26.6 m/s, 27.9 m/s, and 28.9 m/s, respectively. These values may be slightly under estimated due to the 6-hour time interval in the data. It is highly probable that some of the peaks in the wind speed have been missed by the hindcasting methodology.

3.6. Extreme Value Estimates for Waves

The extreme value estimates for waves for return periods of 1-year, 10-years, 25-years, and 50-years and 100-years are given in Table 3.18. Similar to winds, the values were calculated for each month considered separately and for all months combined. The 100-year extreme significant wave height was 13.9 m/s. The 1-year, 10-years, 25-years, and 50-years extreme significant wave heights were 9.6 m, 11.8 m, 12.6 m and 13.3 m, respectively. The highest extreme significant wave height is expected to occur during January. Extreme value estimates were also calculated for the maximum wave heights and for the spectral peak periods associated with the significant wave heights. The extreme significant wave heights, and associated peak periods are presented in Table 3.18. The maximum wave heights are calculated using Oceanweather's software OSMOSIS. Their program evaluates Borgman's (1973) integral:

$$\Pr(H \le h) = \exp \int_{t_a}^{t_b} \log\left[1 - e^{h^2 / a^2(t)}\right] \frac{dt}{T(t)}$$

Table 3.17. Extreme Wind Estimates for Return Periods of 1, 10, 25, 50, and 100 Years at Grid Point # 5400 (45.0 °N; 55.8 °W).

	Wind Speed 1-hr (m/s)				
Month	**1.0**	**10.0**	**25.0**	**50.0**	**100.0**
JAN	21.0	24.7	26.0	27.0	28.0
FEB	20.6	24.3	25.6	26.6	27.6
MAR	19.8	24.6	26.4	27.7	29.0
APR	17.3	20.8	22.1	23.0	23.9
MAY	15.1	18.9	20.3	21.3	22.3
JUN	13.6	17.0	18.3	19.2	20.1
JUL	12.4	15.9	17.2	18.2	19.10
AUG	13.2	17.1	18.5	19.5	20.6
SEP	15.6	20.1	21.7	22.9	24.1
OCT	17.6	22.9	24.8	26.2	27.6
NOV	18.9	22.7	24.0	25.1	26.1
DEC	20.5	24.1	25.4	26.4	27.3
ALL	23.2	26.6	27.9	28.9	29.8
	Wind Speed 10-min (m/s)				
Month	**1.0**	**10.0**	**25.0**	**50.0**	**100.0**
JAN	22.2	26.1	27.5	28.6	29.6
FEB	21.8	25.8	27.2	28.2	29.3
MAR	21.0	26.1	28.0	29.3	30.7
APR	18.4	22.1	23.4	24.4	25.4
MAY	16.0	20.0	21.5	22.5	23.6
JUN	14.4	18.1	19.4	20.4	21.3
JUL	13.1	16.9	18.2	19.2	20.2
AUG	14.0	18.1	19.6	20.7	21.8
SEP	16.6	21.3	23.0	24.3	25.5
OCT	18.7	24.3	26.3	27.8	29.3
NOV	20.0	24.1	25.5	26.6	27.6
DEC	21.8	25.6	26.9	28.0	29.0
ALL	24.6	28.2	29.5	30.6	31.6
	Wind-Speed 1-min (m/s)				
Month	**1.0**	**10.0**	**25.0**	**50.0**	**100.0**
JAN	25.6	30.1	31.7	32.9	34.1
FEB	25.1	29.7	31.3	32.5	33.7
MAR	24.1	30.1	32.2	33.8	35.3
APR	21.1	25.4	26.9	28.1	29.2
MAY	18.4	23.1	24.7	25.9	27.2
JUN	16.5	20.8	22.3	23.4	24.6
JUL	15.1	19.4	21.0	22.2	23.3
AUG	16.1	20.9	22.6	23.8	25.1
SEP	19.1	24.5	26.5	27.9	29.4
OCT	21.5	28.0	30.3	32.0	33.7
NOV	23.1	27.7	29.3	30.6	31.8
DEC	25.1	29.5	31.0	32.2	33.4
ALL	28.4	32.4	34.0	35.2	36.4

Table 3.18. Extreme Wave Estimates for Return Periods of 1, 10, 25, 50, and 100 Years at Grid Point 5400 (45.0 °N 55.8 °W).

	Significant Wave Height (m)				
Month	**1.0**	**10.0**	**25.0**	**50.0**	**100.0**
JAN	7.6	10.9	11.9	12.7	13.4
FEB	7.3	10.2	11.1	11.8	12.4
MAR	6.1	9.6	10.7	11.5	12.2
APR	5.0	7.6	8.4	9.0	9.6
MAY	3.9	6.2	6.9	7.4	7.9
JUN	3.3	4.8	5.3	5.6	5.9
JUL	2.9	4.6	5.0	5.4	5.8
AUG	3.2	5.1	5.7	6.1	6.6
SEP	4.0	6.9	7.8	8.4	9.0
OCT	5.0	8.6	9.6	10.4	11.2
NOV	6.0	9.6	10.7	11.5	12.3
DEC	7.5	10.5	11.4	12.1	12.7
ALL	9.6	11.8	12.6	13.3	13.9
	Maximum Wave Height (m)				
Month	**1.0**	**10.0**	**25.0**	**50.0**	**100.0**
JAN	14.3	20.5	22.4	23.7	25.1
FEB	13.5	19.4	21.1	22.4	23.7
MAR	11.7	18.1	20.0	21.4	22.8
APR	9.4	14.2	15.7	16.8	17.8
MAY	7.6	11.7	12.9	13.8	14.7
JUN	6.3	9.2	10.1	10.7	11.3
JUL	5.6	8.6	9.5	10.2	10.8
AUG	6.2	9.7	10.7	11.5	12.3
SEP	7.6	12.9	14.5	15.7	16.9
OCT	9.4	16.0	17.9	19.4	20.8
NOV	11.3	18.0	20.0	21.5	22.9
DEC	14.1	19.5	21.2	22.4	23.6
ALL	17.9	22.1	23.7	24.9	26.1
	Associated Peak Period (sec)				
Month	**1.0**	**10.0**	**25.0**	**50.0**	**100.0**
JAN	11.8	13.9	14.4	14.8	15.2
FEB	11.7	13.3	13.7	14.0	14.3
MAR	11.6	13.1	13.4	13.7	13.9
APR	10.0	12.1	12.6	13.0	13.4
MAY	9.4	11.2	11.6	12.0	12.3
JUN	8.7	10.0	10.4	10.6	10.8
JUL	8.3	10.1	10.5	10.8	11.2
AUG	8.9	10.5	10.8	11.1	11.3
SEP	9.5	11.5	12.0	12.3	12.6
OCT	10.2	12.2	12.6	12.9	13.2
NOV	11.8	14.3	14.9	15.3	15.8
DEC	11.9	13.4	13.8	14.1	14.4
ALL	13.0	14.0	14.4	14.7	14.9

Where H is the largest wave height; a^2 is the mean square height taken as a function of time, t; t_a and t_b are the beginning and end times of the storm; and T(t) is the wave period.. This integral is based on a Rayleigh distribution function. Oceanweather's program uses a variant of this equation to calculate maximum individual wave height and has the following form:

$$\Pr\{H > h\} = \exp\left[-1.08311\left(\frac{h^2}{8M_0}\right)^{1.063}\right] \text{(Forristall)};\quad T = \frac{M_0}{M_1}$$

Where M_0 and M_1 are the first and second spectral moments of the total spectrum.

3.6.1. Joint Probability of Extreme Wave Heights and Spectral Peak Periods

In order to examine the period ranges of storm events, an environmental contour plot was produced showing the probability of the joint occurrence of significant wave heights and the spectral peak periods using the methodology of Winterstein et al. (1993). The environmental contour plot is presented in Figure 3.48. The wave heights were fitted to a Weibull Distribution and the peak periods to a lognormal distribution. The wave data was divided into bins of one metre for significant wave heights and one second for peak periods. Since the lower wave values were having too much of an impact on the wave extremes, the wave heights below two metres were modeled separately in a Weibull Distribution. The two Weibull curves were combined at two metres, the point where both functions had the same probability.

Three-parameter Weibull Distributions were used with a scaling parameter α, shape parameter β, and location parameter γ. The three parameters were solved by using a least square method, the maximum log likelihood, and the method of moments. The following equation was minimized to get the coefficients

$$LS(\alpha,\beta,\gamma) := \sum_{i=0}^{13}\left[\ln\left(-\ln\left(1-FP_i\right)\right) - \beta\cdot\ln\left[\frac{\left(h_i-\gamma\right)}{\alpha}\right]\right]^2$$

where h_i is the endpoint of the height bin (0.5, 1.5, …) and FP_i is the cumulative probability of the height bin. Using a minimizing function the three parameters α, β and γ were calculated.

A lognormal distribution was fitted to the spectral peak periods in each wave height bin. The coefficient of the lognormal distribution was then calculated. Using the coefficients and the two distribution functions, the joint wave height and period combinations were calculated for the various return periods. The values were plotted and contours produced as shown in Figure 3.48 for return periods of 1-year, 10-years, 25-years, 50-years, and 100-years. Environmental contour plots for each month of the year are contained in Appendix 7 of Oceans (2006).

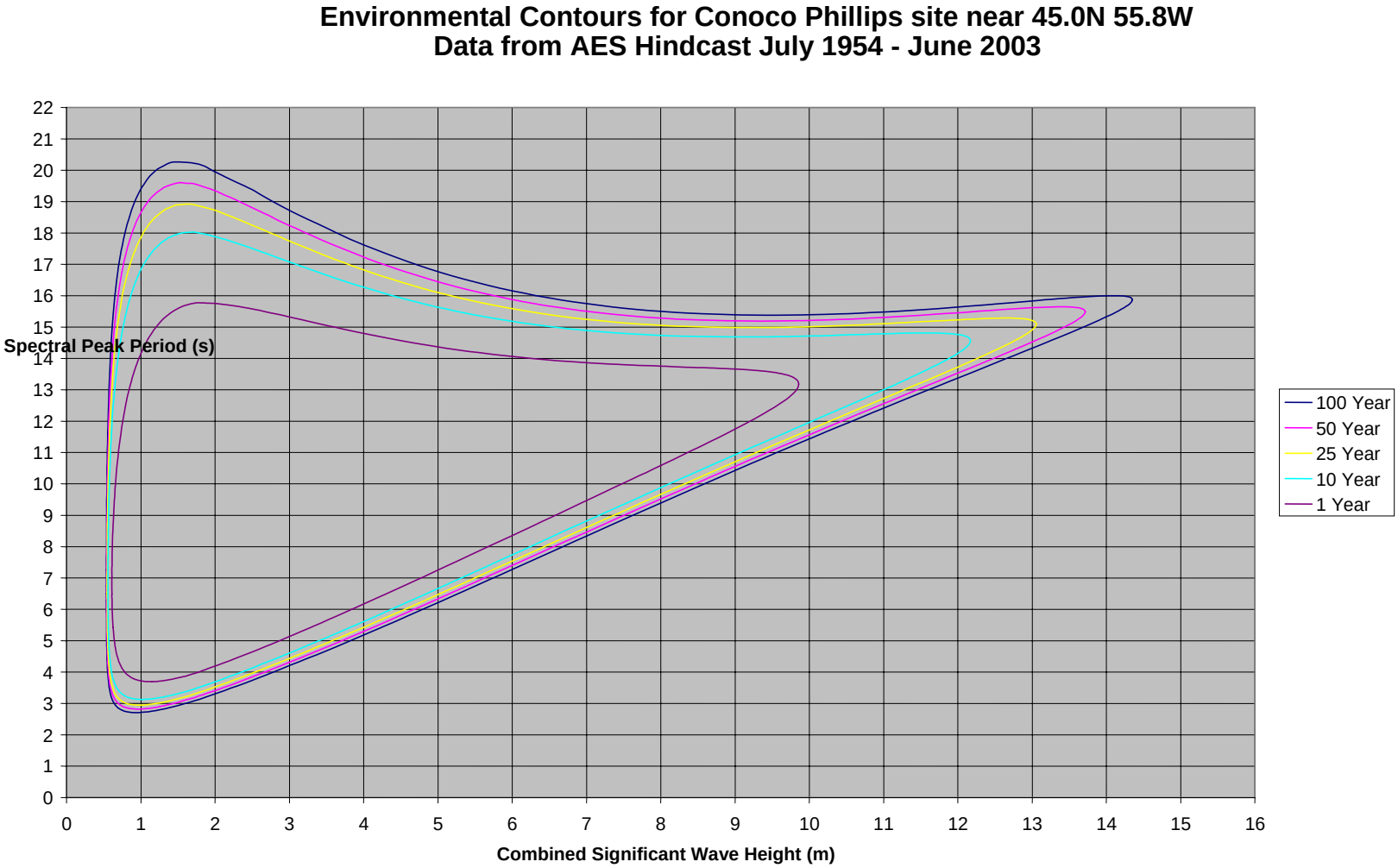

Figure 3.48. Environmental Contour Plot for the Laurentian Sub-basin.

The values for the significant wave height estimates and the associated spectral peak periods are given in Table 3.19. The 100-year extreme wave height using the Weibull Distribution on the complete set was 14.4 m as compared to 13.9 m using a Gumbel Distribution on a selected number of storms.

Table 3.19. Extreme Wave Estimates Together with Spectral Peak Periods.

Return Period (years)	*Significant Wave Height (metres)*	*Spectral Peak Period (seconds)*
1	9.9	11.5
10	12.2	13.3
25	13.1	14.0
50	13.7	14.4
100	14.4	14.9

3.7. Sea-Ice and Icebergs

The following is a description of the ice environment in the Laurentian Sub-basin. The exploration licenses lie in water depths ranging from a little over 2,500 m in the Southeast to 100 m in the north. The Laurentian Sub-basin location is susceptible to seasonal incursions of ice. Two different forms of floating ice are present in this marine environment: (1) sea ice and (2) icebergs.

This description of the ice regime at Laurentian Sub-basin begins with a description of the databases used, followed by a summary of the characteristics of the sea ice cover, then the information on icebergs is presented. Extreme conditions are included because they illustrate how the ice regime varies over time and space. Such variability is important when trying to assess the impact of ice on offshore exploration and development.

3.7.1. Databases

Regional sea ice data were compiled from approximately 28 years of ice observations carried out by the Canadian and US government agencies. Initially, these observations were obtained from airborne reconnaissance. Beginning in the 1970s, satellite images supplemented airborne observations, eventually replacing them as the principal sources of data by the mid-1990s. The data used for this report were extracted from a digital database of (approximately) weekly composite ice charts produced by the Canadian Ice Services (CIS) and the US National Ice Center (NIC). Data are stored in a SIGRID format at a resolution of 15-minute grids of latitude and longitude.

Data on icebergs were compiled from approximately 40 years of iceberg sightings from the International Ice Patrol (IIP). The IIP data have been used in most efforts to quantify and understand iceberg behaviour off eastern Canada. The database accessed for this report contains iceberg sightings and detections that for the most part come from aerial ice reconnaissance flights. Since 1989, iceberg survey data for the Canadian East Coast have been available from Provincial Airlines Ltd. (PAL). These data are particularly notable because the icebergs are visually confirmed after initial detection with radar.

Comparisons of annual total numbers of icebergs sighted in the Laurentian Sub-basin area from both sources indicate a similar distribution. Where differences do occur, they are likely the result of different operating mandates, estimation procedures and uncertainties associated with each survey methodology.

3.7.2. Sea Ice

Sea ice coverage information over the Laurentian Sub-basin was extracted from both the CIS (1972-2001) and NIC (1972-1994) databases. Both databases were queried for the number of weeks of coverage (10 weeks).

Where the data period overlapped, both the CIS and the NIC databases were consistent in their results.

Figure 3.49 shows the results of all sea ice coverage data. Sea ice was present for eight out of the 30 years considered or 26 percent of the time. For those periods when sea ice was present, the duration of coverage ranged from one to three weeks. The mean duration was one week.

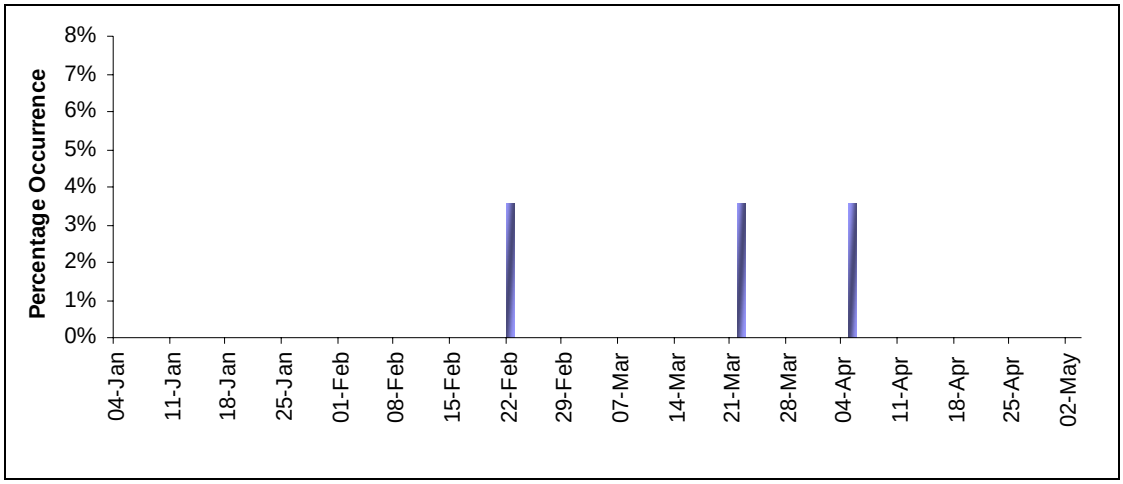

Figure 3.49. Timing of Sea Ice Cover, when Present.

3.7.2.1. Timing of Sea Ice Occurrence

All sea ice observations fall within the period February 22nd to April 5th with the peak influx centred on the month of March. Figure 3.50 shows the probability of sea ice occurrence by week for the Laurentian Sub-basin location.

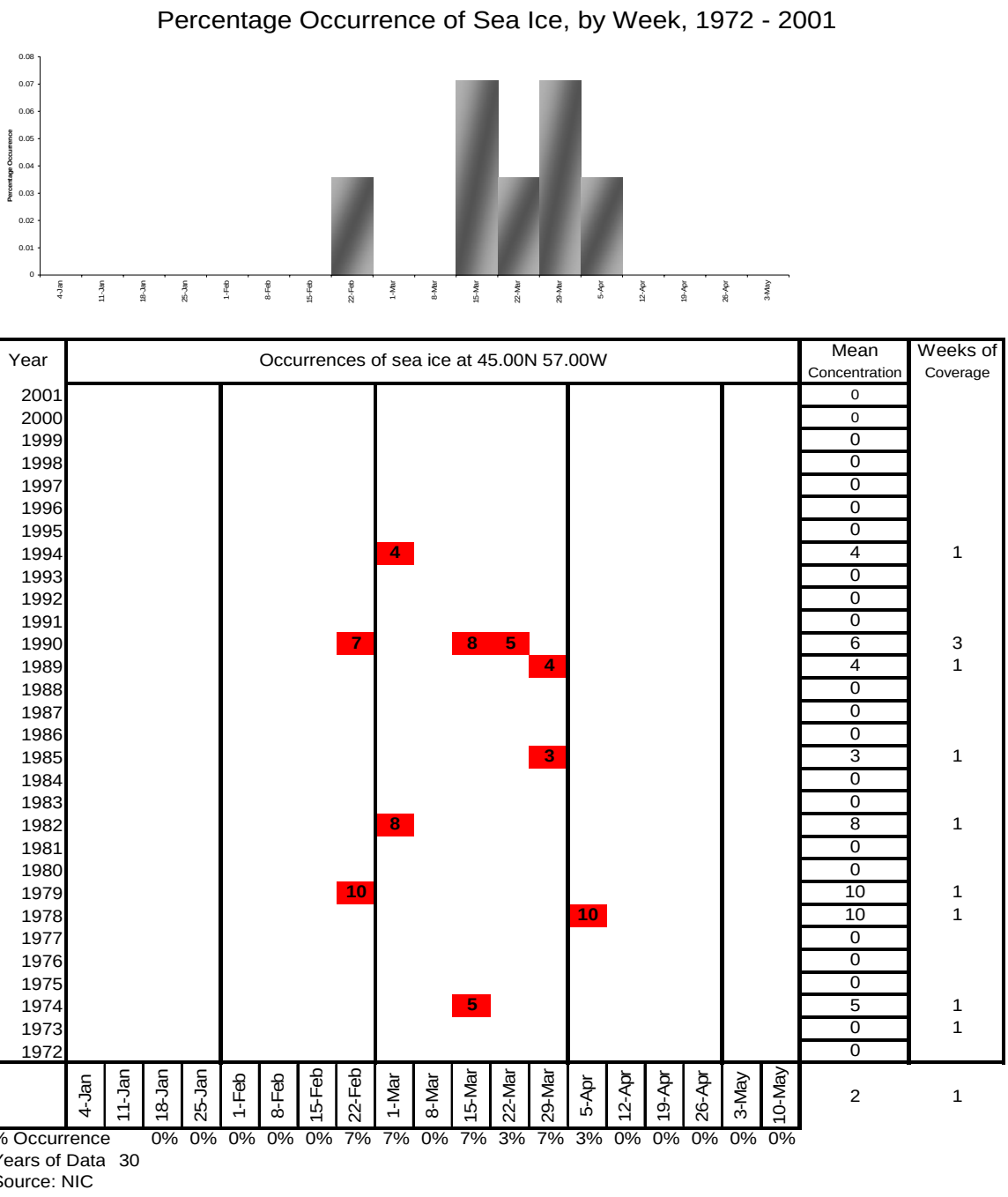

Figure 3.50. Percentage Occurrence of Sea Ice within the Laurentian Sub-basin, by Week, 1972 – 2001.

3.7.2.2. Sea Ice Concentrations

Sea ice concentrations ranged widely from a low of 30 percent to a high of 100 percent. Mean concentrations when ice is present are just over 60 percent. Figure 3.51 shows the mean sea ice concentrations by week for the Laurentian Sub-basin location.

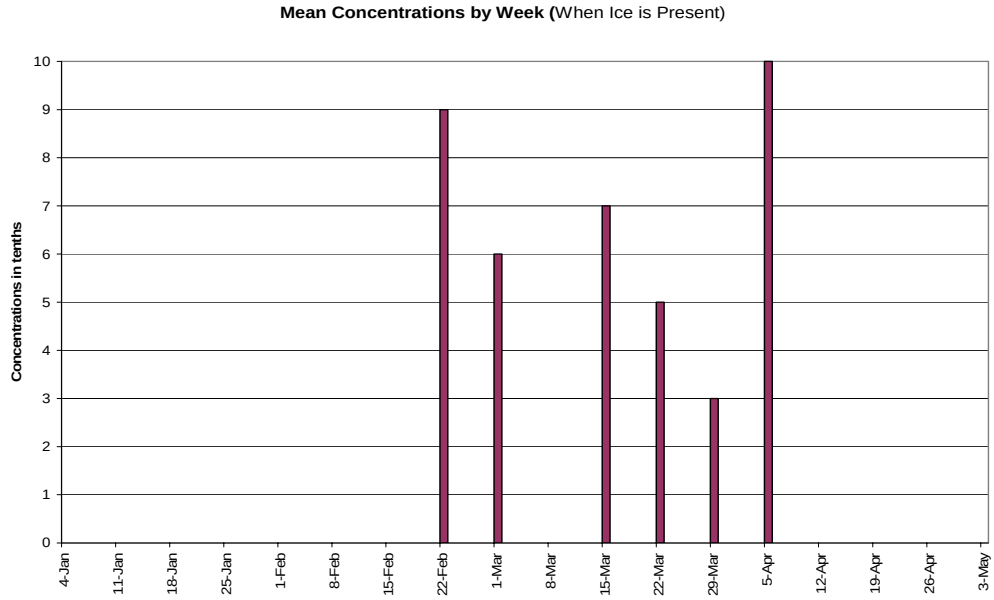

Figure 3.51. Mean Sea Ice Concentrations by Week.

3.7.2.3. Pack Ice Composition

Pack ice composition data were not available from the databases consulted. However, numerous industry and government reports confirm that the pack composition across the marginal ice zone is consistent at between 40 to 60 percent coverage of thin first-year ice (70-120 cm) in small floes.

The Canadian Ice Services Sea Ice Climate Atlas shows that the entire Gulf Pack ice cover in March is comprised of first-year ice and as the Laurentian Sub-basin is at the outer edge of the Gulf Pack it is reasonable to assume that the composition is similar. This assumption is consistent with observations made along the entire marginal ice zone and documented in all Grand Banks environmental assessments.

3.7.2.4. Pack Drift

Detailed drift data were not available from the databases consulted. However, analysis of weekly distributions shows that the pack ice edge advances out of the Gulf of St. Lawrence towards the Laurentian Sub-basin. In years of extreme sea ice distributions, additional ice may advance from the main pack that has rounded Cape Race on the southern tip of Newfoundland (Figure 3.52).

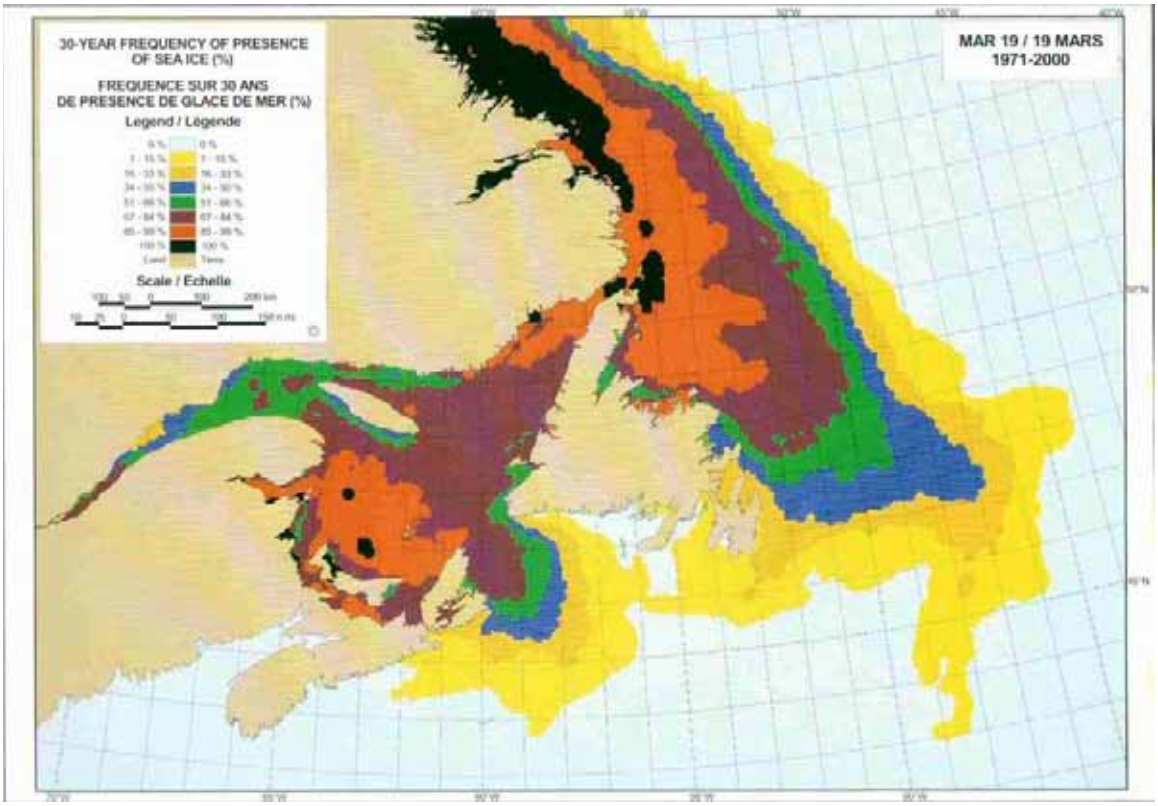

Figure 3.52. Maximum Pack Ice Cover by Frequency.

3.7.3. Icebergs

Iceberg sightings made within the constraints of the following coordinates; 46.00N to 44.00N and greater than 55.00W (the longitude of entry) were extracted from the PERD Iceberg Sighting Database. All sighting were sourced from the International Ice Patrol (IIP). The database was queried on all reports and then by confirmed sightings. Table 3.20 shows the results of those queries.

Table 3.20. Total Iceberg Sightings.

Source	Available Period	Sightings	
		Total Number	Number of Confirmed
IIP	1960 – 2001	517	58

The differences in numbers between all reported and confirmed icebergs is a usual result from this database. The total number of reports includes slow-moving, radar targets, duplicate sightings, and confirmed sightings. Historically, the total number of reports has proven to be considerably higher than the actual number of icebergs present and the standard analysis practice has been to only consider confirmed sightings

3.7.3.1. Iceberg Distribution by Year

The confirmed sightings were then analysed by year, considerable fluctuations in the yearly iceberg distribution are evident in both databases (Figure 3.53). However, the same is true when considering any one-degree block off Canada's East Coast.

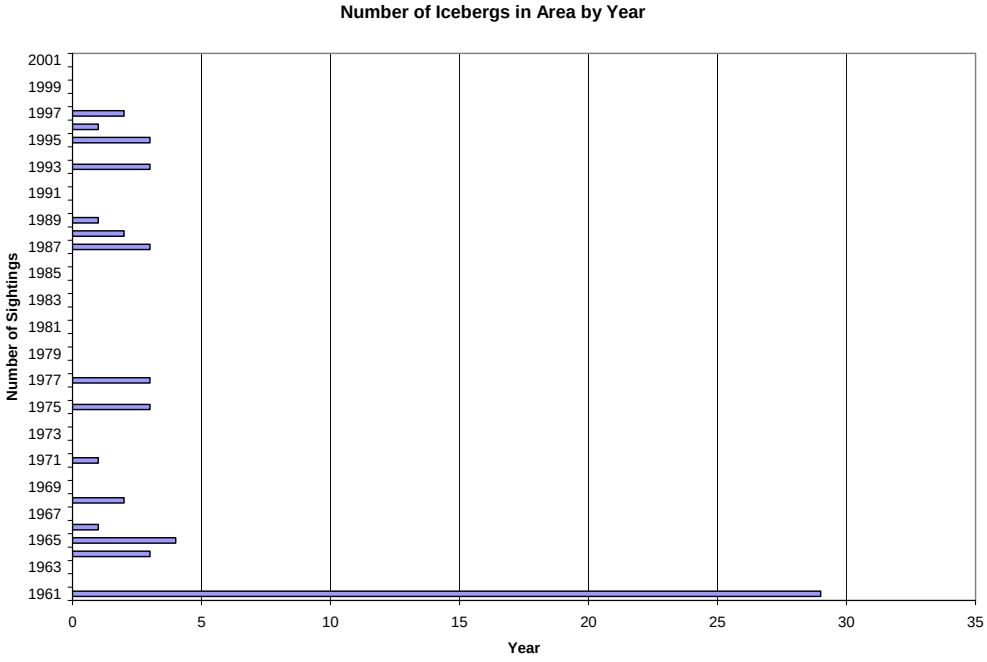

Figure 3.53. Iceberg Distribution by Year.

Table 3.21 shows the distribution range from both databases for Laurentian Sub-basin location and as a comparison, distribution range for the Terra Nova block.

Table 3.21. Iceberg Distribution Range by Year.

Source	Maximum	Minimum	Mean
Laurentian Sub-basin Block			
IIP	29	0	1.4
Terra Nova Block			
PAL	217	0	47

Twenty-six of the 41 years reviewed or 63 percent, showed iceberg free conditions existed at the Laurentian Sub-basin location.

3.7.3.2. Iceberg Distribution by Month

Data on monthly iceberg distribution for the Laurentian Sub-basin block were compiled from the IIP database. Iceberg sightings were present between February through to August and results showed that the peak flux was roughly centred on May month.

Figure 3.54 shows the monthly occurrence of icebergs in the Laurentian Sub-basin block as a percentage of the yearly total.

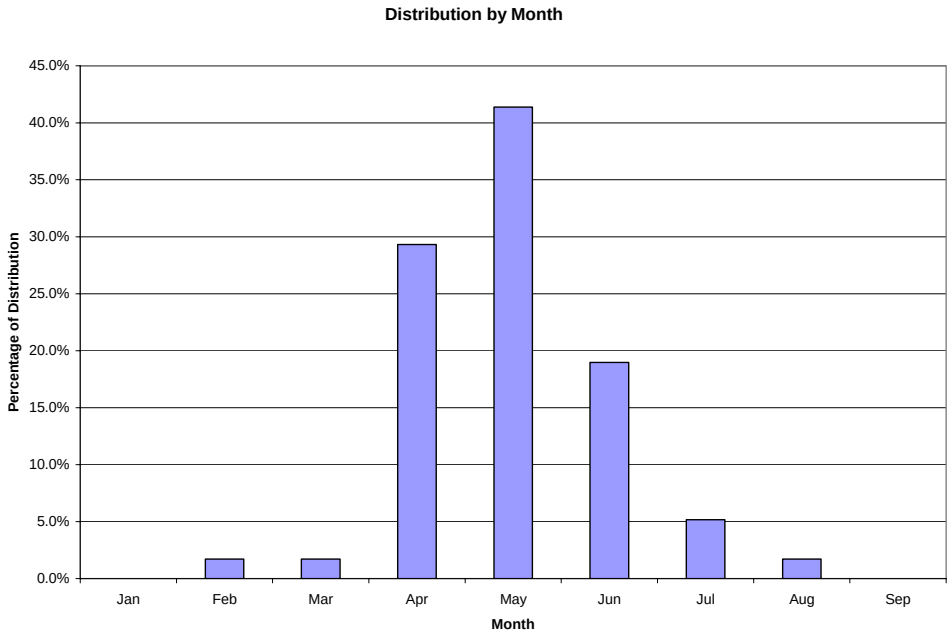

Figure 3.54. Monthly Occurrence of Icebergs as a Percentage of the Yearly Total.

3.7.3.3. Iceberg Size Distribution

Of the 58 icebergs extracted from the IIP database, 50 icebergs had associated size classifications while the remaining eight database entries were recorded as unknown or not reported. The International Ice Patrol visually classifies icebergs according to Table 3.22:

Table 3.22. Iceberg Size.

Category	Height (m)	Length (m)	Approx. Mass (T)
Very Large	> 75	>200	<10 Million
Large	45 -75	120 - 200	2 - 10 Million
Medium	15 - 45	60 - 120	100,000 - < 2 Million
Small	5 - 15	15 - 60	100,000
Bergy Bit	1.0 - 5	5 - 15	10,000
Growler	< 1.0	< 5	1,000

The accuracy of size distributions extracted from the IIP database is questionable, because most data are based on visual estimations and unspecified selection criteria. However, this methodology has been used on many previous studies and reports and is for the most part the only data available for the Laurentian Sub-basin area.

The size distribution for the Laurentian Sub-basin area is shown in Figure 3.55. In general terms, this distribution is very similar to other areas studied; however, as the Study Area is on the extreme range for icebergs there is a noticeable absence of large icebergs in the distribution. While the database does contain one report of a large iceberg, it is likely that it was over-estimated. If this were in fact a large iceberg we would expect additional sightings to have been made either in the same area or further down stream and there were no additional reports in the databases searched.

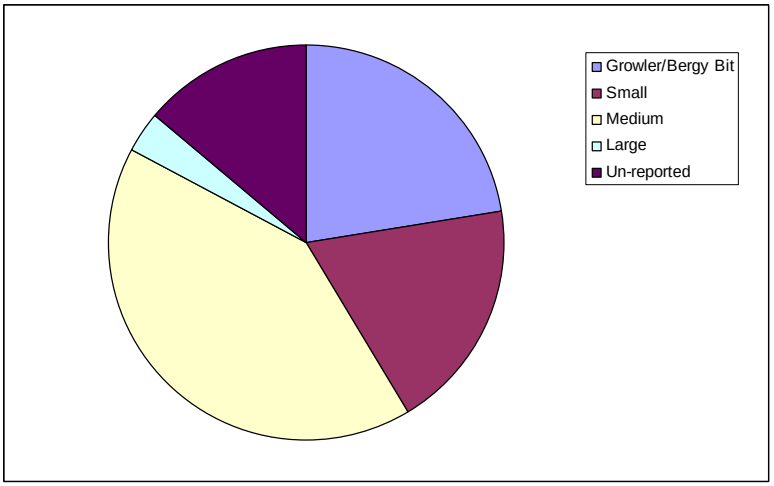

Figure 3.55. Iceberg Size Distributions for the Laurentian Sub-basin Block.

3.7.3.4. Iceberg Drift

Local winds and currents largely determine the movements of free-floating icebergs. There are little quantitative data on iceberg drift in the area of Laurentian Sub-basin. As such, only general iceberg drift information based on regional drift patterns and known distribution data from adjacent blocks can be presented (Figure 3.56).

Regional iceberg drift generally follows two basic patterns. The first is from the main inshore flow down through the Avalon Channel, turning south of Cape Race and drifting across the Saint Pierre Bank while the second approaches from the south and east following the bathymetric contouring of the area.

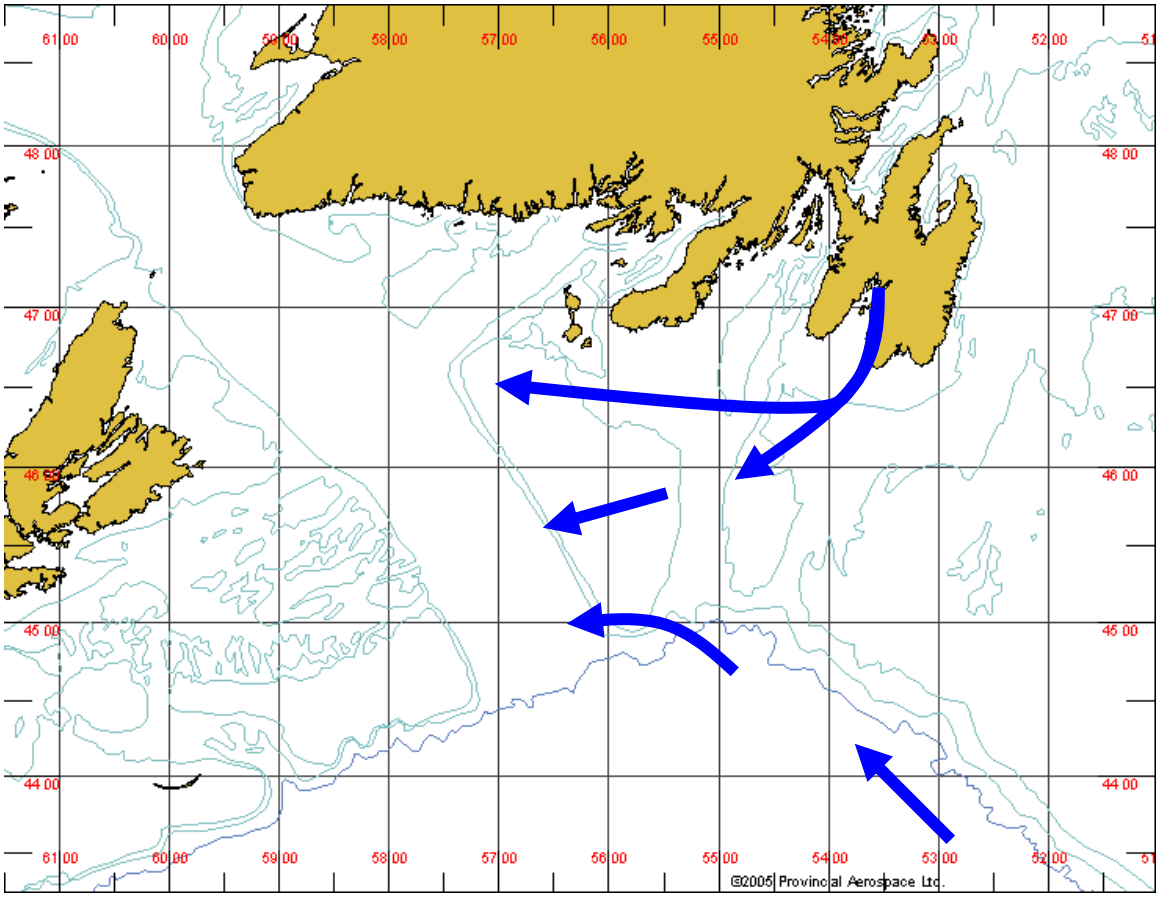

Figure 3.56. Bathymetry and General Iceberg Drift Patterns Surrounding the Laurentian Sub-basin Location.

3.7.3.5. Iceberg Scour

When large icebergs drift into relatively shallow water they can contact the sea floor resulting in a scour. Of the reported icebergs in this area, none have a size sufficient that could scour the sea floor. This area is close to the extreme limit for glacial ice as such any icebergs crossing the area are nearing the end of their melt cycle. However, historical scours have been reported.